Technical Report Documentation Page

1. Report No. FHWA/TX-02/1395-2F	2. Government Accession No.	3. Recipient's Catalog No.
4. Title and Subtitle TOP LATERAL BRACING OF STEEL U-SHAPED GIRDERS		5. Report Date October 1999 *Revised June 2000* *2nd Revision January 2002* 6. Performing Organization Code
7. Author(s) Brian S. Chen, Joseph A. Yura, and Karl H. Frank		8. Performing Organization Report No. Research Report 1395-2F
9. Performing Organization Name and Address Center for Transportation Research The University of Texas at Austin 3208 Red River, Suite 200 Austin, TX 78705-2650		10. Work Unit No. (TRAIS) 11. Contract or Grant No. Research Project 0-1395
12. Sponsoring Agency Name and Address Texas Department of Transportation Research and Technology Implementation Office P.O. Box 5080 Austin, TX 78763-5080		13. Type of Report and Period Covered Final (9/95-8/99) 14. Sponsoring Agency Code

15. Supplementary Notes

Project conducted in cooperation with the U.S. Department of Transportation, Federal Highway Administration, and the Texas Department of Transportation

16. Abstract

Steel box girder systems are being used more frequently for curved bridges because of their torsional stiffness and aesthetic appearance. These systems typically consist of U-shaped girders placed side-by-side with a composite concrete deck acting as the top flange. A critical design stage for these girders occurs during casting of the bridge deck, when the non-composite steel section must support the entire construction load, including the wet concrete. During this period, the top flanges are in compression and are susceptible to lateral-torsional buckling. Lateral bracing, typically in the form of a horizontal truss system, is installed to prevent the flanges from buckling and to increase the torsional stiffness of the girders. There is currently no existing codified design method for the lateral bracing of U-shaped girders.

This research report describes the analytical and experimental tests conducted on steel U-shaped girders with top-flange lateral bracing. The scope of the study focused on X-type top lateral truss systems. A series of pilot tests were also conducted to evaluate the performance of girders with metal deck panels used as a top lateral bracing system. Results include girder buckling loads, buckled shapes, brace forces, and girder torsional stiffnesses. Deficiencies in current code specifications are also discussed.

17. Key Words	18. Distribution Statement
U-Girders, Trapezoidal Girders, Steel Box Girders, Buckling Behavior, Top Lateral Bracing, Brace Forces, Torsional Stiffness	No restrictions. This document is available to the public through the National Technical Information Service, Springfield, Virginia 22161.

19. Security Classif. (of report)	20. Security Classif. (of this page)	21. No. of pages	22. Price
Unclassified	Unclassified	114	

Form DOT F 1700.7 (8-72) Reproduction of completed page authorized

TOP LATERAL BRACING OF STEEL U-SHAPED GIRDERS

by

Brian S. Chen, Joseph A. Yura, and Karl H. Frank

Research Report 1395-2F

Research Project 0-1395

"Trapezoidal Box Girder Systems"

conducted for the

Texas Department of Transportation

IN COORPERATION WITH THE

U.S. Department of Transportation
Federal Highway Administration

by the

CENTER FOR TRANSPORTATION RESEARCH
BUREAU OF ENGINEERING RESEARCH
THE UNIVERSITY OF TEXAS AT AUSTIN

October 1999
Revised June 2000
2nd Revision January 2002

This report was prepared in cooperation with the Texas Department of Transportation and the U.S. Department of Transportation, Federal Highway Administration.

IMPLEMENTATION

The findings in this research report indicate steel form metal decking may provide adequate bracing for the top flanges in steel U-shaped bridge girders. Implementation of these results is not recommended until the entire study has been completed. Recommendations for the bracing of steel U-shaped girders will be presented in the final research report presented by the University of Texas at Austin to the Texas Department of Transportation.

ACKNOWLEDGEMENTS

The researchers would like to acknowledge Arnie Cohn (DES), TxDOT Project Director, for his contributions to this research project. Appreciation is also extended to the TxDOT Project Monitoring Committee, which includes T. Ahmed (GHWA), Jeffery Cicerello (DES), J.C. Liu (HOU), Fred Long (LBB), Michael Smith (CST), Mary Lou Ralls (CSTM), and John Vogel (HOU). The researchers also want to give thanks to the FSEL staff and students for their assistance.

NOT INTENDED FOR CONSTRUCTION,

BIDDING, OR PERMIT PURPOSES

Joseph A. Yura, Texas PE. #29859

Karl H. Frank, Texas P.E. #48953

Research Supervisors

TABLE OF CONTENTS

LIST OF TABLES

LIST OF FIGURES

NOTATION

DIMENSIONS AND SECTION PROPERTIES

b	Distance between girder webs (brace panel width)
s	Distance between adjacent brace points (brace panel length)
A_f	Area of one top flange
S_f	Section modulus for top flange about strong axis
S_g	Section modulus (top) for U-girder
Δ	Lateral deflection of top flange
Δ_o	Initial deflection of top flange
Δ_{lat}	Lateral deflection necessary to accommodate panel shortening
Δ_{sh}	Shortening of a brace panel due to girder bending
θ	Brace angle measured between diagonal brace and cross strut

FORCES AND STRESSES

F_{br}	Diagonal brace force
F_{xs}	Cross-strut brace force
F_{yf}	Force necessary to cause yielding in both top flanges ($F_{yf} = 2A_f F_y$)
P, M	Experimentally applied ram load or moment
P_{cr}	Southwell predicted buckling load
P_e	Euler buckling load
P_{max}, M_{max}	Maximum experimentally applied ram load or moment
P_y, M_y	Ram load or moment causing first yield in top flanges using simple bending theory (calculation uses F_y)
σ_{max}	Maximum first and second-order compressive stress

MATERIAL PROPERTIES

$\boldsymbol{E}$	Modulus of elasticity
$\boldsymbol{F_{sy}}$	Static yield stress from tensile tests
$\boldsymbol{F_y}$	Specified minimum yield stress
$\boldsymbol{G}$	Modulus of rigidity

OTHER

β	Equivalent lateral stiffness of diagonal brace
β_{axial}	Axial stiffness of a tension brace member
$\beta_{coupler}$	Axial stiffness of coupler
β_i	Ideal brace stiffness
$\boldsymbol{I_w}$	Warping torsional constant
$\boldsymbol{K_T}$	St. Venant or pure torsional constant
χ	Torsion proportionality parameter

PREFACE

This report summarizes the research conducted to evaluate the top flange lateral bracing requirements to stabilize the top flanges of U-shaped girders. In Project Report 1239-4F two bracing methods for controlling lateral stability were developed for I-sections, lateral bracing and torsional bracing. The design rules for these two methods are given in Appendix A of that report. In the present project, the applicability of these two bracing methods for U-shaped girders was investigated in Task 5. The contribution of internal diaphragms (torsional bracing) to lateral stability of U-shaped girders was reported in 1395-1, "Buckling Behavior of U-Shaped Girders." That research showed experimentally that internal diaphragms designed using the 1239 design rules could be applied to U-shaped girders.

Report 1239-4F showed that there were two types of lateral bracing, relative and discrete, and only tests with discrete bracing were conducted in that study. The typical top flange diagonal systems used in U-shaped girders are classed as relative lateral brace systems. Since there are no tests on girders with top flange diagonal braces, a series of experiments were conducted on the same specimen used in Report 1395-1. In the research reported herein, it is shown that the design rules for top flange diagonal systems must be adjusted to account for their shortening due to girder bending when diagonals are used for lateral stability and/or torsional stiffness of U-shaped girders.

SUMMARY

Top Lateral Bracing of Steel U-shaped Girders

Steel box girder systems are being used more frequently for curved bridges because of their torsional stiffness and aesthetic appearance. These systems typically consist of U-shaped girders placed side-by-side with a composite concrete deck acting as the top flange. A critical design stage for these girders occurs during casting of the bridge deck, when the non-composite steel section must support the entire construction load, including the wet concrete. During this period the top flanges are in compression and are susceptible to lateral-torsional buckling. Lateral bracing, typically in the form of a horizontal truss system, is installed to prevent the flanges from buckling and to increase the torsional stiffness of the girders. There is currently no existing codified design method for the lateral bracing of U-shaped girders.

This research report describes the analytical and experimental tests conducted on steel U-shaped girders with top-flange lateral bracing. The scope of the study focused on X-type top lateral truss systems. A series of pilot tests were also conducted to evaluate the performance of girders with metal deck panels used as a top lateral bracing system. Results include girder buckling loads, buckled shapes, brace forces, and girder torsional stiffnesses. Deficiencies in current code specifications are also discussed.

CHAPTER 1
Introduction

1.1 OVERVIEW

Trapezoidal box girder systems are being used more frequently for curved bridges because of their torsional stiffness and aesthetic appearance. A typical system consists of two U-shaped girders, usually called "tub" girders, placed side-by-side with a concrete slab connecting the top flanges as shown in Figure 1.1.

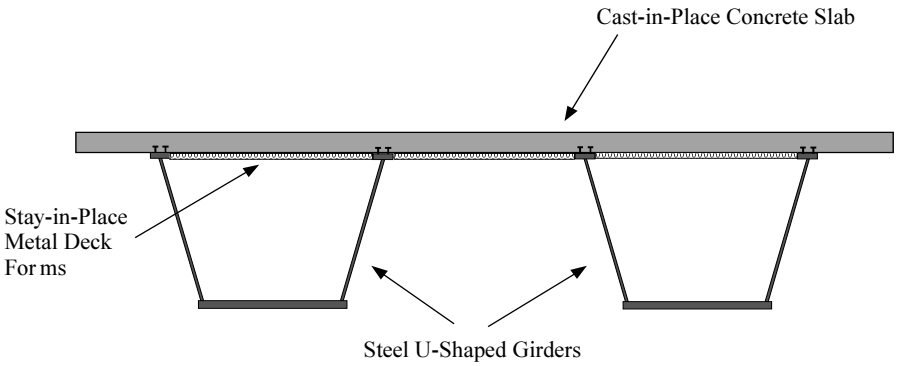

Figure 1.1 Cross Section of a Box Girder Bridge System (Gilchrist, 1997)

Construction of box girder systems occurs in several stages. The steel U-shaped girders are first assembled in a fabrication shop by cutting the webs and flanges from plates and welding them together. The girders are typically fabricated in lengths of 12-35 m (40-120 ft.) so they can easily be transported to the construction site. Figure 1.2 shows a girder section prior to erection. At the job site, the segments are lifted into place and connected using bolted splice plates. After the girders are bolted together, stay-in-place metal deck forms are typically placed across the top and between the two girders. A concrete slab is then poured, usually in longitudinal stages, to control girder stresses and concrete shrinkage. Shear studs, which can be seen in Figure 1.3, allow the girder and deck to act compositely.

Figure 1.2 Cross Section of U-Shaped Girder Segment (Gilchrist, 1997)

Figure 1.3 U-Shaped Girders During Erection (Gilchrist, 1997)

The composite action between the concrete deck and girders creates two closed trapezoidal boxes. The closed section characteristic provides a path for shear flow around the cross section as shown in Figure 1.4, which dramatically increases the torsional rigidity. For comparison, closed cross sections can often have torsional stiffnesses thousands of times greater than similar open sections (Basler and Kollbrunner, 1969).

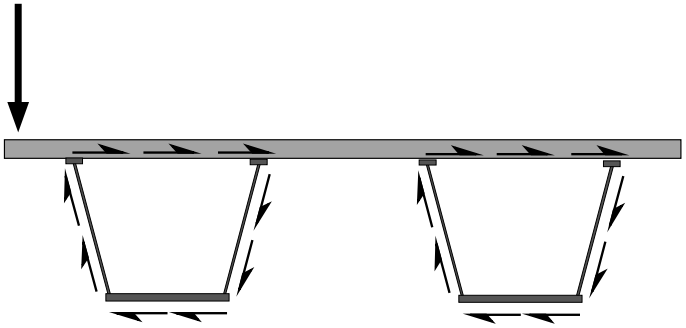

Figure 1.4 Shear Flow Resulting from Eccentric Load (Gilchrist, 1997)

1.2 NEED FOR U-GIRDER BRACING

The steel U-shaped girders generally feature minimal top flanges, especially in the positive bending moment regions where the composite concrete deck can resist the compressive forces. Prior to deck curing, lateral bracing is necessary to prevent the top flanges from buckling under loads encountered during fabrication, transport, erection, and deck placement. The bracing also effectively closes the cross section and enables the curved girders to resist the large torsional moments that occur when construction loads are applied. Once the concrete deck has cured, the bracing is no longer required because the deck provides continuous lateral bracing for the top flanges.

1.3 TOP LATERAL SYSTEMS

Top lateral bracing systems typically consist of a horizontal truss system placed near the top flanges along the entire length of a girder. The truss system can either be a single diagonal, as pictured in Figure 1.3, or an X-brace layout, as shown in Figure 1.5. Connecting the top flanges forms a pseudo-closed cross section that increases the torsional stiffness of a girder significantly. The lateral bracing also resists the differential lateral movement of points along the top flanges that are connected by the bracing (points A and B in Figure 1.5). In addition to horizontal truss systems, it is believed that top lateral systems can consist of metal deck panels attached to the top flanges of a U-girder. Like the truss systems, locations where the deck panels are attached to the top flanges are braced from differential lateral movement.

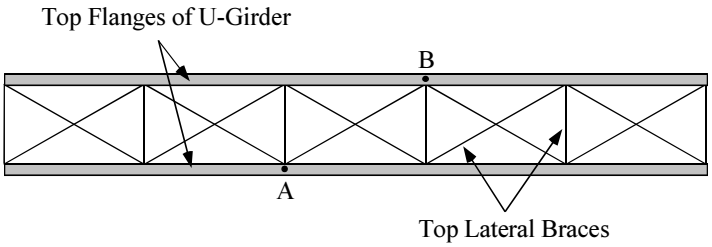

Figure 1.5 Top Lateral X-Brace System

In theory, top lateral systems force the top flanges of a U-girder to buckle between the brace points, which increases the bending capacity of the girder. These systems do not, however, prevent torsional distortion of the cross section. Torsional distortion occurs when torsional forces are applied to noncircular cross sections. Distortion of the cross section can as seen in Figure 1.6 is commonly controlled by internal diaphragms, such as those pictured in Figure 1.2.

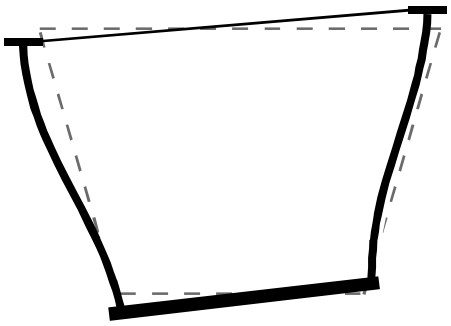

Figure 1.6 Torsional Distortion of Cross Section

1.4 CURRENT DESIGN CODE

The current American Association of State Highway and Transportation Officials (AASHTO) *LRFD Bridge Design Specifications* provides very limited information on the lateral bracing requirements for the top flanges of steel box girders. Section 6.11.5.1 of the specification states:

The individual box section geometry shall be maintained throughout all phases of construction, including placement of the concrete deck. The need for temporary or permanent intermediate interior diaphragms or cross-frames, exterior diaphragms or cross-frames, and top lateral bracing, or other means shall be investigated to ensure that deformations of the box section are adequately controlled during fabrication, erection, and placement of the concrete deck.

To be an effective brace point, a lateral brace must have both adequate strength and stiffness (Winter, 1960). Currently, the AASHTO specifications provide no strength or stiffness requirements for lateral bracing of U-shaped girders. There is also no existing design method for lateral bracing of U-shaped girders.

1.5 OBJECTIVES OF RESEARCH

The work presented herein was part of research project 1395, "Trapezoidal Box Girder Systems," sponsored by the Texas Department of Transportation. The objective of this research project was to develop a reliable design approach for trapezoidal bridge systems.

The aim of this portion of the project was to determine the minimum lateral bracing required to resist construction loads for U-shaped girders. The current specifications provide no means for determining the lateral bracing necessary to resist torsional loads and prevent lateral-torsional buckling of the top flanges. It is important to minimize the bracing placed in U-shaped girders since this bracing is not utilized after the concrete deck of the box girder system has cured. Currently, the material and fabrication costs of the lateral bracing system make up a significant portion of the total box girder costs. For example, the top lateral bracing used in a bridge unit constructed in Houston, Texas, shown in Figure 1.3, increased the weight by nearly 12%. By reducing the amount of bracing currently being used for U-shaped girders and simplifying the connection details, trapezoidal box girders can become a more cost effective bridge system.

The effect of top lateral bracing systems on both the bending and torsional behavior of U-shaped girders was considered in this research. Because the bending and torsional behavioral aspects each represent distinct problems, the results are presented separately.

Chapters 2 through 7 deal with the effect of the top-flange lateral bracing on the bending strength of U-shaped girders. In this portion of the report, an analytical study was first conducted using elastic finite element modeling. Bifurcation loads and buckling modes obtained in the analysis were used to guide the selection of appropriate experimental test cases. Experimental tests were then conducted on scale models of U-shaped girders. The two types of bracing systems used were an X-brace truss system and metal deck panels fixed to the top flanges. Variable parameters included brace stiffness, geometry, initial pretension force, connection detail, and deck panel layout. Experimental test results provided girder buckling loads and buckled shapes to compare with the analytical results. Brace forces, which could not be obtained in the analytical program, were measured to compare with current design provisions. Lastly, the performance of the metal deck bracing system was evaluated through comparison with the truss-type system. Chapters 7 through 10 deal with the effect of top-flange lateral bracing on the torsional stiffness of a U-shaped girder. Specifically, the purpose was to examine the increase in torsional stiffness that a metal deck top lateral bracing system would produce.

Part I: Bending Behavior

CHAPTER 2
Analytical Program

2.1 GENERAL

Part I of this research study will focus on the in-plane bending behavior of U-shaped girders with top lateral bracing systems. In order to identify the critical parameters governing the behavior of these braced girders, an analytical program was undertaken. In this study, a finite element model of an experimental test specimen was created to analyze the effects of variation in the number of brace points and brace stiffness. Results were then used to select appropriate test cases for the experimental program.

2.2 GIRDER MODELING

The buckling behavior of a U-shaped girder can be understood by modeling the girder as two separate "half-girders" connected by a bottom flange. The wide bottom flange adds both torsional and lateral restraint to the half-girders. If either girder twists during buckling, the bottom flange must bend as illustrated in Figure 2.1. Therefore, the bottom flange restraint can be idealized as a torsional brace running continuously along the length of the girder. The stiffness of the continuous brace varies depending on whether the bottom flange bends in single or reverse curvature. Also, if the bottom of the girder is to move laterally, the bottom flange must bend about the weak axis of the girder. However, because the lateral moment of inertia of the bottom flange is so large the lateral restraint can be idealized on the half-girder as a continuous lateral support as shown in Figure 2.2.

The top-flange lateral bracing can be approximately modeled as discrete lateral springs. The stiffness of the lateral springs is based on the stiffness of the brace, the geometry of the brace layout, and whether the bracing is a tension-only or tension-compression system. To obtain the buckling load for a complete U-girder, the buckling load of the half-girder is doubled.

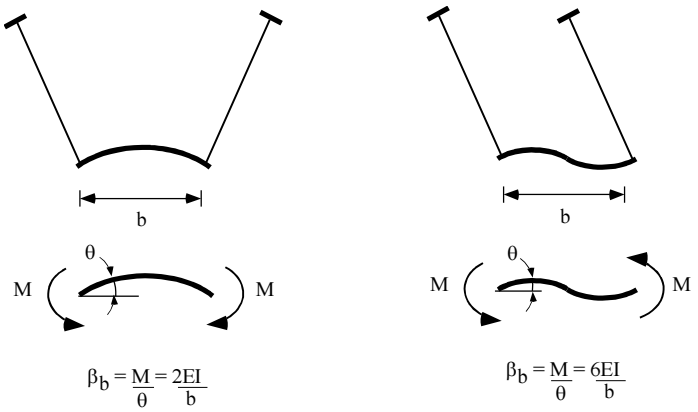

Figure 2.1 Torsional Restraint of Bottom Flange (Gilchrist, 1997)

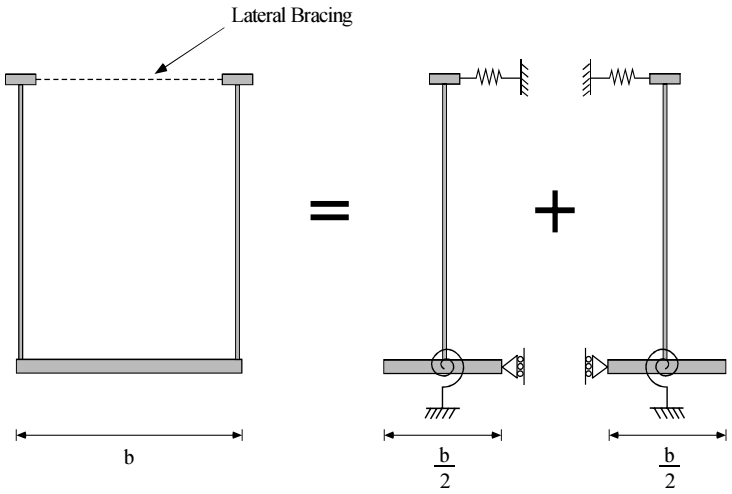

Figure 2.2 Half-Girder Model of a U-Girder with Top-Flange Lateral Bracing

2.3 BUCKLING BEHAVIOR OF U-GIRDERS

2.3.1 Column Analogy for Top-Flange Bracing

The bracing of the top flange of a U-Girder is similar to that of a column. Column bracing provides stability so that the column can support higher loads. The lateral bracing of a U-girder can similarly increase the buckling capacity by forcing the top flanges to buckle between brace points.

A relative brace controls the movement of adjacent stories or points along the length of a column or beam. Winter (1960) developed the dual parameters of strength and stiffness for bracing. In a relative column brace, the brace force is related to the initial column out-of-straightness, Δ_o, and the brace stiffness, β. The relative brace, shown as the spring at the top of the column in Figure 2.3, controls the movement at the top, Δ, relative to the column base. Summing moments about the base yields

$$P\Delta_T = \beta L\left(\Delta_T - \Delta_o\right) \qquad (2.1)$$

where $\Delta_T = \Delta + \Delta_o$. For initially perfectly straight members where $\Delta_o = 0$, the brace force $F_{br} = \beta L$. The brace stiffness necessary to attain the buckling load between braces, P_o, is referred to as the ideal stiffness, β_i. In this case, $\beta_i = P_o/L$.

The relationship between P, β, and Δ_T is plotted in Figure 2.4. If $\beta = \beta_i$, the load can reach P_o only at very large displacement levels. Since $F_{br} = \beta L$, the resulting brace forces are also very high. If the brace stiffness is above ideal, P_o can be reached with much smaller deflections and brace forces. For example, if $\beta = 2\beta_i$, then $\Delta = \Delta_o$ at P_o. As the brace stiffness increases, the brace force decreases.

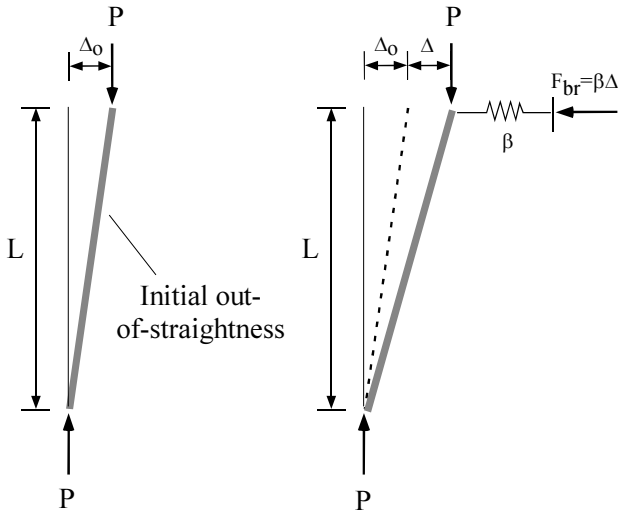

Figure 2.3 Relative Brace

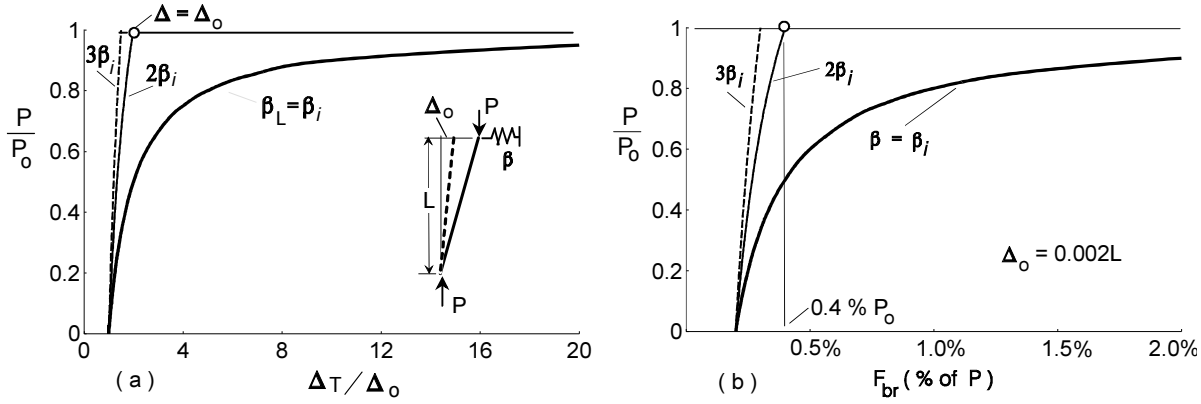

Figure 2.4 Effects of Increasing Brace Stiffness (Yura, 1993)

2.3.2 Description of BASP Computer Program

BASP, short for Buckling Analysis of Stiffened Plates, is a two-dimensional elastic finite element program developed at the University of Texas at Austin (Akay, 1977; Choo, 1987). The program provides eigenvalue buckling modes for stiffened I-shaped beams and T-sections. It considers local and lateral-torsional buckling including cross-section distortion. It will handle many types of restraints including lateral and torsional braces at any node point along the span as well as transverse and longitudinal stiffeners. BASP has been previously used to analyze braced beams. The solutions have been consistent with other finite element programs such as ABAQUS and are consistent with the works of others (Gilchrist, 1997; Yura, 1993).

A BASP model was created based on the half-girder analogy presented in Section 2.2. The model dimensions were based on the test specimen used in the experimental program. It consisted of a girder 12.19 m (40 ft.) in length, with pin supports located 1.83 m (6 ft.) from each end. Load was applied at each end of the girder, creating an 8.53 m (28 ft.) uniform moment region between supports, as shown in Figure 2.5. The cross-sectional dimensions are shown in Figure 2.6.

The boundary conditions for the model included lateral displacement restraints, rotational springs, and lateral springs and are shown in Figure 2.5. The continuous torsional restraint of the bottom flange was modeled as a series of discrete nodal springs. Their stiffnesses were calculated based on the dimensions of the bottom flange and the spacing of the nodes along the length of the girder. Lateral displacement was restrained at the load and support cross sections due to the presence of internal stiffening frames in the U-girder. Top-flange lateral braces were modeled using lateral springs at various locations along the top flange.

Discrete and relative braces are two classifications for lateral beam braces. Relative braces control the relative lateral movement of two points along the length of a member. A truss system installed near the top flanges of a U-shaped girder is an example of a relative brace. Discrete braces, on the other hand, connect a point on the member to an independent point not on the member. Temporary guy cables are an example of a discrete brace. To achieve the same performance, discrete braces require greater stiffnesses than relative braces (Yura, 1993).

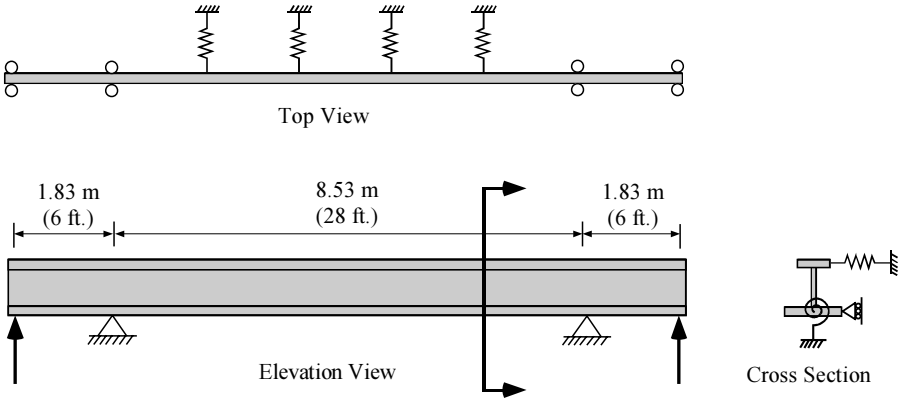

Figure 2.5 Boundary Conditions for BASP Model

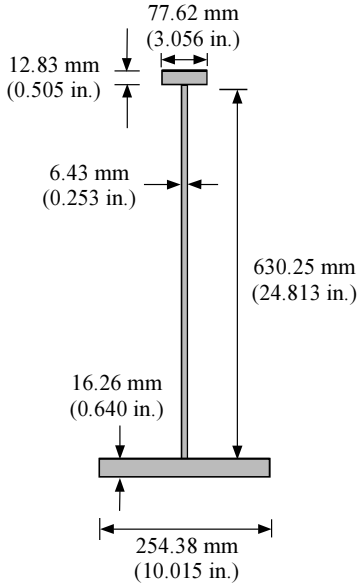

Figure 2.6 Cross-Sectional Dimensions of BASP Model

The top-flange lateral bracing system used in the experimental program was a relative bracing system. Because of the difficulties associated with modeling relative bracing on a single half-girder, discrete lateral springs were used to approximate the true relative bracing. The results, however, were used only for guidance in selecting appropriate experimental test cases.

2.3.3 Effect of Bottom-Flange Torsional Bracing

The wide bottom flange of the U-girder was modeled as a continuous torsional brace attached to the bottom flange of each half-girder. The stiffness of this brace was based on the width and thickness of the bottom flange as well as whether the bottom flange bent in single or reverse curvature during buckling.

Gilchrist (1997) studied the effects of bottom-flange torsional bracing on the buckling behavior of unstiffened half-girders. Figure 2.7 illustrates how increasing the torsional brace stiffness increases the buckling strength of the half-girder non-linearly. The buckling moment, M, is normalized by M_y, the moment necessary to cause yielding of the top flange of the half-girder using simple bending theory. The yield stress was taken to be 345 MPa (50 ksi), the minimum specified yield stress of the flanges of the test specimen used in the experimental program.

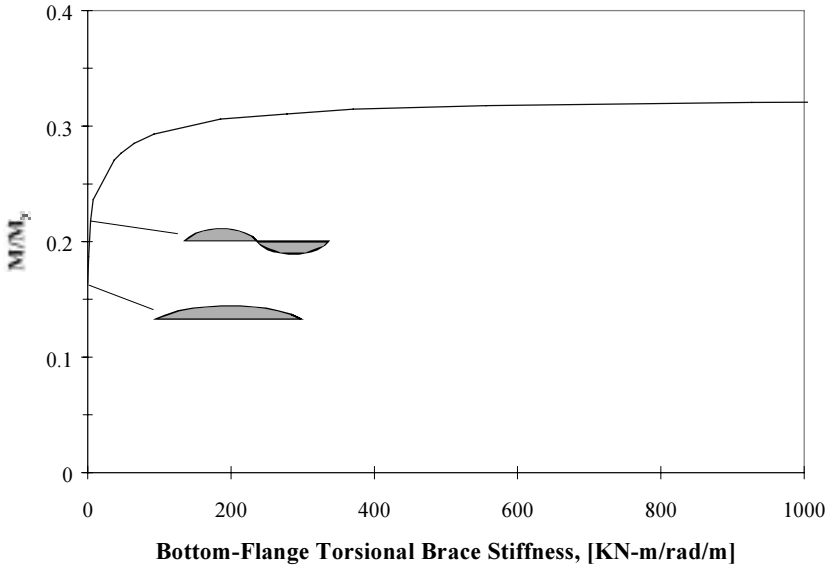

Figure 2.7 Effect of Increasing Bottom-Flange Torsional Brace Stiffness

With no torsional bracing, the half-girder buckled into a single-wave between the supports at M/M_y = 0.16. A torsional brace of only 3.7 KN-m/rad/m (0.83 k-in/rad/in) was required to cause the girder to buckle into two-waves at M/M_y = 0.22. For a U-girder with a 254 mm (20 in.) wide bottom flange bending in single curvature, this corresponded to a bottom flange thickness of only 3.8 mm (0.15 in.). Increasing the brace stiffness beyond 200 KN-m/rad/m (45 k-in/rad/in) provided virtually no increase in buckling capacity. This was due to the effect of cross section, which is illustrated in Figure 2.8. The introduction of torsional bracing by the bottom flange of the U-shaped girder caused the first mode of buckling to be two-waves rather than the expected single-wave. This phenomenon was validated both in this experimental program as well as by Gilchrist (1997).

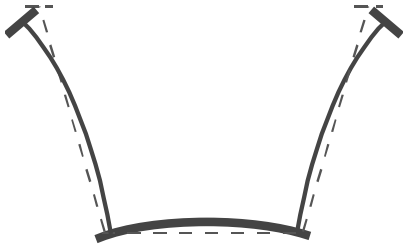

Figure 2.8 Cross-Section Distortion (Gilchrist, 1997)

2.3.4 Effect of Cross-Section Distortion

Yura (1993) determined that even small amounts of web distortion have significant effects on the buckling load of torsionally braced beams. Gilchrist (1997) showed that by reducing web distortion with transverse stiffeners, the buckling capacity of the half-girder model could be increased substantially. Figure 2.9 shows that minimizing cross-section distortion allows higher buckling modes to be attained. By placing eight equally spaced 10 x 0.25 cm web stiffeners along the length of the half-girder, the buckling load reached was nearly twice that of the girder with the unstiffened web. This corresponded to a four-fold increase in buckling strength over the girder with no web stiffeners or bottom-flange torsional bracing. The third and fourth buckling modes were attained at torsional stiffnesses of 185.3 KN-m/rad/m (41.7 kip-in/rad/in) and 926.7 KN-m/rad/m (208.3 kip-in/rad/in), respectively.

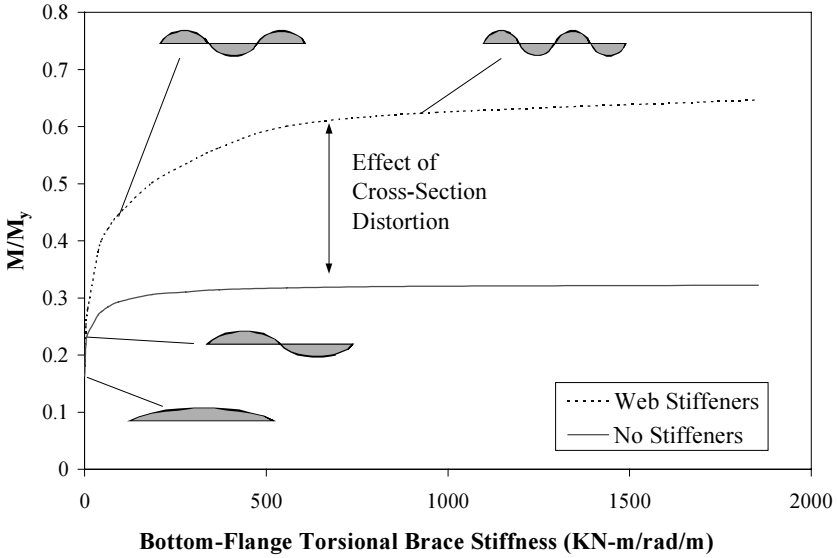

Figure 2.9 Effect of Cross-Section Distortion (Gilchrist, 1997)

2.3.5 Effect of Bottom-Flange Lateral Restraint

As discussed in Section 2.2, the lateral moment of inertia of the bottom flange of a U-girder is so large that it acts like a continuous lateral brace. Yura (1993) has shown that the position of a lateral brace along the beam height has a very significant effect on the buckling load. Lateral braces located on the compression flange are the most effective, while ones placed on the tension flange are almost ineffective. The BASP solution in Figure 2.10 verifies that lateral bracing placed on the bottom tension flange provides virtually no increase in buckling capacity.

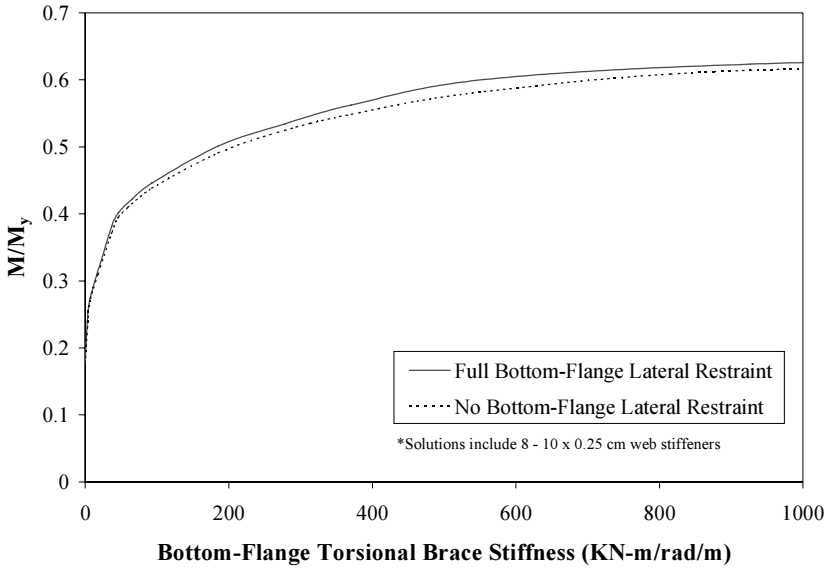

Figure 2.10 Effect of Bottom-Flange Lateral Restraint (Gilchrist, 1997)

2.3.6 Effect of Top-Flange Lateral Bracing

Top-flange lateral bracing systems for U-girders can be approximately modeled as discrete lateral springs placed on the top flange of each half-girder. The stiffness of the lateral brace is dependent upon the axial stiffness of the diagonal bracing members, the geometry or size of the brace panels, and whether the bracing system is tension-only or tension-compression.

The boundary conditions for the half-girder model with top-flange lateral bracing are shown in Figure 2.5. Rotational springs were placed at nodes along the length of the bottom flange. Because top-flange lateral bracing forced both flanges to buckle in the same direction, the torsional stiffness calculated was based on the bottom flange bending in reverse curvature ($6EI/b$). The value used for the torsional springs was 843 KN-m/rad/m (190 kip-in/rad/in). In addition, lateral restraints were placed along the bottom flange to prevent any lateral movement of the bottom flange. Again, this was done because the out-of-plane bending stiffness of the wide bottom flange was extremely high. Lateral springs were placed along the top flange of the girder to model the top-flange lateral bracing. By varying their stiffness and spacing, the effect of the top-flange lateral bracing on the buckling behavior was isolated.

Like bottom-flange torsional bracing, top-flange lateral bracing increased the buckling capacity of the girder non-linearly. The amount of increase depended on both the brace stiffness and geometry. For a given number of brace panels, increasing the brace stiffness increased the girder's capacity until buckling between brace points was achieved, as illustrated in Figure 2.11. Unlike bottom-flange torsional bracing, top-flange lateral bracing was not affected by cross-section distortion.

The torsional restraint provided by the bottom flange caused the first buckling mode to be in two-waves at $M/M_y = 0.32$. As brace stiffness increased, the buckled shape entered intermediate shapes until the ideal stiffness caused buckling between brace points. For the case with five brace panels, the top-flange lateral bracing increased the girder's capacity by 100% to $M/M_y = 0.64$. For the ten brace panel test case, buckling between brace points corresponded to a buckling load greater than the yield load. The yield load for the girder corresponded to a 210% increase in the buckling load.

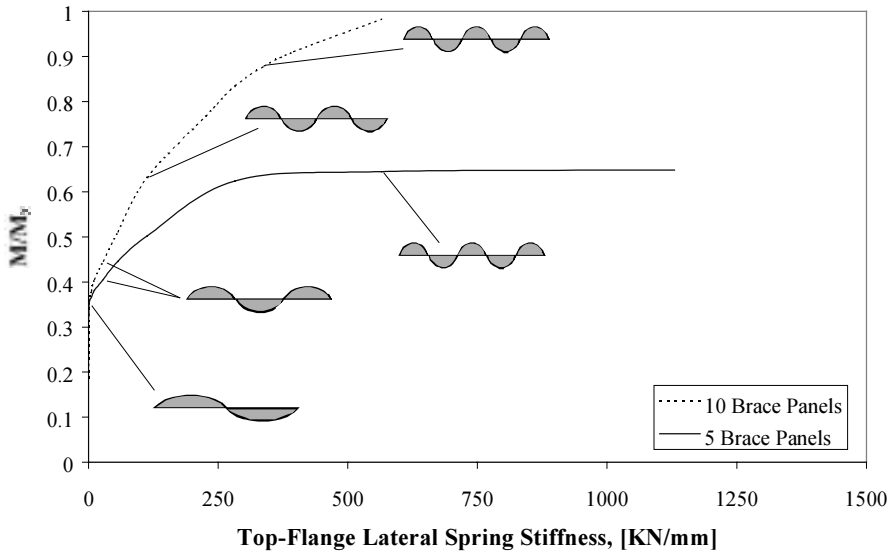

Figure 2.11 Effect of Top-Flange Lateral Brace Stiffness

2.3.7 Effect of Top-Flange Torsional Restraint

The modeling of the top-flange lateral braces as discrete lateral springs was only an idealization of true experimental test conditions. Unlike the analytical model, the actual attachment of the bracing to the top flanges would introduce some level of torsional restraint. The effect of torsional restraint about the strong axis of the top flanges is shown in Figure 2.12. If the top flanges are fully restrained from rotation at each brace point node, the increase in capacity can be substantial. However, at 84 KN-m/rad/node (740 kip-in/rad/node) the girder's response is primarily governed by the top-flange lateral spring stiffness. For comparison, the largest restraint provided by any of the test cases in the experimental program was conservatively estimated to be 8.5 KN-m/rad/node (75 kip-in/rad/node) and was obtained by assuming reverse curvature bending (6*EI/L*) of the bracing. Therefore, torsional restraint introduced by the lateral bracing was not considered to dominate the buckling behavior of the girder.

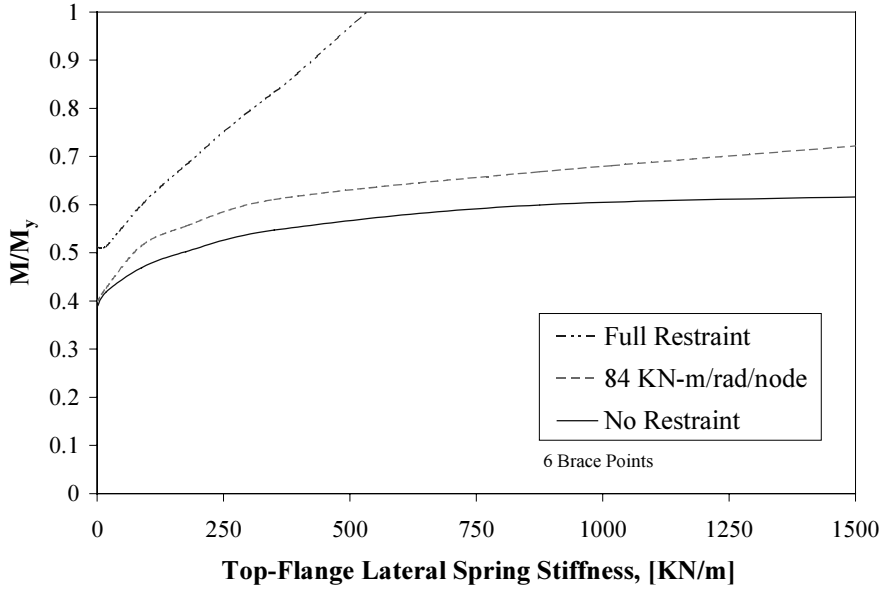

Figure 2.12 Effect of Top-Flange Torsional Restraint

CHAPTER 3
Experimental Program

3.1 GENERAL

This portion of the experimental program consisted of a series of laboratory experiments designed to study the buckling behavior of U-shaped girders with top-flange lateral bracing. Twenty-one tests were conducted on a rectangular girder and four on a trapezoidal girder. The rectangular girder tests used an X-brace horizontal truss system as seen in Figure 3.1. The variable parameters in these tests included brace geometry, stiffness, initial pretension force, and flange connection detail. The trapezoidal girder tests, pictured in Figure 3.2, used metal deck panels attached to the top flanges as the bracing system.

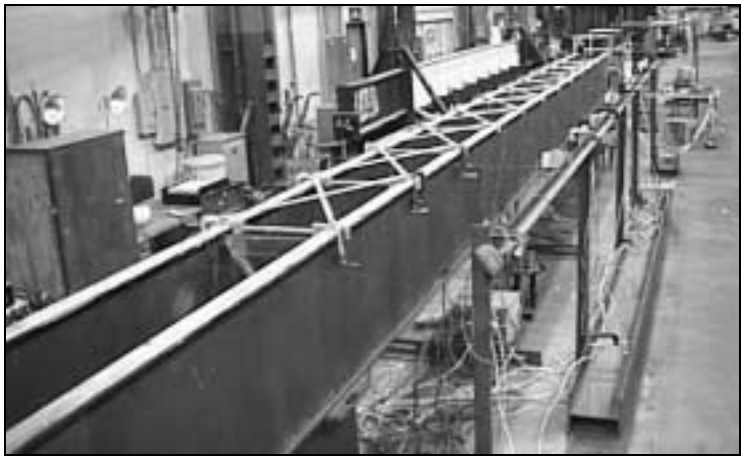

Figure 3.1 Overall Test Setup for Rectangular Girder Tests

Figure 3.2 Overall Test Setup for Trapezoidal Girder Tests

The test girder was 12.19 m (40 ft.) long and simply supported over an 8.53 m (28 ft.) span with 1.83 m (6 ft.) overhangs at each end as shown in Figure 3.3. Loading was applied at the ends of the girder to produce uniform moment between the supports.

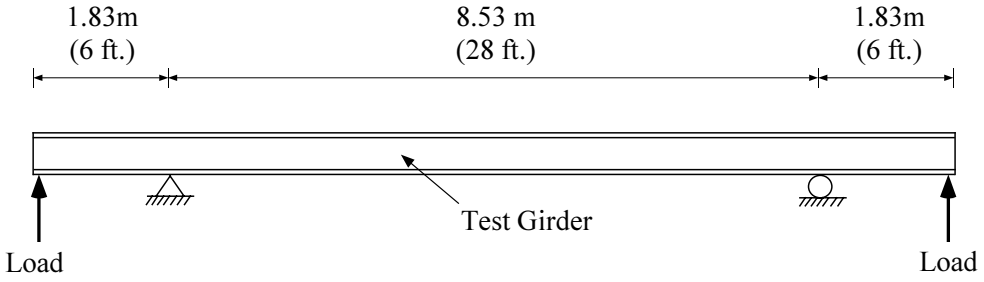

Figure 3.3 Profile of Test Setup (Gilchrist, 1997)

3.2 TEST SETUP

3.2.1 Test Specimens

Both the rectangular and trapezoidal girders were fabricated using steel with a specified minimum yield stress of 345 MPa (50 ksi) for the top and bottom flanges and 250 MPa (36 ksi) for the webs. Tensile tests were conducted on specimens taken from the rectangular girder in accordance with ASTM standards. Average static values were obtained and are summarized in Table 3.1. Additional test information may be found in Appendix A.1. The cross-sectional dimensions and properties of the girders are shown in Figure 3.4.

Table 3.1 Tensile Test Data

	F_y MPa (ksi)	F_u MPa (ksi)
Top Flange	320 (46)	443 (64)
Web	300 (44)	422 (61)
Bottom Flange	315 (46)	444 (64)

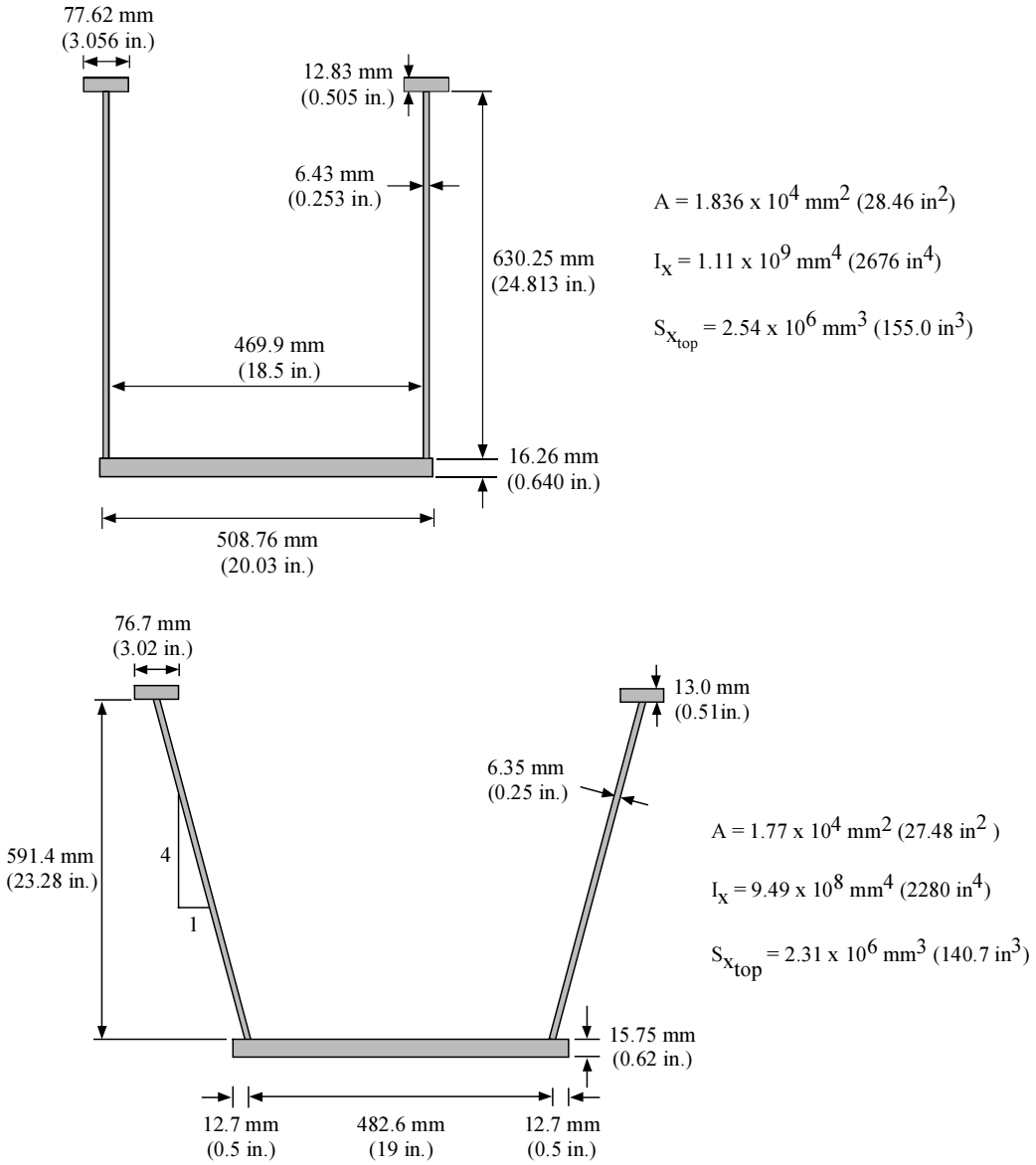

Figure 3.4 Cross-Sectional Properties of Test Girders

3.2.2 Loading and Support System

The girder supports consisted of two 61 cm (24 in.) long W920 x 223 (W36 x 150) beams oriented perpendicular to the long axis of the U-girder as shown in Figure 3.5. The supports very closely approximated simple support conditions because the webs of the support beams were unstiffened and very slender. If the support beams were conservatively considered fully fixed to the test floor, the rotational stiffness of the support ($4EI/L$) would provide a restraining moment of just 1.3% of the yield moment. Finite element analysis has also shown support restraint to have virtually no influence on the buckling capacity and behavior of the girder (Gilchrist, 1997).

Load was applied to the test specimen 11.43cm (4.5in.) from the ends using two hydraulic rams as seen in Figure 3.6. The rams were connected in parallel to a single pump, ensuring equal force was applied to the girder ends at all times. Roller/bearing assemblies were placed in between the ram and girder so when the girder ends deflected, the line-of-action of the ram force remained vertical.

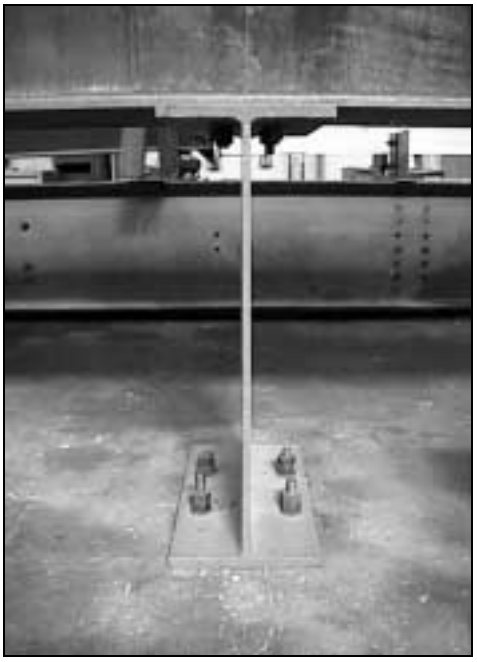

Figure 3.5 Support Beam

Figure 3.6 Load Ram, Load Cell, and Roller/Bearing Assembly

Four internal stiffening cross frames were located at each of the support and load points. These internal braces eliminated web crippling and local buckling failure modes at the concentrated load points.

Two external deflection stops were used to limit lateral deflection of the top flanges. These deflection stops, located at midspan and the south quarter point, were frames built around the test girder as shown in Figures 3.7 through 3.11. Outward lateral deflections were controlled by the sides of the frame and inward lateral deflections were controlled by two threaded rods fixed through the frame top.

Figure 3.7 X-Brace at Support Location

Figure 3.8 K-Brace at Location of Concentrated Load

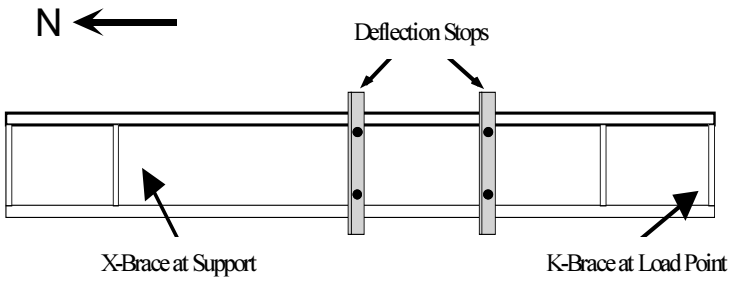

Figure 3.9 Location of Deflection Stops (Plan View of Girder)

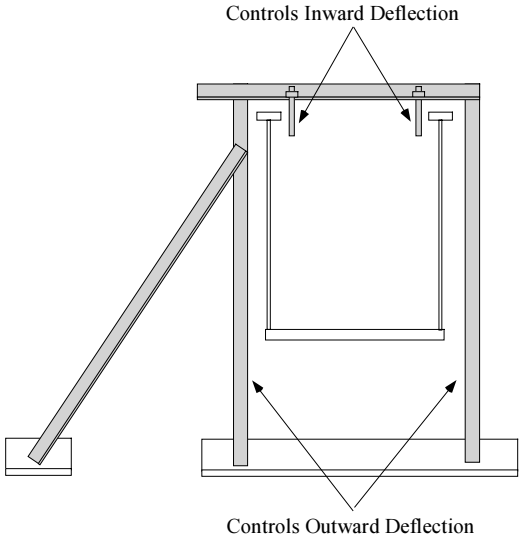

Figure 3.10 Deflection Control of Stop Frames

Figure 3.11 Lateral Deflection Stop Frames

3.2.3 Instrumentation

Lateral top flange deflections, midspan vertical deflection, ram load, hydraulic pressure, and brace force strain data were collected using a computerized data acquisition system. Lateral deflections of both top flanges were also monitored using transits. The midspan vertical deflection was measured using an electronic linear displacement potentiometer that had an accuracy of 0.0254 mm (0.001 in.). This measurement was taken to verify that the girder remained in the elastic range during testing.

The lateral deflections of the east top flange were measured using electronic linear displacement string potentiometers as shown in Figure 3.12. The string pots were mounted at flange level more than 0.9 m (3 ft.) away to minimize the effect of vertical displacement of the girder during loading. The gages had an accuracy of 0.0254 mm (0.001 in.). The points along the top flange that were measured varied with the each particular test case.

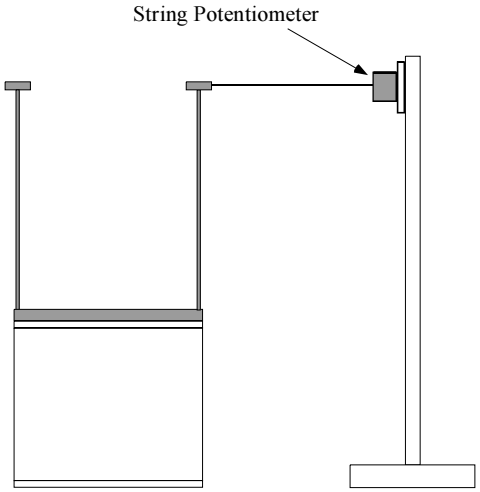

Figure 3.12 Top-Flange Lateral Displacement Gages

The lateral deflections of both flanges were also measured using transits located at one end of the specimen as shown in Figure 3.13. The transits were sighted parallel to the two supports. The lateral deflection readings were used to produce deflected shapes of the top flanges. The accuracy of these readings was 1.0 mm (0.04 in.).

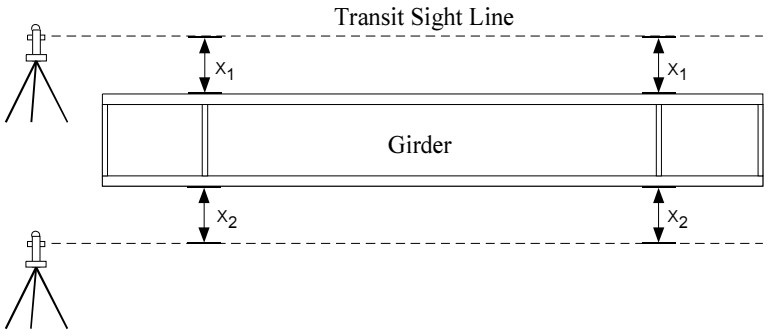

Figure 3.13 Transit Locations (Plan View)

Loads were obtained from load cells placed in series with each of the rams and the girder as shown earlier in Figure 3.6. The load cells had a capacity of 444.8 KN (100 kips) and a maximum absolute error of 0.63%. Hydraulic ram pressure was monitored using a pressure transducer as a secondary measure of the applied load.

3.3 X-BRACE SYSTEM

The top-flange lateral bracing system used in the rectangular girder tests was a tension-only X-brace system placed within the constant moment region between the supports. Figure 3.14 shows a test case with five brace panels. The end brace points were located 76.2 mm (3 in.) to the interior of the support cross frames. All other brace points were evenly spaced to produce equal sized brace panels.

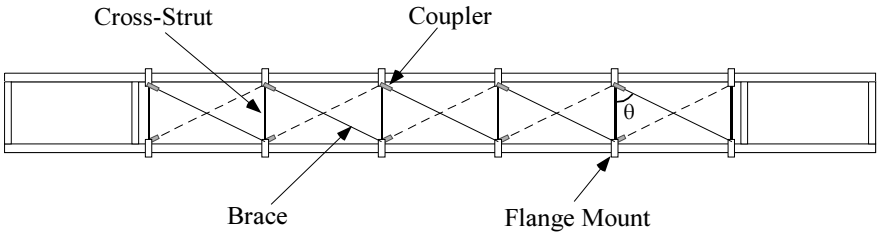

Figure 3.14 X- Brace System

3.3.1 Braces

The braces, with the exception of the final test case, were fabricated using T6061-T6 and T6063-T1 aluminum flat bars with moduli of elasticity of 69,000 MPa (10,000 ksi) and specified yield stresses of 260 MPa (38 ksi) and 150 MPa (22 ksi), respectively. Aluminum was the material of choice because of its high strength and low relative stiffness when compared to steel. Depending on the test case, the sizes varied from 3.175 mm x 12.7 mm (1/8 in. x 1/2 in.) to 6.35 mm x 25.4 mm (1/4 in. x 1 in.) wide. Cross-strut braces that connected directly opposite points on the two flanges were made from 12.7 mm x 19.05 mm (1/2 in. x ¾ in.) aluminum bars. All diagonal braces and cross-struts were T6061-T6 grade aluminum except the 3.175 mm x 12.7 mm (1/8 in. x 1/2 in.) bars, which were a T6063-T1 alloy.

The final test case used 3.175 mm x 12.7 mm (1/8 in. x 1/2 in.) A36 steel flat bars. Steel braces were used in this test case because the connection detail required welding the braces directly to the top flanges of the girder.

3.3.2 Connection to Flange

Three mounting schemes were used to attach the braces to the top flanges of the girder. The original flange mount connection was designed so the attachment to the flanges was not permanent, allowing for easy variation of the brace geometry or number of brace points. Subsequent tests modified the original design to isolate the effects of particular test parameters.

The original connection design, pictured in Figure 3.15, attached the braces and couplers to the flanges of the girders using removable flange mounts. The mounts, which were machined from T6061-T6 aluminum, gripped the flanges with two opposing set screws, as shown in Figure 3.16. This design connected the diagonal braces and cross-struts at the same pin location, but had a 76.2 mm (3 in.) eccentricity from the flange centroid.

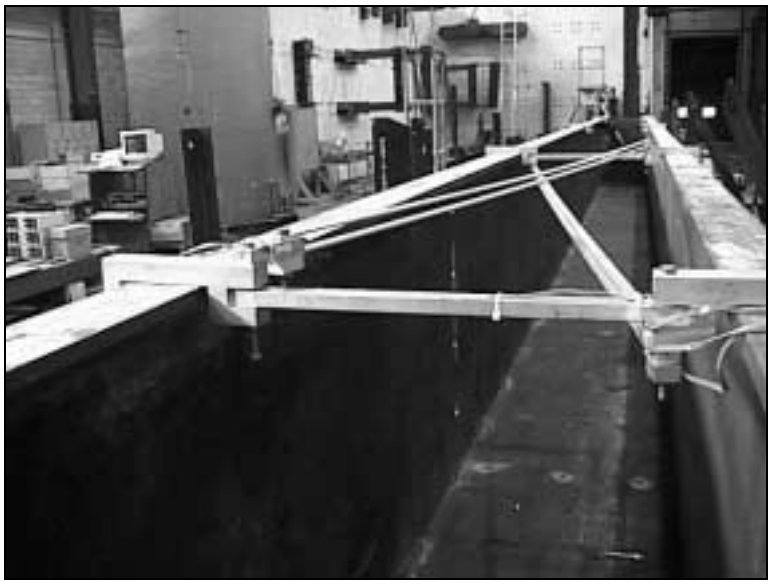

Figure 3.15 Original Brace, Coupler, and Flange Mount Connection

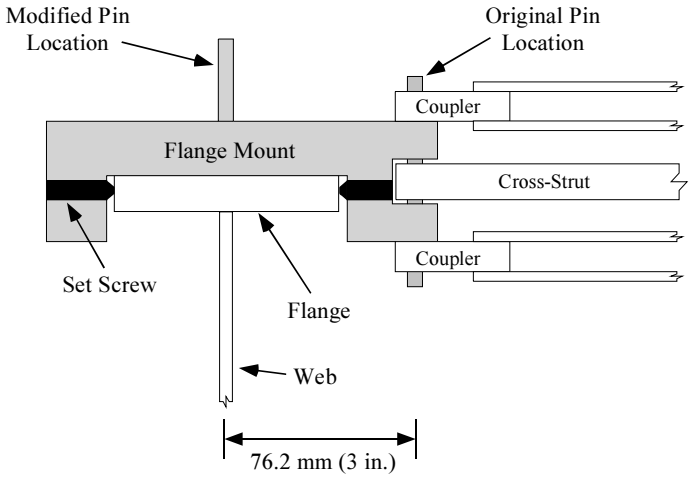

Figure 3.16 Original and Modified Flange Mount Connection (Profile)

The modified connection detail, also shown in Figure 3.16, moved the pin location from its eccentric position to the center of the flange. The purpose of this detail change was to investigate the effect of out-of-plane flange rotations on the brace behavior. The final connection detail, shown in Figure 3.17, involved directly welding the braces to flange of the girder. The flange mounts were still used to connect the cross-struts. The purpose of this detail was to investigate the effect of connection stiffness on the brace behavior.

Figure 3.17 Welded Brace Connection Detail

3.3.3 Brace Force Measurement

Strain gages were used to obtain forces in all the brace members. Gages were placed directly on the cross-strut members and on the diagonal brace members with the modified and welded connections. For diagonals attached with the original flange mount connection, brace forces were acquired by placing a coupler device that was strain gaged in series with the braces as shown in Figure 3.18.

The coupler was designed as a bolted splice connector. One end was bolted to the flange mount and the other was bolted to two diagonal braces for symmetry. The vertical pin shown in Figure 3.18 connected the braces to the coupler. This pin pressed against a horizontal screw in the coupler. Tightening this screw removed any slack or introduced pretensioning in the braces prior to girder loading. As force developed in the brace, the vertical pin was free to pivot as illustrated in Figure 3.19. This assured equal force in each brace. The design also allowed for only tensile force transfer because any compressive movement would cause the vertical pin to slide within the coupler.

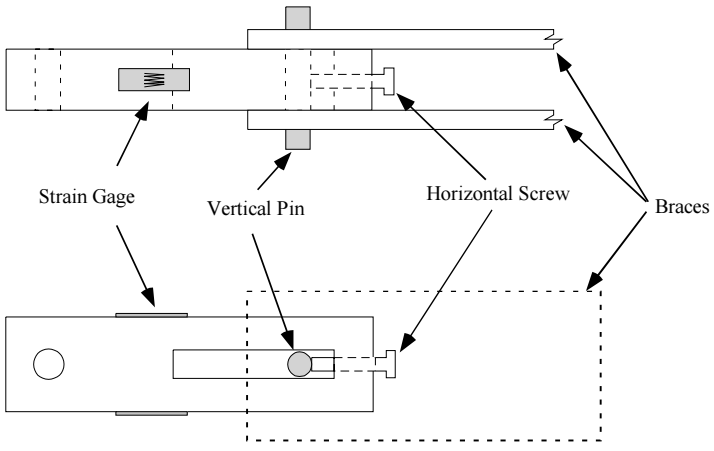

Figure 3.18 Coupler-Brace Connection

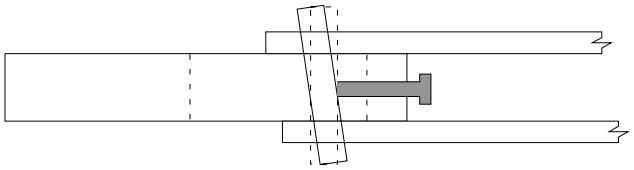

Figure 3.19 Rotational Freedom of Coupler Pin Allows Force Redistribution

3.3.4 Coupler Calibration

To obtain diagonal brace forces, two strain gages were placed on the opposite sides of each coupler, as shown in Figure 3.18. If the cross section of the couplers were uniform, the brace force would easily be obtained by:

$$F_{brace} = E \cdot A \cdot \varepsilon \tag{3.1}$$

where F_{brace} is the brace force, E is the modulus of elasticity, A is the cross-sectional area of the coupler, and ε is the average strain from the gages. However, because the cross sections were not uniform, Equation (3.1) did not produce the correct brace force. Therefore, calibration of the couplers was necessary.

The couplers were calibrated in a universal testing machine to determine the force associated with a given strain gage output. A typical calibration plot is shown in Figure 3.20. A linear regression analysis was used to calculate the calibration factor for each coupler. This calibration factor was used in place of the product of E and A. Both the loading and unloading data were used in the regression analysis. The average calibration factor was 140% greater than the product of E and A. A summary of the calibration factors for all the couplers is listed in Appendix A.2.

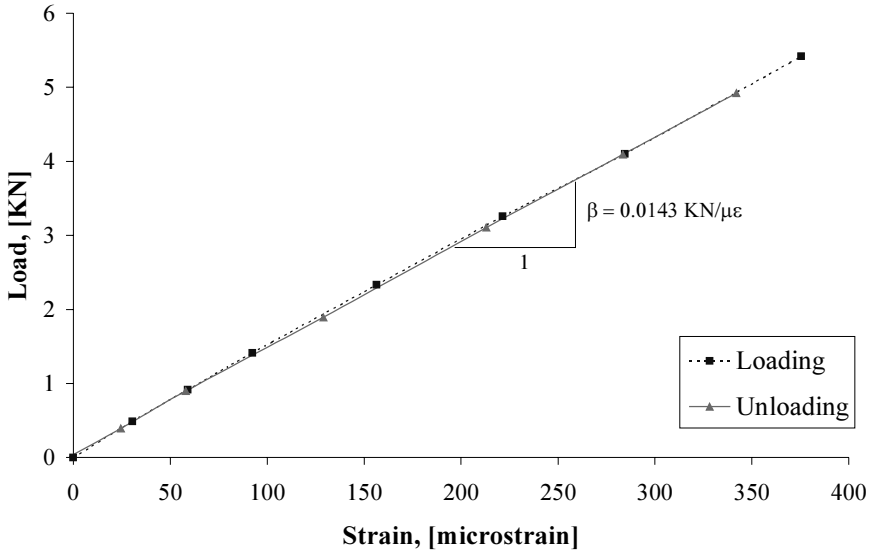

Figure 3.20 Typical Strain Gage Calibration Curve

Since the couplers were connected in series with the diagonal bracing, the stiffness of the couplers affected the overall stiffness of the diagonal bracing system. The stiffness of the couplers was obtained by using the force-displacement measurements from the universal testing machine tests. A typical force

versus displacement plot is shown in Figure 3.21. The stiffness at lower load levels was markedly different than at higher load levels. Because the brace forces in all of the experimental test cases that used the couplers did not exceed 1.6 KN (350 lbs.), the calculation of stiffness was based on load levels less than this value. The data points used in the regression analyses for the loading and unloading stages are indicated by the bold data points in Figure 3.21. The two stiffness values obtained were then averaged to produce the coupler's stiffness. The average stiffness obtained from the various calibration tests was found to be 4.4 KN/mm (25 kips/in).

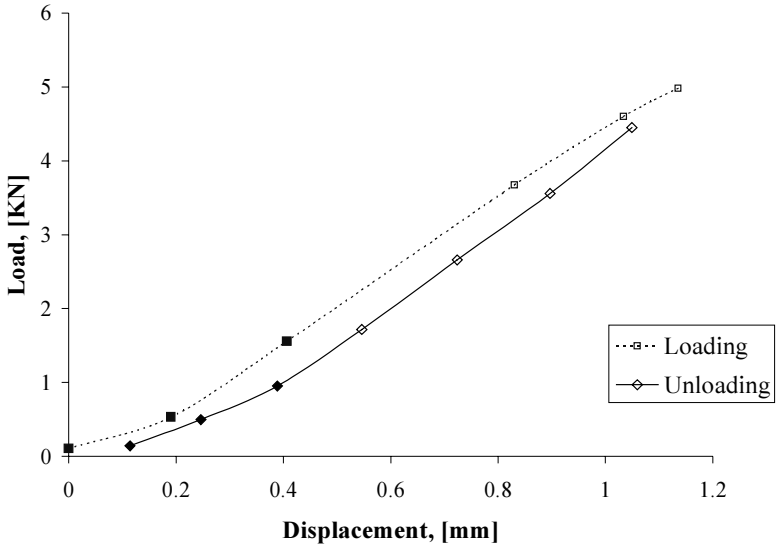

Figure 3.21 Typical Coupler Force vs. Displacement Response

3.4 METAL DECK BRACING SYSTEM

The type of metal decking used for the bracing system was a Vulcraft 2VLI20 form deck with a 2 in. rib height. The metal deck panels were oriented with their ribs perpendicular to the length of the girder and were attached to the inside lips of the top flanges using Hilti ENPH2-21-L15 powder actuated fasteners. The fasteners were approximately 5 mm (0.2 in.) in diameter and had a specified static shear capacity of 20 kN (4.5 kips). Eight fasteners, one in each of the four troughs that contacted the top flanges, were used to attach each panel.

3.5 TEST VARIABLES

There were several variable parameters that were considered in the scope of the X-brace tests. These parameters were brace geometry, brace stiffness, initial brace pretension force, and connection detail. For the metal deck bracing tests, only the number and distribution of deck panels was varied.

3.5.1 Brace Geometry

The brace geometry was based on the number of brace panels located between the supports. The brace angle, θ, was the angle between the diagonal brace and perpendicular cross-struts (see Figure 3.14). Three brace geometry cases were examined: four, five and ten brace panels.

3.5.2 Brace Stiffness

The effective lateral brace stiffness was dependent on both the brace geometry and the axial stiffness of the braces used. The axial stiffness, β_{axial}, of a tension member was:

$$\beta_{axial} = \frac{EA}{L} \tag{3.2}$$

where E was the modulus of elasticity, A was the total cross-sectional area of the all the bars in a diagonal, and L was the length of the brace. When the coupler was placed in series with the diagonal braces, the stiffness of the brace system was equivalent to the stiffness of two springs in series. The cosine function was necessary to convert the diagonal brace to an equivalent brace perpendicular to the flanges. The equivalent lateral stiffness of a diagonal brace was then:

$$\beta = \left(\frac{\beta_{axial}\beta_{coupler}}{\beta_{axial} + \beta_{coupler}} \right) \cos^2 \theta \tag{3.3}$$

3.5.3 Brace Pretension Force

The horizontal screw on the couplers allowed the initial tension in the diagonal braces to be selected. In most of the test cases, the horizontal screw was hand tightened to remove any slack in the braces after installation. In a few cases, the coupler screw was tightened an additional amount before any load was applied to the girder to create a pretension force in the braces.

3.5.4 Connection Detail

The three connection details described in Section 3.3.2 were used to investigate their effect on the bracing system and girder's buckling behavior. The modified detail with the pin located at the center of the flange investigated the effect of flange rotations on the effectiveness of the diagonal braces while the welded connection detail investigated the effect of the previous details on the brace stiffness.

A top-flange lateral bracing system attempts to control the relative movements of adjacent brace points. In a tension-only system, the braces are effective only when the end points where they are attached move apart. Figure 3.22 shows how the relative lateral translation of adjacent brace points along the top flange cause the diagonal lengths to change.

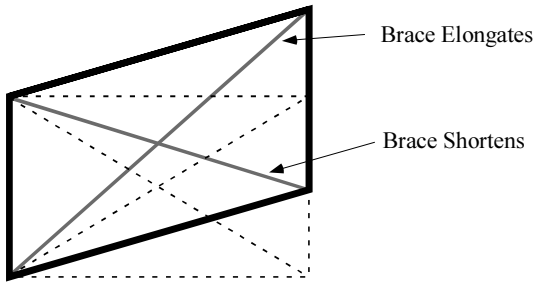

Figure 3.22 Brace Length Change Due to Flange Lateral Translation

The original location of the pin connection point between the diagonal braces, cross-struts, and flange mounts was 76.2 mm (3 in.) to the interior of the center of the top flange. The rotation of the flanges associated with buckling might have contributed to the relative movement of the brace ends due to the mount eccentricity and is illustrated in Figure 3.23. In order to investigate the contribution of this rotational effect, the pin location was moved to the center of the flange in later tests (see Figure 3.16). The eccentricity of the brace-mount connection also introduced torsional restraint to the top flanges. As discussed in Section 2.3.7, torsional restraint of the top flanges had a negligible effect on the buckling behavior of the girder.

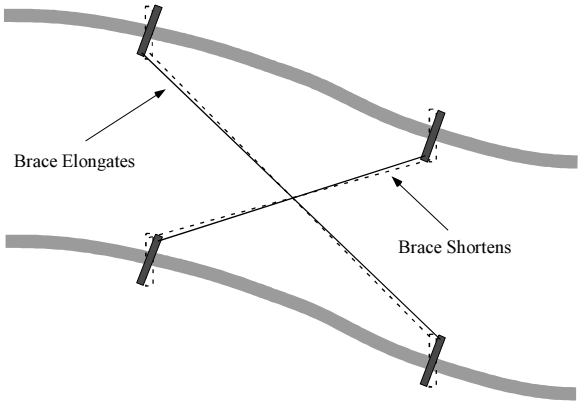

Figure 3.23 Brace Length Change Due to Flange Rotation

During some of the test runs, the forces in the diagonal braces caused the flange mounts to rotate about their long axis. This slight movement may have decreased the stiffness of the diagonal bracing system to a degree where they became inadequate. In order to verify this, a test case was conducted in which the braces were welded directly to the flanges. This connection detail ensured no loss of stiffness from movement at the connection mount and provided a high level of confidence that the theoretical brace stiffness was equal to the experimental brace stiffness.

3.6 TEST CASES

A series of twenty-one tests were conducted on the rectangular girder and four on the trapezoidal girder. The rectangular girder test cases were initially chosen based on the results from BASP analysis and are summarized in Table 3.2. As testing progressed and results were obtained, the test cases were modified. Some variables thought to have an influence on the results did not. Cases were then developed to isolate the critical parameters governing the girder's response. The four trapezoidal test cases are shown in Figure 3.24.

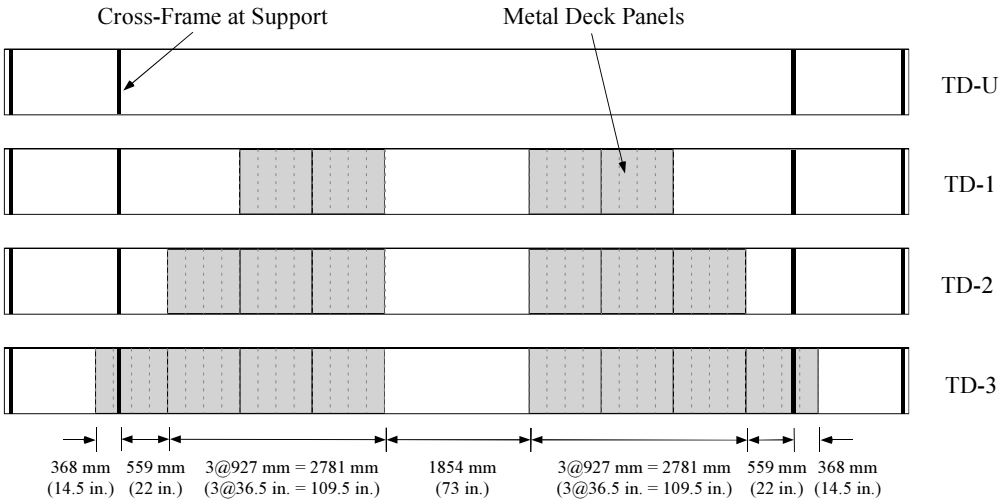

Figure 3.24 Trapezoidal Girder Test Cases

Table 3.2 Rectangular Girder Test Cases

Test Case	Brace Angle, θ	Brace Stiffness		Couplers	Pin Location	Pretension	Comments
	Degrees	KN/mm	x Ideal				
RU-1	-	-	-	-	-	-	
RU-2	-	-	-	-	-	-	After flange yielding in R4-4
R4-1	81.4	0.11	0.4	Yes	Offset	-	
R4-2	81.4	0.11	0.4	Yes	Offset	Yes	
R4-3	81.4	0.11	0.4	Yes	Offset	Yes	
R4-4	-	-	-	-	-	-	Only cross struts
R4-5	81.4	0.33	1.2	Yes	Offset	-	
R5-1	-	-	-	-	-	-	Only cross struts
R5-2	79.3	0.75	0.7	Yes	Offset	-	
R5-3	79.3	0.75	0.7	Yes	Offset	Yes	
R5-4	79.3	1.28	1.2	Yes	Offset	-	
R5-5	74.3	2.09	2.0	No	Center	-	
R5-6	74.3	2.09	2.0	No	Center	-	
R5-7	74.3	1.31	1.2	Yes	Center	-	
R5-8	74.3	0.42	0.4	Yes	Center	-	
R10-1	60.7	5.53	5.3	No	Center	-	
R10-2	60.7	5.53	5.3	No	Center	-	
R10-3	60.7	5.53	5.3	No	Center	-	
R10-4	60.7	5.53	5.3	No	Center	-	
R10-5	60.7	5.53	5.3	No	Center	-	
R10-W	60.7	4.36	4.0	No	-	-	Welded connection

For the rectangular girder tests, the test case identifier designates the number of brace panels between the supports as well as the test run number. For example, test RU-2 refers to the second test run for the unbraced rectangular girder while R5-3 refers to the third test conducted using five brace panels. The brace angle, θ, is the angle between the diagonal brace and perpendicular cross strut, as shown earlier in Figure 3.14. The ideal brace stiffness was the value obtained from BASP analysis that caused buckling between brace points and serves as a reference value.

Of the twenty-one tests conducted on the rectangular girder, eighteen were intended to be confined to the elastic range. The first test case, RU-1, determined the experimental unbraced buckling capacity of the girder. During test R4-4, some yielding occurred in the top flanges, so a second unbraced case was conducted to determine if the buckling capacity had been affected. Tests R10-4 through R10-W were conducted to determine the ultimate strength of the girder. Near the final stages of loading test R10-4, a brace mount slipped from its attachment to the flange. Therefore, an additional test, R10-5, was conducted. Test R10-W employed the welded connection detail. This test failed the girder.

The four tests conducted on the trapezoidal girder were selected to investigate the effectiveness of the metal decking as a bracing system and are shown in Figure 3.24. The initial placement of deck panels attempted to create three similar unbraced lengths within the span of the girder. Before the first deck

panels were attached, an unbraced test case, TD-U, was conducted. All metal deck tests were confined to the elastic range.

3.7 TEST PROCEDURE

Load was applied to the girders in deflection-controlled incremental stages. Each load increment was selected by monitoring the point of maximum lateral deflection of the top flange. At each increment, a computerized data acquisition system was used to record the instrumentation data. This included load cell, pressure transducer, strain gage, and displacement potentiometer data. Periodically, the deflected shapes of the top flanges were recorded using the two transits as described in Section 3.2.3.

For the elastic tests, loading continued until the stresses in the top flanges were close to yield. This was achieved by monitoring both the applied load and the maximum lateral deflection. The first-order compressive stress was calculated using the applied moment and girder section modulus. The maximum second-order stress was based on the point of maximum lateral deflection. By keeping the sum of the first and second order stresses below yield, the test was confined to the elastic range. Whitewash applied to the top flanges provided a visible method for detection of yielding and was monitored periodically during the tests.

CHAPTER 4
Test Results

4.1 DETERMINATION OF BUCKLING LOADS

The U-girders used in the experimental program were designed to buckle elastically, which means the top flanges of the girder would buckle at loads less than the yield moment, M_y. This allowed multiple test cases to be run on the same girder without causing any permanent deformation. The top flanges, however, were not perfectly straight and had initial imperfections. Load applied to the girder would cause lateral deflection of the top flanges. The additional *P-Δ* moments added to the in-plane bending stresses could lead to yielding of the flanges at load levels less than the buckling load. In order to keep the girder in the elastic range and still obtain the girder buckling loads, an extrapolative load-deflection plotting technique was used.

4.1.1 Southwell Method

Southwell (1932) developed a method to predict the buckling load of initially imperfect columns without having to test the column to failure. By plotting the results of a column test in a certain manner, it would be possible to determine that a column's buckling load was, for example, 100 KN (22.5 kips) even though the maximum load reached during the test was 85 KN (19.1 kips).

The typical behavior of a column in the form of load versus mid-height deflection is shown in Figure 4.1. Perfect columns with no initial out-of-straightness exhibit no lateral deflection at load levels less than the Euler buckling load. For columns with small initial imperfections there is some lateral deflection that occurs before the Euler load is attained. The *P-Δ* moments in columns with large initial imperfections will cause yielding before the elastic buckling load can be reached.

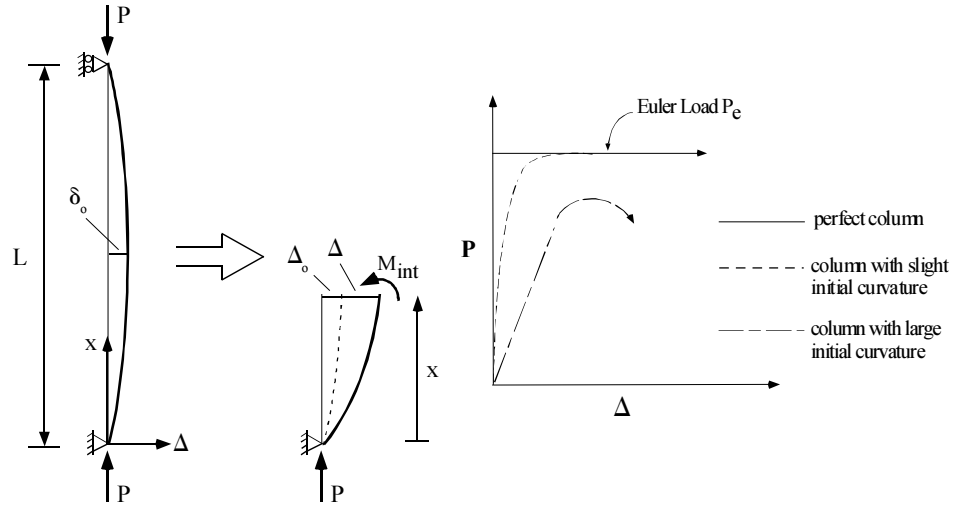

Figure 4.1 Buckling of Imperfect Columns

Southwell assumed the initial shape of the column to be a half-sine wave with an initial imperfection at mid-height equal to δ_o. The equation for the initial shape is characterized by

$$\Delta_0(x) = \delta_o \sin\left(\frac{x\pi}{L}\right) \tag{4.1}$$

The load-deflection relationship based on this initial shape can then be approximated (Timoshenko, 1961) as

$$\Delta_{Total} = \Delta_0 + \Delta = \left(\frac{1}{1 - P/P_e}\right) \cdot \Delta_0 \tag{4.2}$$

where Δ_{Total} is the total lateral deflection, Δ the lateral deflection from the initial shape, P is the axial load in the column, and P_e is the Euler buckling load. Solving in terms of Δ yields

$$\Delta = \frac{P}{P_e}\left(\frac{\Delta_o}{1 - P/P_e}\right) \tag{4.3}$$

and rearranging further gives

$$\frac{\Delta}{P} = \frac{1}{P_e}\Delta + \frac{\Delta_o}{P_e} \tag{4.4}$$

By considering Δ/P and Δ as variables, Equation (4.4) takes the form of the equation of a straight line and can be plotted as shown in Figure 4.2. This Southwell plot produces a linear relationship within the elastic range. The inverse slope of the data represents the predicted buckling load. The variable, Δ, is not the absolute deflection, but the deviation from the initial shape and can easily be measured in the laboratory. The accuracy of this method increases as the maximum test load approaches the actual buckling load, or the ratio P/P_e approaches the value of 1.0. Predicted buckling loads are within 5% for $P/P_e \geq 0.6$ and within 2% for $P/P_e \geq 0.8$ (Southwell, 1932).

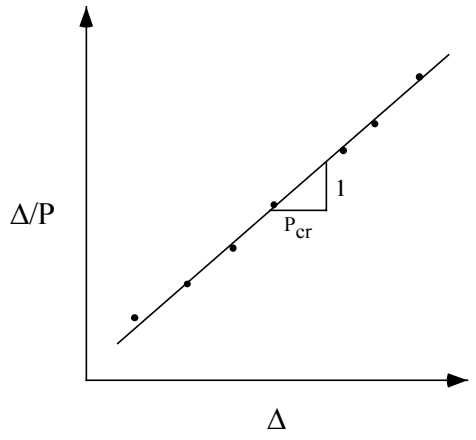

Figure 4.2 Southwell Plot (Gilchrist, 1997)

The Southwell method can only be applied to members in the elastic range. The method also depends on the assumption that the final buckled shape is of the same mode as the initial shape. In cases where this does not occur or where the deflection is very small, the Southwell plots will produce very errant results (Gilchrist, 1997). For example, consider the case of a column braced at mid-height with a single-wave initial imperfection as shown in Figure 4.3. Initial loading of the column will cause deflection to continue in the one-wave shape. However, if loading is continued and the brace is adequate, the column will buckle into two-waves. If lateral deflection for this case is measured at the first quarter point, the initial deflection readings will be in one direction but subsequent readings will be in the opposite direction. This difference in initial and final shapes produces poor Southwell plots, an example of which is shown in Figure 4.4.

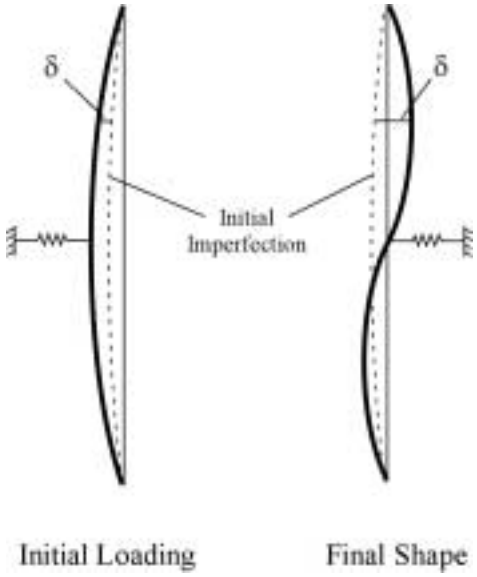

Figure 4.3 Deflection Reversal when Initial and Final Shapes Are Different

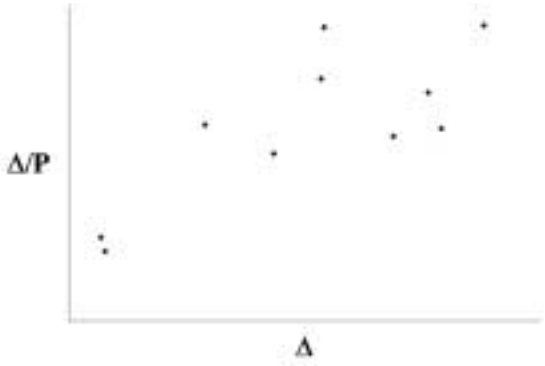

Figure 4.4 Typical Poor Southwell Plot

The Southwell plotting method is not limited only to columns. The scope of application includes any type of buckling problem where there is a hyperbolic load-deflection response similar to Equation (4.2). It is only necessary to have data relating load to a deformation characteristic such as deflection, rotation, or twist. Trahair (1969) and Meck (1977) successfully applied this method and variations of it to predict buckling loads for beams.

4.2 INITIAL IMPERFECTIONS

Before load was applied to the rectangular girder, the initial imperfections of the top flanges were recorded. Measurements were made using two transits sighted parallel to the two supports as described in Section 3.2.3. The imperfections for the east and west flanges are shown in Figure 4.5 and Figure 4.6, respectively.

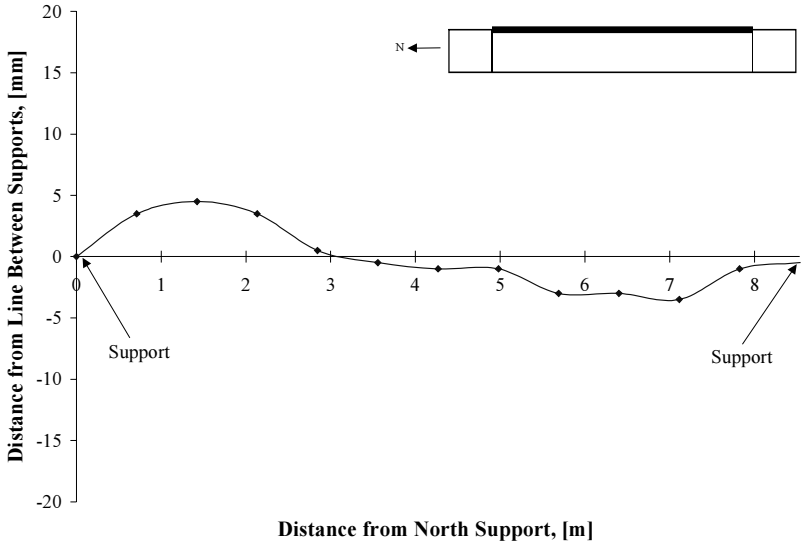

Figure 4.5 Initial Imperfections of East Flange of Rectangular Girder

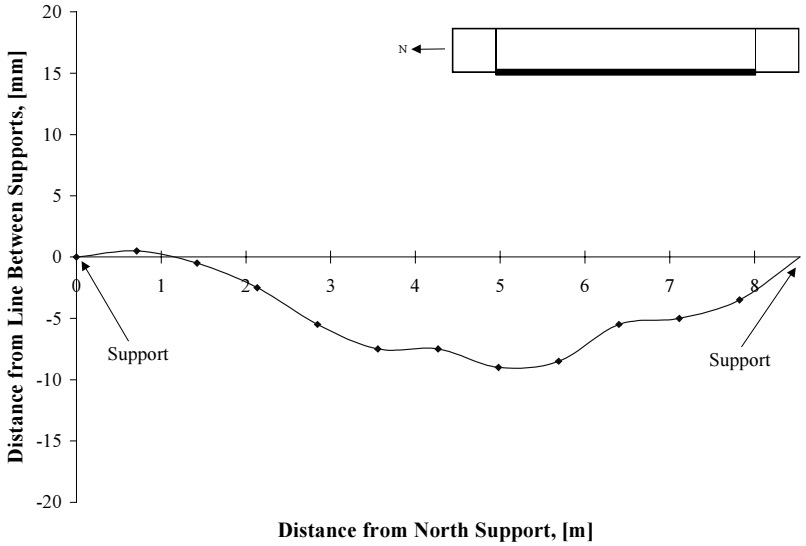

Figure 4.6 Initial Imperfections of West Flange of Rectangular Girder

Out-of-straightness values for each test case were calculated by dividing the relative lateral displacement between brace points, Δ_o, by the brace panel size, s. The results are summarized in Table 4.1.

Table 4.1 Maximum Out-of-Straightness of Brace Panels

Test Case	Δ_o/s
Unbraced	0.0010 (1/900)
4 Brace Panels	0.0030 (1/330)
5 Brace Panels	0.0038 (1/260)
10 Brace Panels	0.0060 (1/167)

Out-of-straightness values for specific brace panels in each of the brace geometry cases can be found in Appendix A.3.

4.3 DETERMINATION OF BRACE FORCES

The brace forces for the elastic tests were obtained by using the strain-gaged couplers described in Section 3.3.3. For the inelastic tests, strain gages were placed directly on selected diagonal brace members. Brace forces are typically normalized by the load necessary to cause buckling between braces. However, this value changed with each brace geometry and, in the case of ten brace panels, exceeded the girder's yield strength. To maintain consistency, the diagonal brace forces, F_{br}, and the cross-strut forces, F_{xs}, were normalized as a percentage of the force necessary to cause yielding in both girder flanges. The flange yield force, F_{yf}, was calculated as the product of the specified minimum yield stress of the flanges, 345 MPa (50 ksi), and the area of both flanges and was equal to 686.4 KN (154.3 kips).

4.4 X-BRACE TESTS - ELASTIC

A series of eighteen tests were conducted in which the rectangular girder was confined to the elastic domain. The purpose of these tests was to investigate the increase in buckling strength provided by X-brace top lateral system with different brace stiffnesses and geometries. This test series included no bracing, four, five, and ten brace panel test cases. Inspection of the whitewashed top flanges during the tests provided a visible verification of elastic behavior.

4.4.1 Buckling Loads

Southwell plots were created using load-deflection data from the string potentiometers measuring lateral deflection of the girder's top flange. A typical Southwell plot is shown in Figure 4.7. A linear regression analysis was used to calculate the slope of the trendline through the data points. The inverse of the slope of this line is the predicted Southwell elastic buckling load, P_{cr}. The data points chosen for use in the regression analysis were the last several data points recorded. The number of data points used was based on providing an R-squared value greater than 0.9975. This was done to ensure a sufficient number of data points were used in the regression analysis and to maintain consistency in data sampling between the test cases.

During the beginning stages of each test, the data points do not align with the linear portion near the latter test stages. This is due in part to uplift of the girder and settlement of fixtures and braces during the initial loading. The deviation can be mostly attributed to the fact that when P/P_e is small, the higher order terms that were neglected in the approximate solution of Equation (4.2) no longer have negligible effects (Bažant, 1991). That is, Equation (4.2) was derived using a Fourier sine series characterization for the initial deflected shape. When P/P_e is not small, the leading term in the series dominates the response, while the higher order terms have only a negligible contribution. This leading term is the expression seen in Equation (4.2).

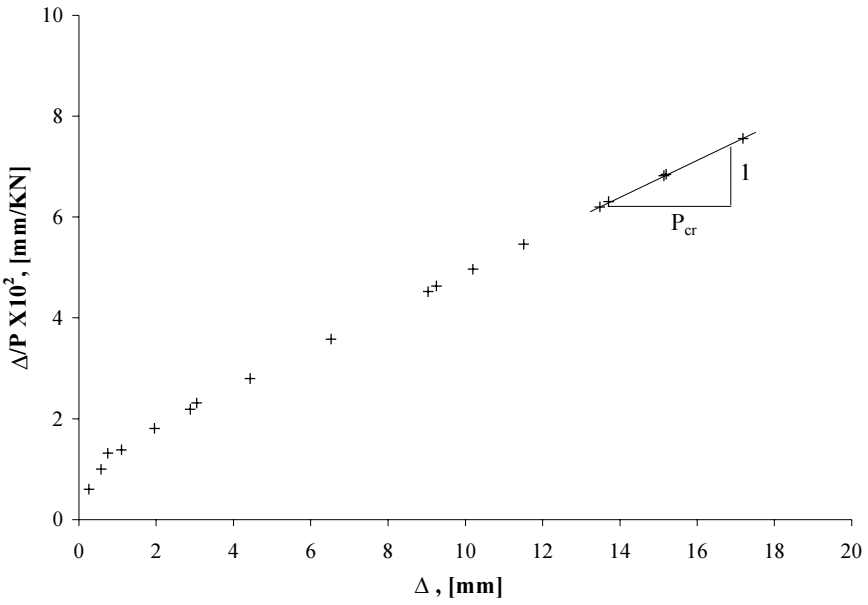

Figure 4.7 Typical Southwell Plot

To maintain consistency, lateral deflection data used to calculate the Southwell buckling loads was measured from the same location on the top flange. The Southwell method typically yields better results with data based on larger deflections. Therefore, the potentiometer chosen was near the point of maximum lateral deflection. This point, shown in Figure 4.8, was 3.2 m (10.5 ft.) from the south support and was near the point of maximum deflection for all test cases.

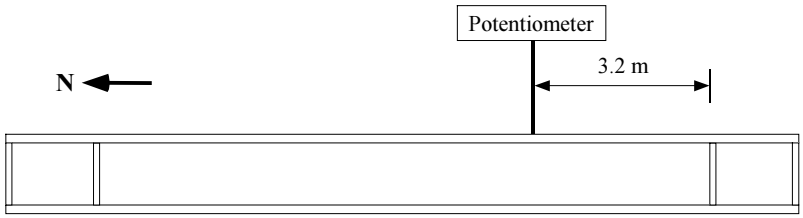

Figure 4.8 Potentiometer Used for Southwell Displacement Data

Table 4.2 provides a summary of the Southwell predicted buckling loads. Applied test loads and buckling loads are reported in terms of the ram force, P, which is directly proportional to the stress in the top flanges. Reported values are normalized by P_y, the ram load necessary to cause yielding in the top flanges based on simple elastic bending theory. The value for P_y for the rectangular girder was equal to 478.7 KN (107.6 kips).

During test R4-4, some yielding occurred that was visibly observed in the whitewashed top flanges. The permanent set of the top flanges was recorded and can be found in Appendix A.4. An additional test, RU-2, was conducted to see if the yielding had affected the buckling strength of the unbraced girder. The results indicated a slight decrease in the predicted Southwell buckling load from $0.50P_y$ to $0.47P_y$.

Table 4.2 Southwell Predicted Buckling Loads

Test Case	Maximum Applied Test Load (P_{max}/P_y)	Southwell Predicted Buckling Load (P_{cr}/P_y)
RU-1	0.415	0.50
RU-2	0.415	0.47
R4-1	0.475	0.58
R4-2	0.458	0.54
R4-3	0.467	0.55
R4-4	0.476	0.54
R4-5	0.453	0.54
R5-1	0.426	0.53
R5-2	0.425	0.58
R5-3	0.427	0.58
R5-4	0.421	0.55
R5-5	0.443	0.58
R5-6	0.447	0.59
R5-7	0.410	0.56
R5-8	0.418	0.57
R10-1	0.511	0.73
R10-2	0.509	0.89
R10-3	0.490	0.81

4.4.2 Buckled Shapes and Brace Behavior

Figures 4.9 through 4.12 show the typical buckled shapes of the top flanges between the two supports for the various brace geometries. The braces were visually inspected during each test to determine whether they were engaged, slack, or buckled. Engaged diagonal braces are denoted by bold lines, while buckled or slack braces are shown as dotted lines.

The final buckled shape for all of the brace geometries and stiffness cases was two-waves between the supports. The flanges of the unbraced girder buckled independently of one another because cross struts were not present to maintain the distance between flanges.

During the beginning stages of loading, all of the diagonal bracing visibly slackened from their initially taught position as shown in Figures 4.13 and 4.14. This was observed in all of the test cases and was especially apparent in the cases with fewer brace panels. The shortening of the top compression flange under loading caused the bracing to slacken. As the top flanges began to deflect laterally, some braces engaged to prevent the panel distortion while others remained slack. As an example, the second brace panel from the north in the four brace panel case had a diagonal brace engage as the panel attempted to distort (Figure 4.10). However, the adjacent brace panel to the north also distorted, but the diagonal brace did not engage. The lateral deflection or panel distortion necessary to elongate the brace in the first panel was not sufficient to make up for the slack that was introduced when the brace panel shortened.

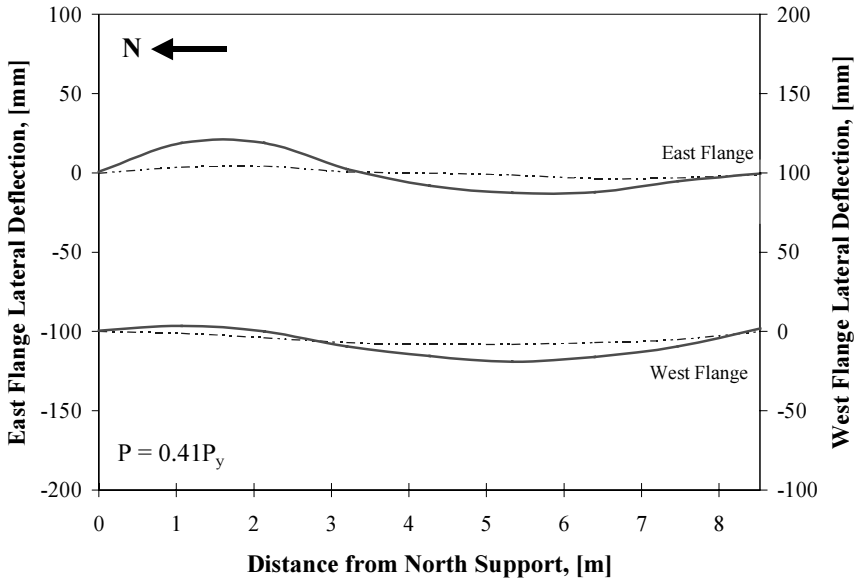

Figure 4.9 Typical Buckled Shape for Unbraced Girder

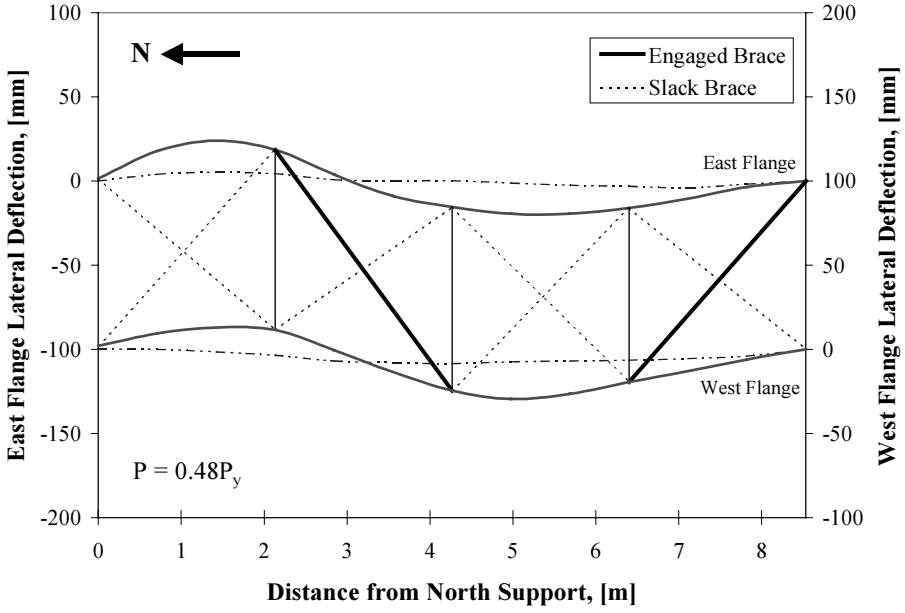

Figure 4.10 Typical Buckled Shape for 4 Brace Panels

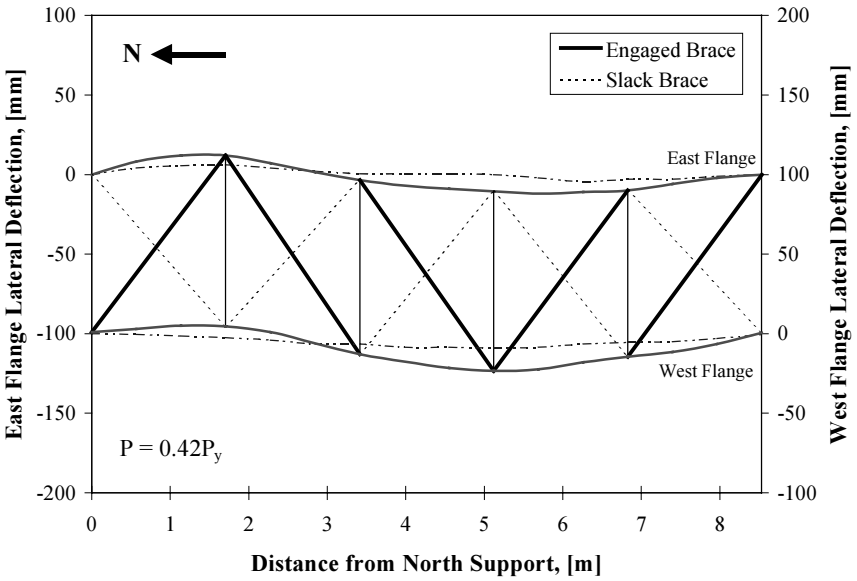

Figure 4.11 Typical Buckled Shape for 5 Brace Panels

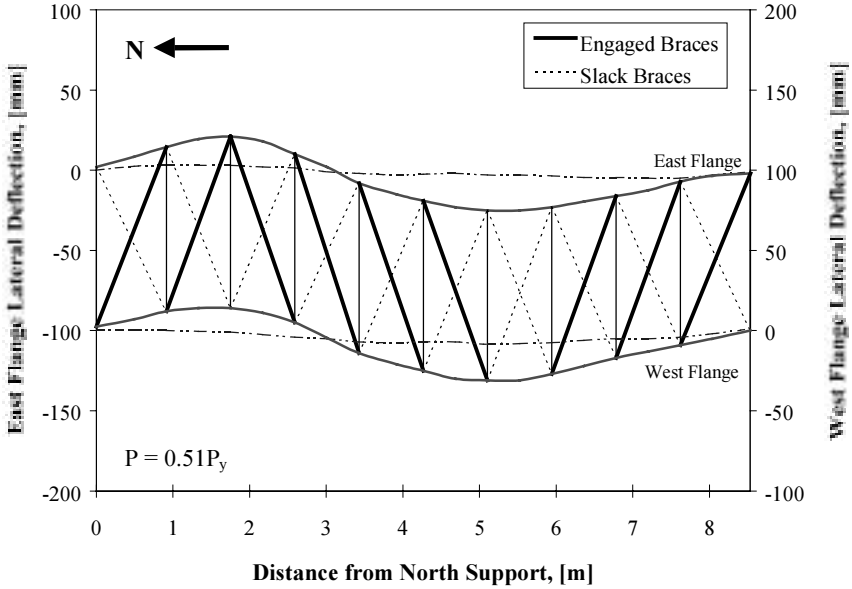

Figure 4.12 Typical Buckled Shape for 10 Brace Panels

Figure 4.13 Bracing Taught before Loading

Figure 4.14 Bracing Slack during Initial Loading

4.4.3 Brace Forces

The general distribution of brace forces was very similar within each brace geometry case. Typical brace force distributions for the four and five brace panel test cases are shown in Figures 4.15 and 4.16. The diagonal brace P2a in both the four and five brace panel test cases attracted the highest brace forces. As visually observed during the tests, the number of braces that developed significant forces increased as the number of brace panels increased. The four brace panel test cases had only two active braces while the five brace panel cases typically had five. A summary of the maximum brace forces reached in each test is shown in Table 4.3. A dash indicates those particular brace forces were not measured during a given test.

Table 4.3 Maximum Brace Forces for Elastic Tests

Test Case	P_{max}/P_y	Diagonal Braces (F_{br}/F_{yf})	Cross Struts (F_{xs}/F_{yf})	
		Tension	Tension	Compression
R4-1	0.48	0.23%	0.41%	-0.11%
R4-2	0.46	0.24%	0.25%	-0.12%
R4-3	0.47	0.29%	0.34%	-0.13%
R4-4	0.48	-	0.61%	-0.13%
R4-5	0.45	0.27%	0.33%	-0.03%
R5-1	0.43	-	0.26%	-0.10%
R5-2	0.42	0.17%	0.22%	-0.34%
R5-3	0.43	0.19%	0.23%	-0.33%
R5-4	0.42	0.11%	0.18%	-0.34%
R5-5	0.44	-	-	-
R5-6	0.45	-	-	-
R5-7	0.41	-	-	-
R5-8	0.42	0.11%	0.18%	-0.20%
R10-1	0.42	-	0.53%	-0.40%
R10-2	0.51	-	0.51%	-0.28%
R10-3	0.49	-	0.54%	-0.31%

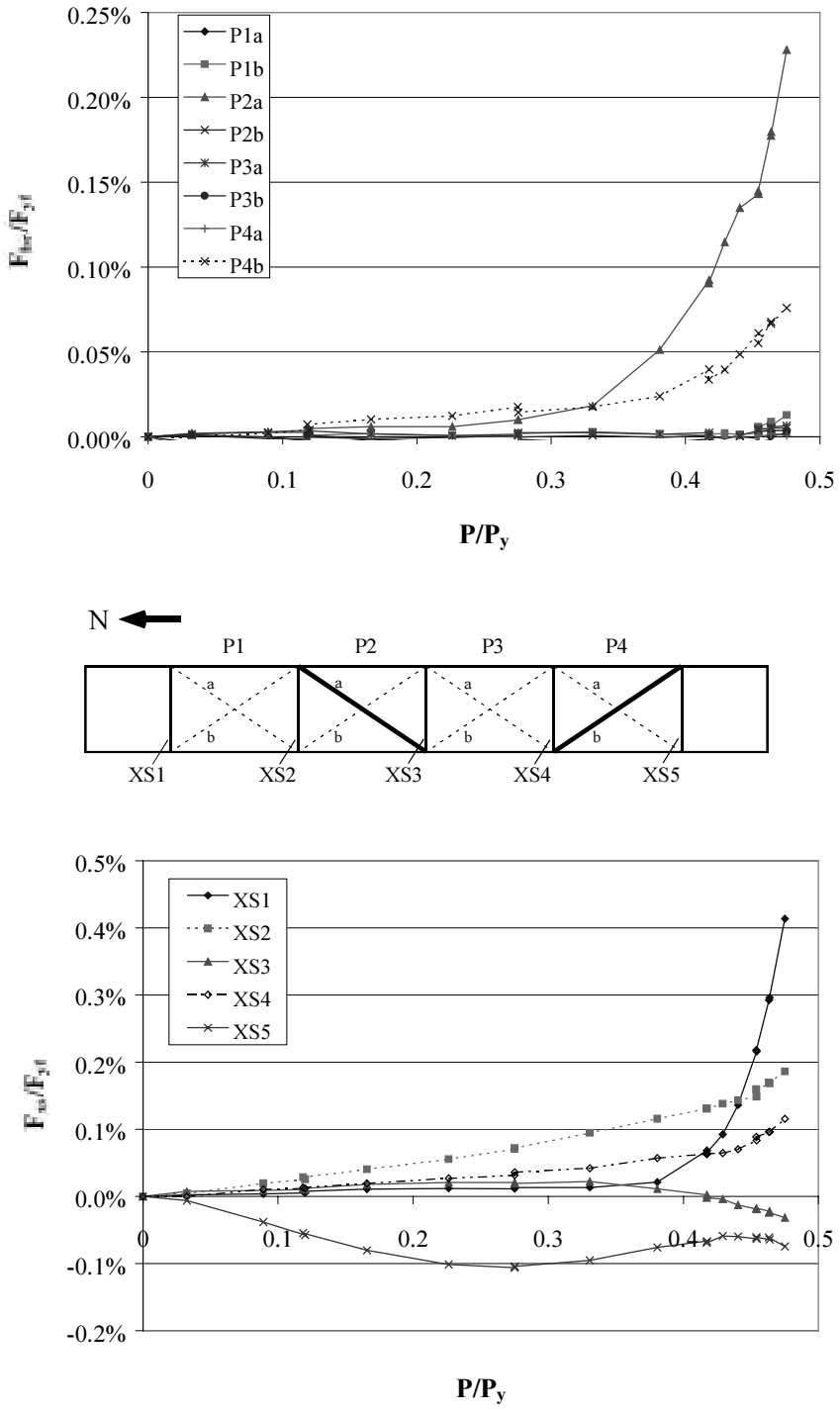

Figure 4.15 Typical Brace Force Distribution for 4 Brace Panels

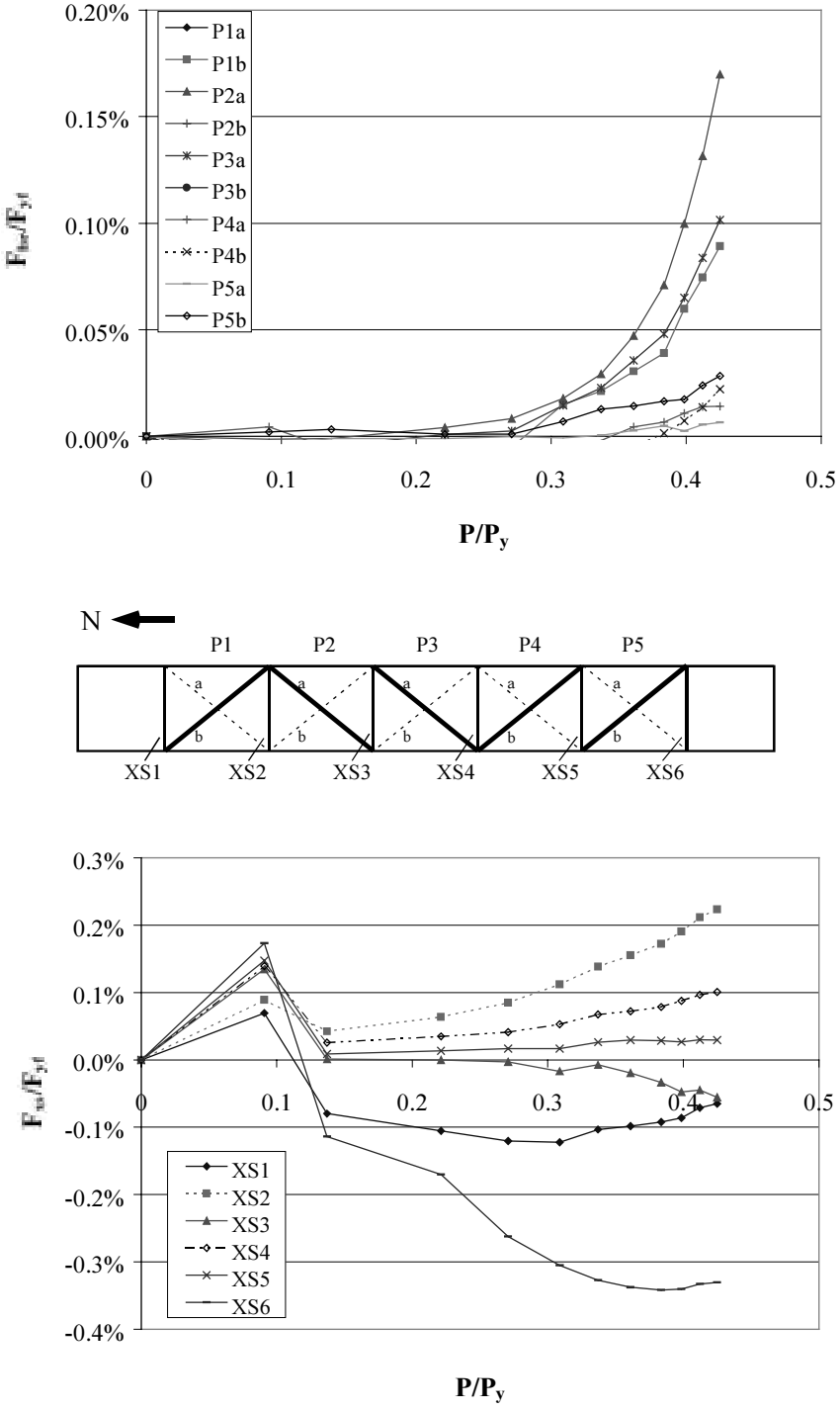

Figure 4.16 Typical Brace Force Distribution for 5 Brace Panels

4.5 X-BRACE TESTS - INELASTIC

A series of three tests were performed in which the rectangular girder was taken into the inelastic range. The goal of these tests was to obtain the true maximum load carrying capacity of the braced girder.

4.5.1 Tests R10-4 and R10-5

The purpose of tests R10-4 and R10-5 was to verify the accuracy of the predicted Southwell buckling loads obtained from the elastic girder tests. During the final stages of loading for test R10-4, a brace mount slipped from the top flange, causing premature termination of the test. Therefore, a second test, R10-5, was conducted to verify the maximum load carrying capacity of the girder.

Before test R10-5 was conducted, the slight permanent set of the top flanges caused by the previous test was recorded and can be found in Appendix A.6. Results from test R10-4 were very similar to R10-5 and may be found in the Appendix A.5.

The load versus lateral deflection response for R10-5 is shown in Figure 4.17. Lateral deflection data was recorded from the same linear string potentiometer as the elastic girder tests and was located near the point of maximum lateral deflection. The load-deflection response indicates the maximum load carrying capacity of the girder was reached because lateral deflection occurred with very little increase in load. Also, the deviation of the load versus midspan vertical deflection from linear indicates inelastic behavior, which was visibly observed by yielding in the whitewashed top flanges. The maximum load achieved was only $0.55P_y$. By contrast, the Southwell predictions for this test (from R10-1 through R10-3) varied between $0.73P_y$ and $0.89P_y$.

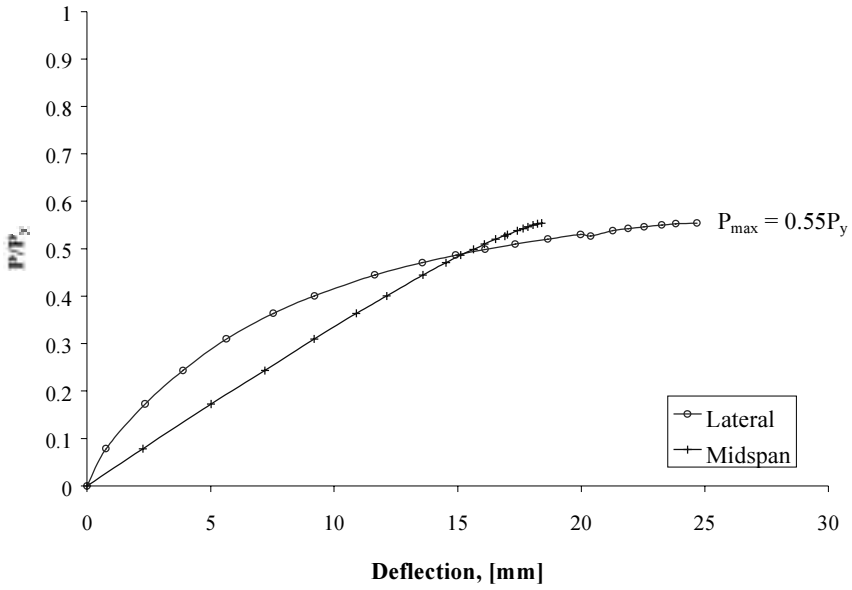

Figure 4.17 Load-Deflection Response for Test R10-5

The brace forces measured included three diagonal braces and six cross struts and are shown as the heavy lines in Figure 4.18. The location of the instrumented members are denoted by the heavy dashed lines in the plan view. The maximum diagonal brace force reached was 0.82% of the flange yield force, while the maximum cross-strut force reached 0.53% in compression and 0.23% in tension.

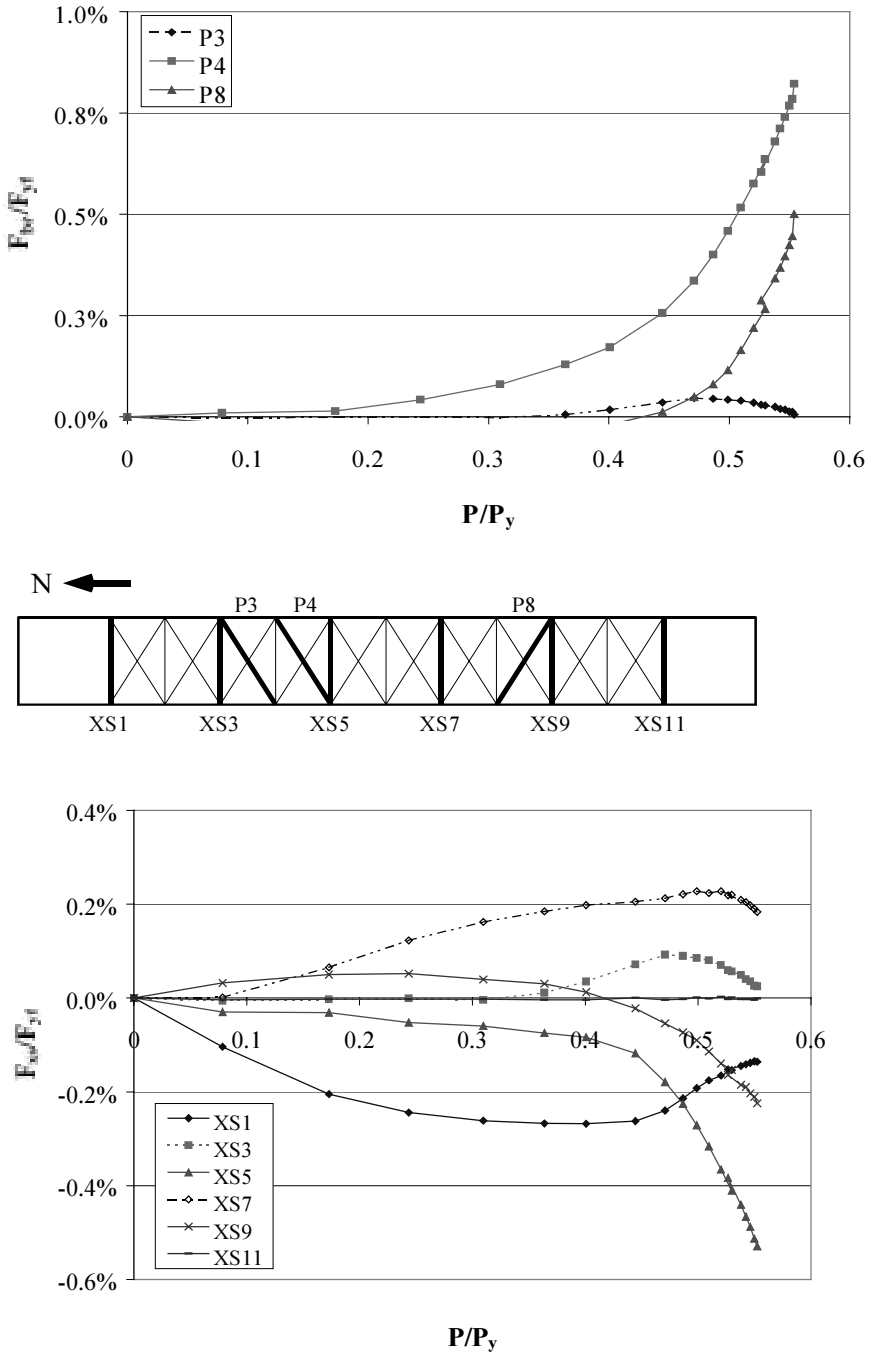

Figure 4.18 Brace Force Distribution for R10-5

4.5.2 Test R10-W

The purpose of test R10-W was to determine if the connection details used in the previous test cases had reduced the effective stiffness of the lateral bracing. This test employed the welded connection detail described in Section 3.3.2. The load-deflection response for test R10-W is shown in Figure 4.19. Lateral deflection data was, again, obtained from the same potentiometer used in the previous tests. The maximum test load achieved before failure was $0.76P_y$, an increase of 21% from the previous test case with the non-welded connection detail.

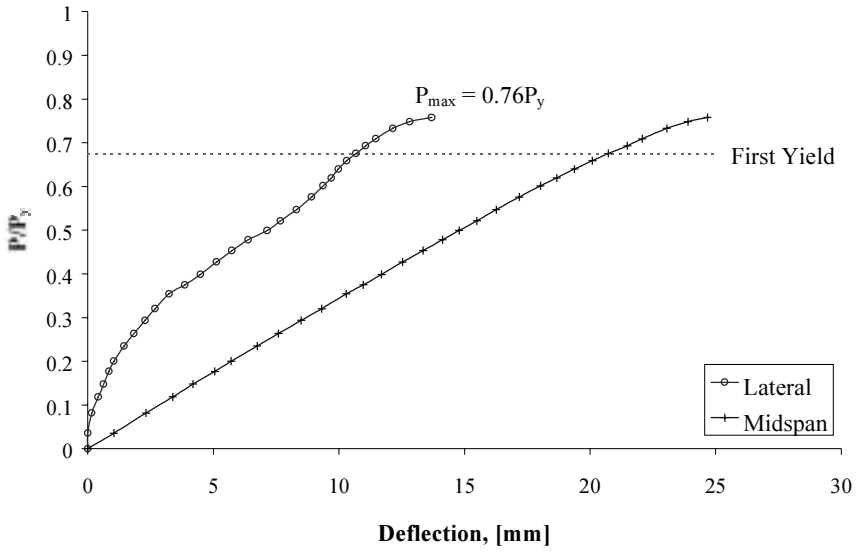

Figure 4.19 Load-Deflection Response for Test R10-W

Failure of the girder occurred by the formation of plastic hinges in the center of the third brace panel from the north support. Once these plastic hinges formed, the top flanges were free to buckle, despite the presence of the diagonal bracing. That is, the flanges could buckle laterally while still maintaining the same diagonal distance between the end points of the tension brace. The locations yielding visibly observed in the whitewashed top flanges are shown in Figure 4.20 and the failure mechanism is shown in Figures 4.21 through 4.23.

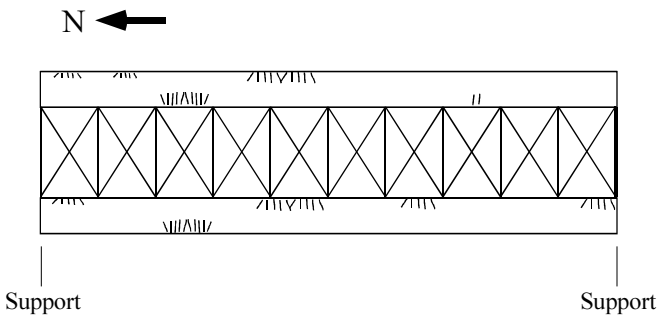

Figure 4.20 Locations of Flange Yielding

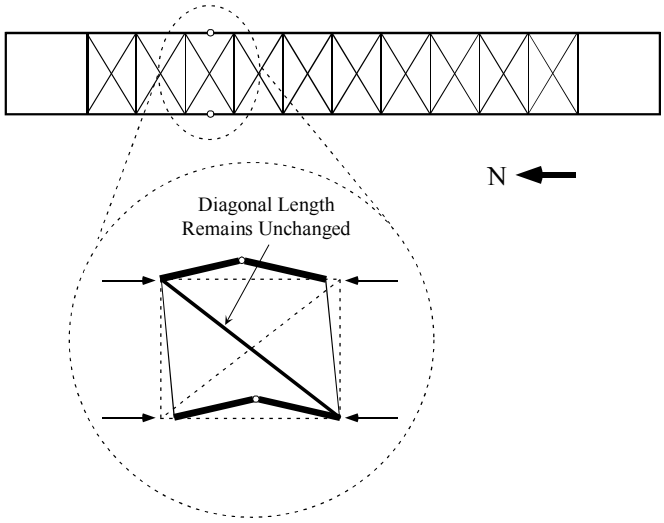

Figure 4.21 Flanges Free to Buckle Once Plastic Hinges Form

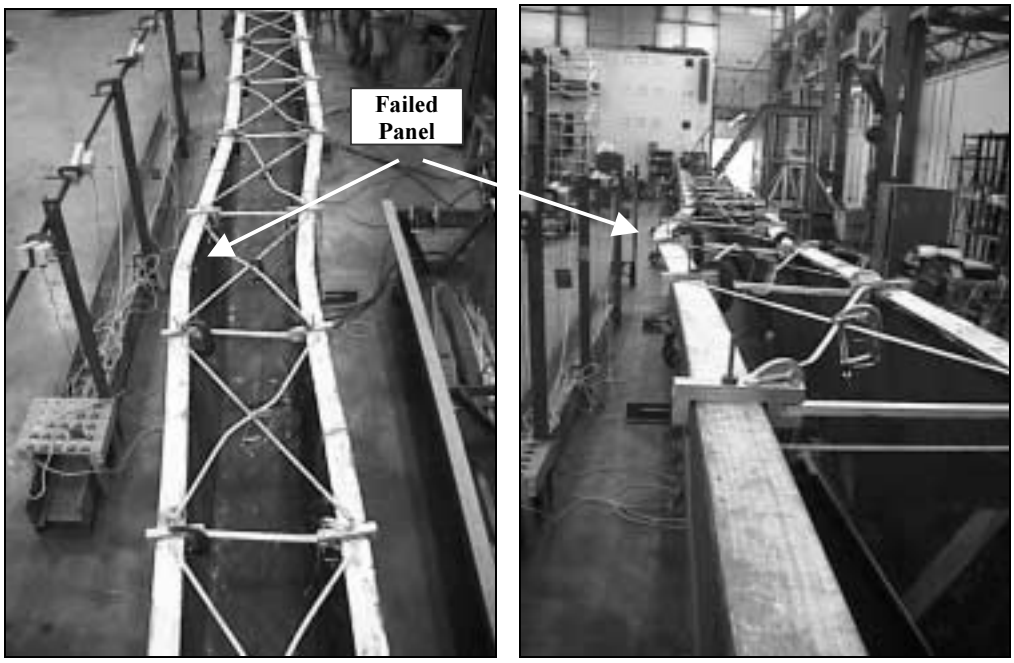

Figure 4.22 Girder after Reaching Failure Mechanism

Figure 4.23 Tension Braces Still Intact after Failure

The out-of-plane buckled shape of the girder just before failure, as seen in Figure 4.24, was the same two-wave shape seen in previous tests. However, the magnitudes of the lateral deflections were not as great for the same levels of applied load.

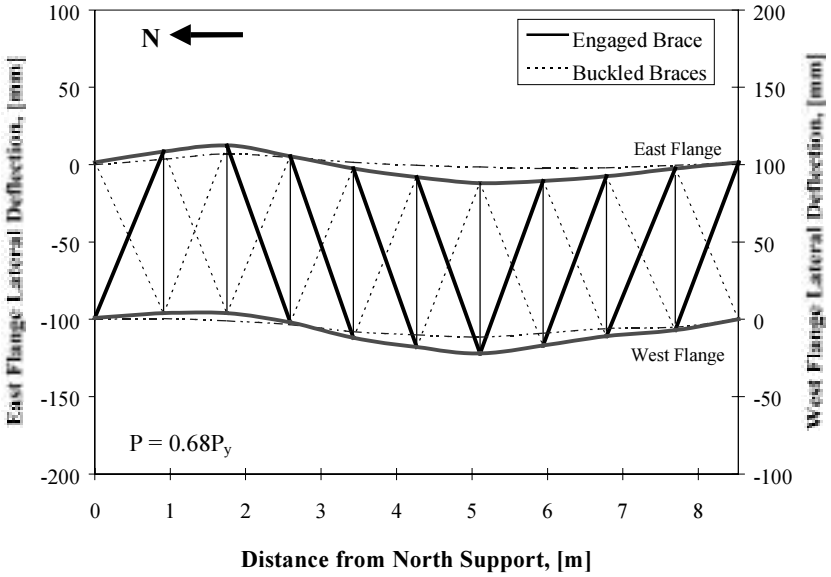

Figure 4.24 Buckled Shape for R10-W

The brace forces measured included two diagonal braces and eight cross-strut members and are shown as the heavy lines in Figure 4.25. Yielding was visibly observed in the whitewashed top flanges at an applied load of $0.68P_y$. The maximum measured diagonal brace force reached 2.33% of the flange yield force, nearly three times the maximum achieved in any of the previous tests. The cross-strut forces reached a maximum of 1.22% of the flange yield force in both tension and compression, twice the maximum any of the previous tests.

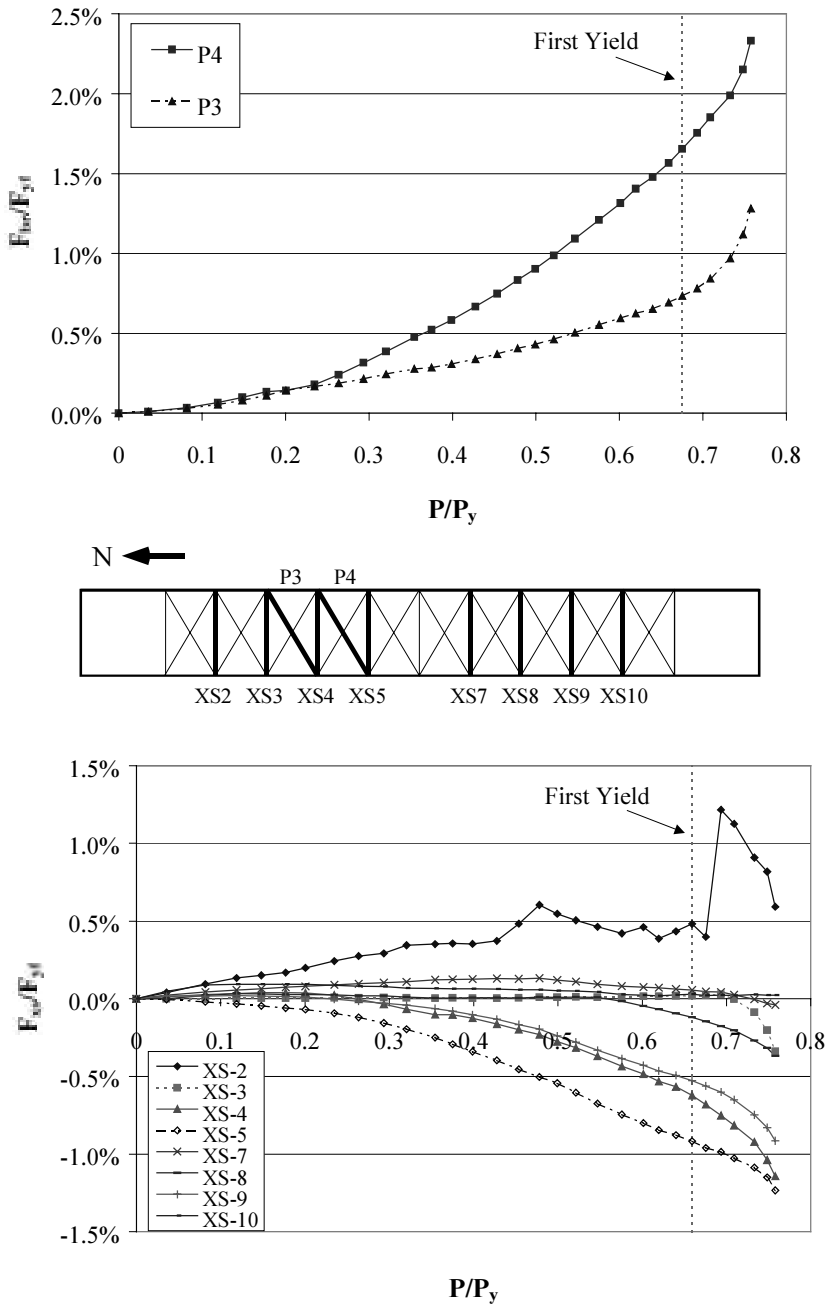

Figure 4.25 Brace Force Distribution for R10-W

4.6 BEHAVIOR OF DIAGONAL BRACES IN COMPRESSION

The diagonal braces in test R10-W were mechanically clamped together at their crossing point with C-clamps. All of the braces in compression buckled and are denoted by the dotted lines in Figure 4.24. With the exception of the two braces in the second brace panel from the north, all of the compression braces buckled into two-waves as shown in Figure 4.26. Both braces in the second brace panel were both in compression and both buckled into a single-wave. The engaged tension braces of the other brace panels served as brace points for the compression braces, reducing their unbraced length by one half.

Figure 4.26 Diagonal Brace with Overlap Point Serving as Brace Point

4.7 METAL DECKING TESTS

A series of four pilot tests were conducted on the trapezoidal girder with a metal decking top lateral bracing system. The purpose of these tests was to examine whether the use of metal decking as a top lateral bracing system would produce similar increases in bending strength that the X-brace system did. Because the test specimen was to be used in subsequent experiments, all test cases were confined to the elastic domain.

The load-deflection response of the girder is shown in Figure 4.27. Lateral deflections were measured 3.3 m (132 in.) from the north support. For a given load level, the lateral deflections markedly decreased as the number of deck panels increased.

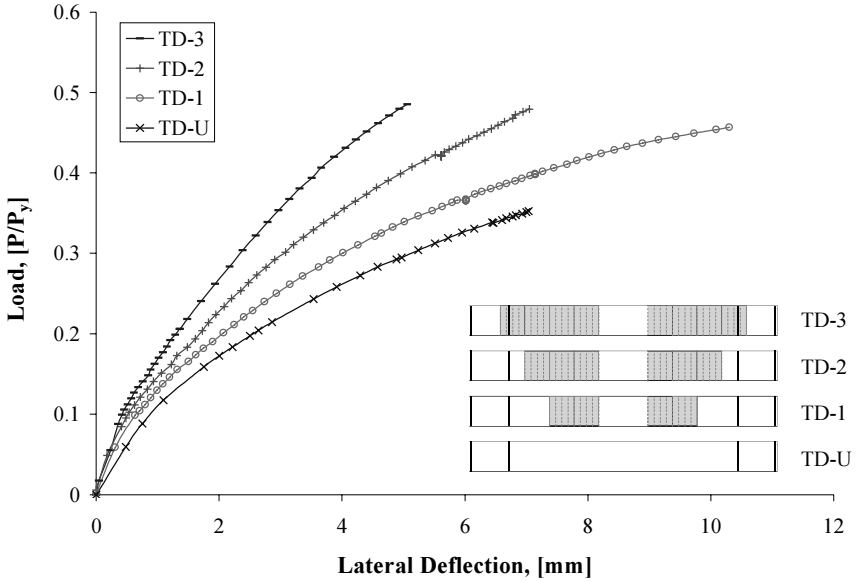

Figure 4.27 Load versus Lateral Deflection Response for Metal Deck Tests

Table 4.4 provides a summary of the Southwell predicted buckling loads. Applied test loads and buckling loads are reported in terms of the ram force, P, which is directly proportional to the stress in the top flanges. Reported values are normalized by P_y, the ram load necessary to cause yielding in the top flanges based on simple elastic bending theory. The value of P_y for the trapezoidal girder was equal to 434.5 KN (97.8 kips).

Table 4.4 Southwell Predicted Buckling Loads

Test Case	Maximum Applied Test Load (P_{max}/P_y)	Southwell Predicted Buckling Load (P_{cr}/P_y)
TD-U	0.35	0.66
TD-1	0.46	0.63
TD-2	0.48	0.87
TD-3	0.49	0.93

CHAPTER 5
Analysis of Results

5.1 EVALUATION OF SOUTHWELL BUCKLING LOAD PREDICTIONS

Gilchrist (1997) showed that the Southwell buckling load predictions for torsionally-braced beams may not yield accurate results for buckled shapes that are more complicated than a sine wave. The Southwell predictions for the U-girder with top-flange lateral bracing exhibited similar inconsistencies. Predictions based on measurements of lateral deflection at different points along the top flange differed by significant amounts. Table 5.1 shows the typical variation in the predicted buckling loads. The locations of the string potentiometers on the top flange are shown in Figure 5.1. As with the web stiffened results presented by Gilchrist (1997), the variation in buckling loads may be caused by a buckled shape that is more complicated than a simple sine curve.

Table 5.1 Typical Variation of Southwell Predictions Using Different Lateral Deflection Data (R5-3)

Pot #	Predicted Buckling Load (P_{cr}/P_y)	Difference from Average
1	0.60	2.3%
2	0.56	4.6%
3	0.48	17.2%
4	0.63	8.8%
5	0.58	0.1%
6	0.58	1.0%
7	0.65	11.8%
Average	0.58	--

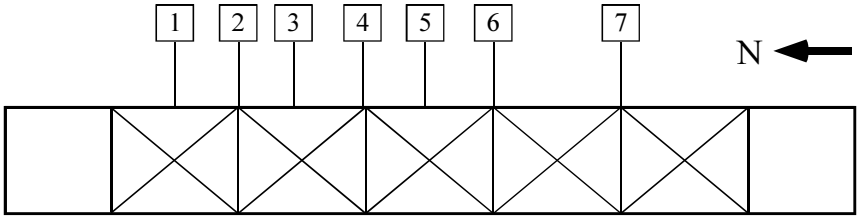

Figure 5.1 String Potentiometer Locations

The Southwell buckling load predictions were also very dependent on the level of load that was applied to the girder. For a given test, the Southwell predictions made using deflection data at lower applied loads differed from those made at higher load levels. This is because the Southwell method predicts buckling loads based on the assumption that elastic buckling will occur. In cases where inelastic buckling occurs,

Southwell tends to overestimate the true buckling load. In these cases, the Southwell buckling loads will initially overestimate the actual buckling load, but will approach the true buckling load as the applied load approaches the true buckling load.

Figure 5.2 illustrates how the Southwell buckling load prediction decreased as the applied load increased. If only data at moderate load levels were considered, the Southwell buckling load prediction was $0.84P_y$. As the applied load increased, the slope of the data points on the Southwell plot increased, corresponding to a decrease in the predicted buckling load. The buckling load prediction when the applied load was near the true load capacity of the girder was $0.56P_y$. As the applied test load increased, the Southwell prediction converged on the true experimental buckling load of $0.55P_y$. Therefore, Southwell predictions should not be used if the buckling load, P_{cr}, exceeds the first yield load.

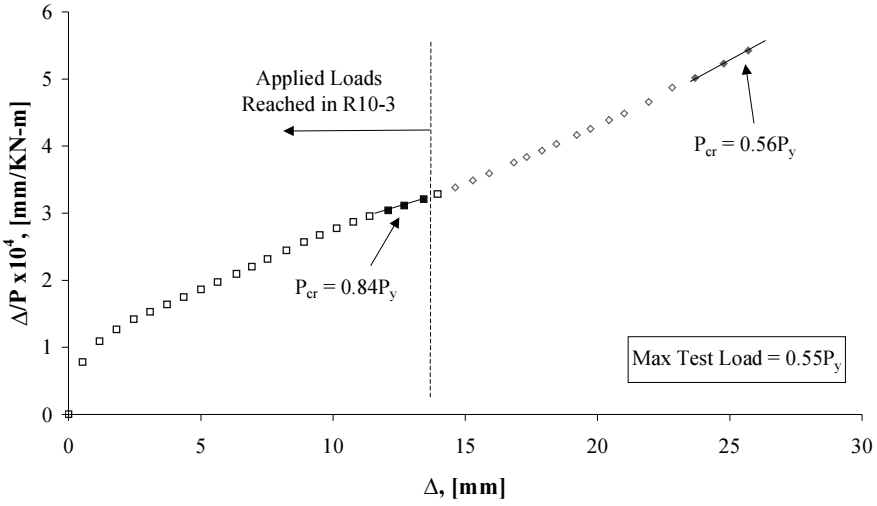

Figure 5.2 Comparison of Southwell Buckling Loads Based on Level of Applied Load (R10-4)

5.2 BRACE STIFFNESS LOSS FROM CONNECTION

The non-welded connection detail used in the X-brace tests did not adequately attach the diagonal bracing to the top flanges of the girder. Flexibility in the connection detail reduced the effective stiffness of the bracing system. This resulted in a significant reduction in the buckling capacity of the girder.

A comparison of tests R10-5 and R10-W isolates the effect of the brace connection detail. Test case R10-5 had the same brace geometry and even a slightly higher brace stiffness than R10-W, but the connection detail used was the removable flange mounting brackets described in Section 3.3.2. The maximum load reached during test R10-5 was $0.55P_y$, only a 17% increase from the unbraced buckling load prediction of $0.47P_y$. By contrast, the welded connection in test case R10-W reached $0.76P_y$, a 62% increase over the unbraced case. Figure 5.3 compares the load versus lateral deflection responses for these two test cases. For a given load level, the lateral deflections in R10-W were much lower than in R10-5, indicating the lateral bracing was more effective at preventing lateral deflection of the top flanges. The flexibility of the non-welded connection detail decreased the effective lateral brace stiffness, thereby reducing the buckling capacity of the girder. This effect was illustrated in Section 2.3.6. Also, the lower brace stiffness of R10-5 allowed larger lateral deflections for the same load levels. The load versus midspan vertical deflection responses shown in Figure 5.4 were very similar for both test cases. Because the diagonal bracing members in test R10-W were very slender, their compressive capacity did not significantly contribute to the in-plane bending stiffness of the girder. At moderate load levels, the

midspan vertical responses were nearly identical. At an applied load of about $0.35P_y$, the in-plane response of R10-5 began to deviate from linear as a result of inelasticity associated with the large lateral deflections. The deviation from linear of test R10-W occurred at an applied load of approximately $0.50P_y$. This corresponded to a significantly higher load level than test R10-5. The deviation from linear in the load versus midspan deflection response for both tests occurred at a lateral deflection of approximately 7 mm.

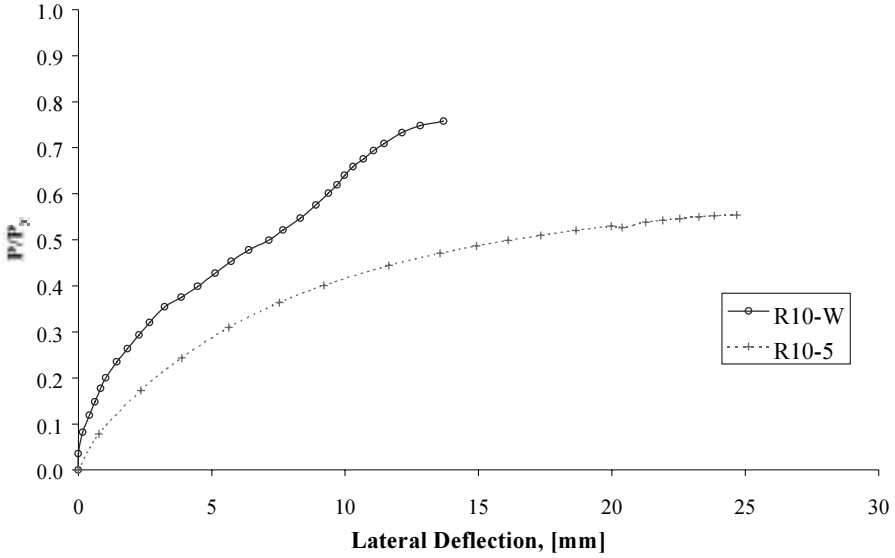

Figure 5.3 Comparison of Load vs. Lateral Deflection Responses

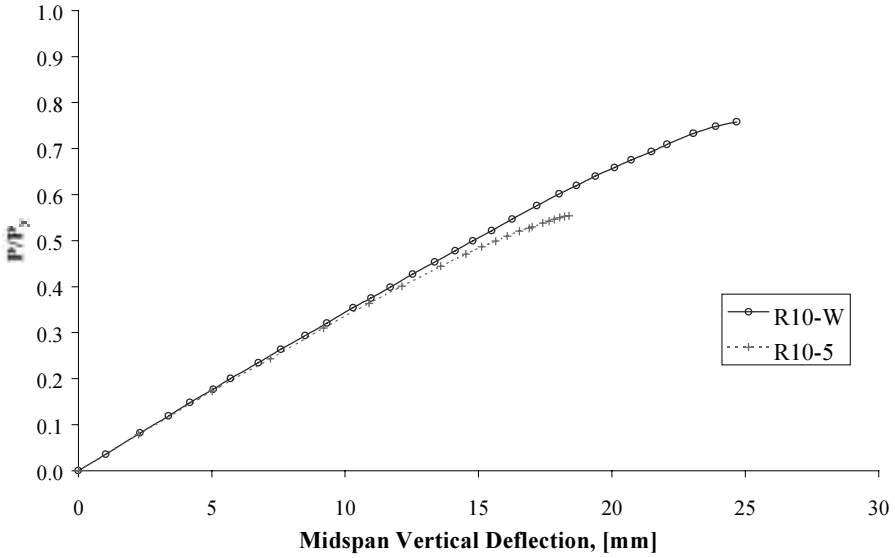

Figure 5.4 Comparison of Load vs. Midspan Vertical Deflection Responses

5.3 SHORTENING EFFECT

5.3.1 Girder Capacity Reduction

Girder bending causes shortening in the diagonal bracing such that lateral displacement must occur before the braces can return to their original length and engage. These lateral displacements, added to the initial imperfections, create second-order bending stresses in the top flanges that cause yielding to occur before P_y can be reached.

In design, the top-flange lateral bracing system is typically treated independently from the girder. In reality, however, the connection between the top flange and the bracing enforces displacement compatibility between the two. When the girder bends under loading, points along the top flange shorten due to compressive stresses. Consequently, the attached bracing also shortens, introducing slack. In order for the braces to engage, the distance between the endpoints of the diagonal braces must return to their original length. This is accommodated by lateral translation of the top flanges as illustrated in Figure 5.5.

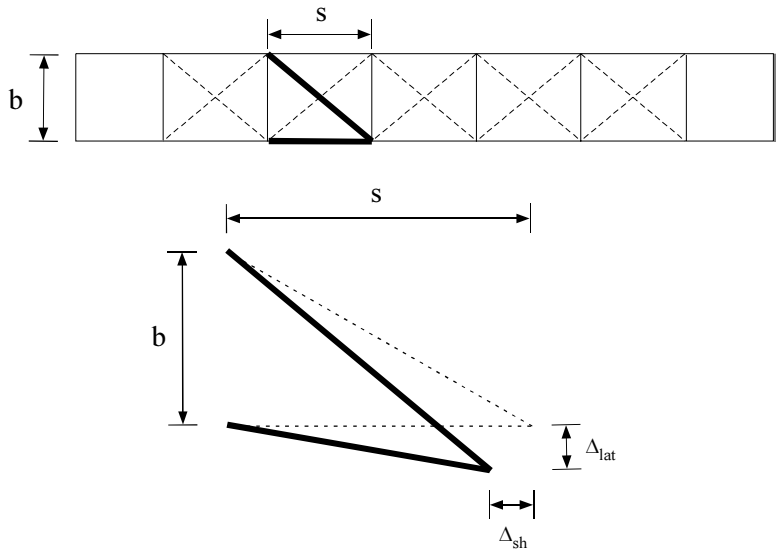

Figure 5.5 Lateral Translation of Top Flange Due to Shortening

The amount of lateral translation associated with a given amount of shortening can be obtained through simple geometry. Equating the length of a diagonal brace before and after shortening gives

$$\sqrt{s^2 + b^2} = \sqrt{\left(s - \Delta_{sh}\right)^2 + \left(b + \Delta_{lat}\right)^2} \tag{5.1}$$

where s is the brace panel size or brace spacing, b is the distance between the connection to the flanges, Δ_{sh} is the longitudinal shortening of the top flanges due to girder bending, and Δ_{lat} is the lateral translation necessary to accommodate the shortening. Rearranging and solving for Δ_{lat} yields

$$\Delta_{lat} = \sqrt{s^2 + b^2 - \left(s - \Delta_{sh}\right)^2} - b \tag{5.2}$$

From simple bending theory, the strain multiplied by the brace panel length gives the shortening of a brace panel as

$$\Delta_{sh} = \varepsilon \cdot s = \left(\frac{M}{S_g E} \right) \cdot s \tag{5.3}$$

where M is the bending moment, S_g is the section modulus for the top of the girder, and E is Young's modulus.

The maximum compressive stress in the top flange is the sum of the first-order bending stress and second-order stress due to the lateral translation associated with shortening. The maximum lateral deflection due to shortening depends on the buckled shape of the girder. For U-shaped girders, the torsional restraint provided by the bottom flange causes the first buckling mode to be two-waves between the supports. Therefore, if the deflected shape is assumed to be a full sine wave, the maximum lateral deflection at each peak is the sum of the lateral translations of the brace panels between the support and the peak. Thus, the maximum compressive stress in the top flange equals

$$\sigma_{\max} = \frac{M}{S_g} + \frac{P\left(n \cdot \Delta_{lat}\right)}{S_f} \tag{5.4}$$

where P is the force in one flange, n is the number of brace panels contributing to the maximum lateral deflection, and S_f is the section modulus of a top flange about its strong axis. If the stress distribution in the top flange is approximated as uniform, then the flange force, P, is equal to

$$P = \frac{M}{S_g} A_f \tag{5.5}$$

where A_f is the area of one top flange. To find the bending capacity of the braced girder considering the effects of shortening, the yield stress of the top flanges, F_y, is substituted for σ_{max}. Combining Equations (5.4) and (5.5) gives

$$F_y = \frac{M}{S_g}\left[1 + \frac{A_f}{S_f} n \cdot \Delta_{lat}\right] \tag{5.6}$$

Substituting Equations (5.2) and (5.3) into (5.6) yields

$$F_y = \frac{M}{S_g}\left[1 + \frac{A_f}{S_f} n \cdot \sqrt{s^2 + b^2 - \left(s - \frac{M \cdot s}{S_g E}\right)^2} - \frac{A_f}{S_f} b\right] \tag{5.7}$$

Solving for M gives the bending capacity of a girder considering the effects of elastic shortening.

5.3.2 Comparison of Theoretical Capacity and Results from R10-W

The "Full Bracing" criteria developed by Winter was defined as forcing buckling between brace points and considering the brace points themselves to be unyielding supports. For a girder with no initial imperfections and unyielding brace points, the load capacity would either be governed by buckling between brace points or flange yielding. In the case of test R10-W, buckling between brace points corresponded to a load above the yield load, P_y. Analysis using Winter's "Full Bracing" criteria would

predict a load capacity equal to P_y, but the experimental test reached a maximum applied load of only $0.76P_y$.

An analysis was conducted to determine the capacity of the girder with ten brace panels, considering the effects of shortening as described in the previous section. The yield stress used was the average static yield stress of the top flanges obtained from the tensile tests, F_{sy}, and was equal to 320 MPa (46.4 ksi).

The maximum moment was obtained by numerically solving for the moment, M, in Equation (5.7). Since the buckled shape was two-waves between the supports, one-quarter of the brace panels were estimated to contribute to the maximum lateral deflection. The value of n was estimated to be equal to 2.5, the total number of brace panels between supports, ten, divided by four. Although the value of n was not an integer and the true peaks were not located at the quarter points, the calculation provides a reasonable approximation of the maximum lateral deflection due to girder shortening. The results of this analysis indicated that the top flanges of the girder would yield at an applied load of $0.72P_y$, within 5% of the experimental result. Thus, the effects of shortening alone can reduce the bending capacity of a U-shaped girder by a significant amount.

A comparison of the girder's strength with varying brace angles is shown in Figure 5.6. The curve plotted represents the load at which first yield would occur in the top flanges due to the combined first and second-order stresses. Increasing the brace angle, θ, decreases the girder's capacity non-linearly because the lateral deflections due to shortening increase with increasing brace angles.

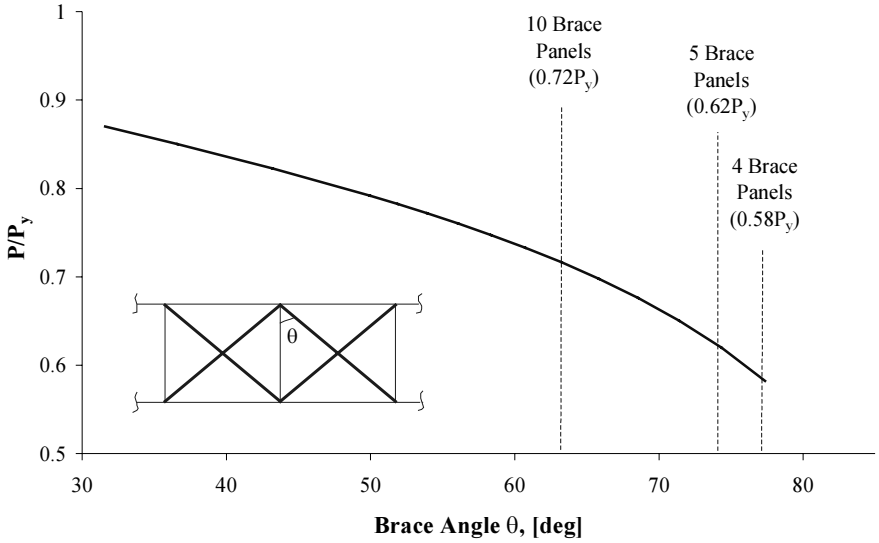

Figure 5.6 Effect of Shortening on Girder Capacity

The previous analysis was not intended to reproduce the experimental load capacity analytically, but to illustrate the detrimental effects of shortening. Some additional factors which were not considered in the analysis include lateral deflections due to initial imperfections of the top flanges or elongation of the brace members, additional compressive stresses induced in the top flanges by tension brace forces, strain hardening, and residual stresses.

The nominal flexural resistance of the U-girder was also calculated using the current *AASHTO LRFD Bridge Design Specifications*. Similar results would have been obtained using the *AISC LRFD Specification for Steel Buildings*. Using the unbraced length of the ten brace panel geometry and the average static yield stress, F_{sy}, the nominal flexural strength calculated was $0.95P_y$, 25% higher than the

experimental flexural strength. Details of the calculations may be found in Appendix B.1. By comparison, the flexural strength of the girder considering the effects of shortening was $0.72P_y$. This discrepancy can be attributed to the fact that the current specifications do not account for the effects of shortening.

5.4 BRACE FORCES

Current design recommendations for beam lateral bracing follow from the column analogy presented in Section 2.3.1. The value of the brace force at arbitrary applied loads is given by

$$F_{brace} = \frac{M/h}{\cos\theta}\left(\frac{\Delta_o}{s}\right)\left(\frac{1}{1-\frac{M/h}{s\beta}}\right) \tag{5.8}$$

where M is the girder moment, h is the height of the girder, Δ_o/s is the initial out-of-straightness of the brace panel, and β is the effective lateral (perpendicular) brace stiffness (Yura, 1993, also refer to Figure 2.3 and Appendix B.2). The ratio M/h represents an equivalent compressive beam flange force and is applicable for both the elastic and inelastic regions. Predicted values were obtained both considering and not considering the effects of shortening. Shortening increases the brace forces by effectively increasing the out-of-straightness of a brace panel. The initial out-of-straightness term Δ_o is replaced by $\Delta_o+\Delta_{sh}$. Brace geometries with larger brace angles (fewer brace panels) exhibit larger brace force increases because Δ_{sh} is greater for larger brace angles.

A comparison between the brace forces calculated using Equation (5.8) and the experimentally measured values obtained in test R10-W is shown in Figure 5.7. The average initial out-of-straightness values of 0.003 and 0.0045 for were used for brace panels three and four, respectively (see Table A.5). Brace force predictions when the effects of shortening were not considered compared favorably with the measured results for P3 but underestimated P4. When shortening was considered, calculated values agreed well with measured results for P4 but overestimated P3. Differences between calculated and measured results stem from both the sensitivity to the value chosen for the initial out-of-straightness, as well as the theoretical predicted deflections due to shortening. Results obtained using Equation (5.8), however, follow the general trend exhibited by the measured brace forces.

Cross-strut forces can be determined from the value of the diagonal brace forces and the brace geometry. Using the measured diagonal brace force in the fourth brace panel of test R10-W, the two cross-strut forces for that panel were calculated using simple statics. The small compressive force associated with buckling of the compression diagonal was ignored. A comparison of the measured and calculated values is shown in Figure 5.8. The calculated cross-strut force compares favorably with the average of the two measured forces. The difference between the two strut forces was due to the lateral bending stiffness of the flanges.

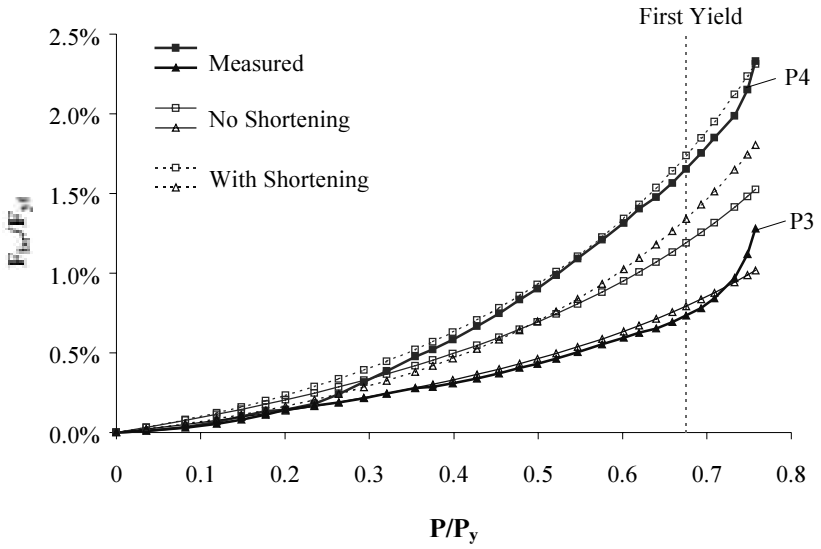

Figure 5.7 Comparison of Measured and Calculated Brace Forces (R10-W)

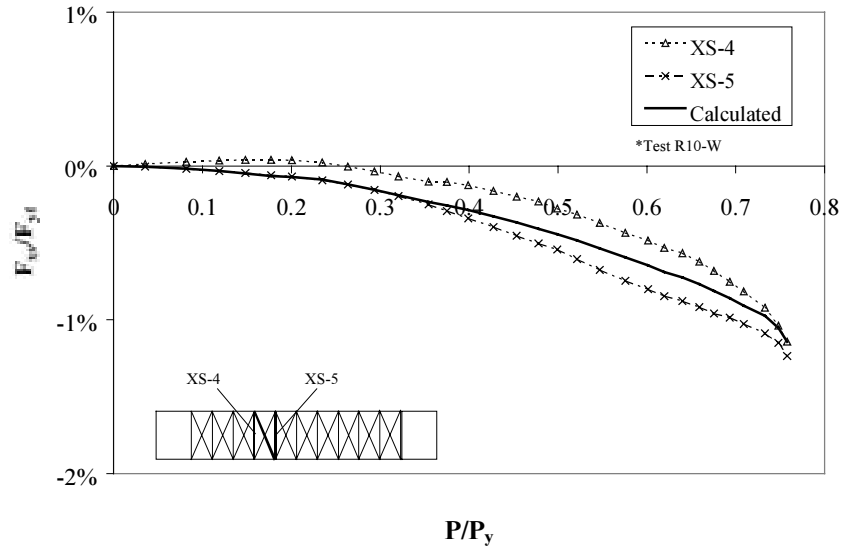

Figure 5.8 Comparison of Calculated and Measured Cross-Strut Forces

5.5 COMPARISON OF BUCKLED SHAPES

The buckled shape of the girder for all the test cases was two-waves between the supports. A comparison of the buckled shapes for the various test cases at similar load levels is shown in Figure 5.9. Despite variations in the brace spacing or stiffness, the eventual buckled shape of the girder remained the same.

The diagonal bracing was unable to force a higher buckling mode partly because of the effects of shortening. Even for an infinitely stiff tension-only brace, shortening would accommodate some lateral deflection of the top flanges. As a result, the girder would be able to deflect into its preferred buckled shape. In this case, the torsional restraint of the bottom flange made the preferred shape two-waves.

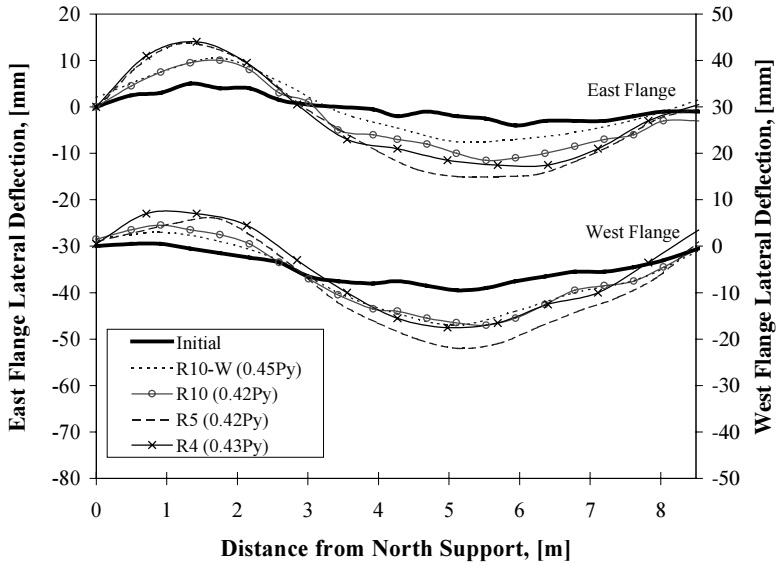

Figure 5.9 Comparison of Deflected Shapes for Different Brace Geometries

5.6 TENSION-ONLY VS. TENSION-COMPRESSION BRACING SYSTEMS

Unlike tension-only bracing systems, tension-compression X-brace systems increase the bending stiffness of the girder by attracting a portion of the flange stresses. The bending behavior of a girder with a tension-compression top-flange lateral bracing system can be analyzed by effectively increasing the area of the top flanges (Fan, 1999).

Girder shortening affects both tension-only and tension-compression systems alike. The difference between the two systems is tension-compression systems have a nominal compressive resistance. As the panel attempts to distort, the compression brace can help prevent such movement. However, since the buckling capacity of the diagonal braces is typically very low, design neglects the stiffness provided by the braces in compression. For X-brace systems, only two braces, one in each of the adjacent brace panels, and not four are considered to contribute to the lateral brace stiffness at a particular brace point.

The advantage of the tension-compression system is the increase in girder stiffness that the bracing provides. By attracting some of the girder bending stresses, the bracing reduces the flange stresses. This in turn increases the load at which the flanges will buckle and decreases the effects of shortening. The drawback of a tension-compression system is the diagonal braces attract large axial and bending forces (Fan, 1999). Therefore, the connection detailing must have adequate ductility to accommodate brace buckling.

5.7 EFFECTIVENESS OF METAL DECK BRACING

The pilot tests involving the metal deck panels used as a top lateral bracing system qualitatively demonstrated increases in the bending strength for similar to the X-brace system. A comparison of load-deflection responses between the X-brace and metal deck tests, shown in Figure 5.10, illustrates similar reductions in the lateral deflections when the bracing systems are used. These decreased lateral deflections for a given load level are indicative of higher girder buckling loads.

Although the cross sections of the X-brace and metal deck tests were different, both girders had similar cross-sectional properties. The moment of inertia of the trapezoidal girder was approximately 15% less than that the rectangular girder. As a result, the trapezoidal girder required smaller applied loads to

produce the same stress level in the top flanges. It should be noted that the load parameter used in Figure 5.10 is normalized by the yield loads for each of the respective girder cross sections. This effectively presents the load as a level of stress in the flanges and provides a reasonable foundation for comparison.

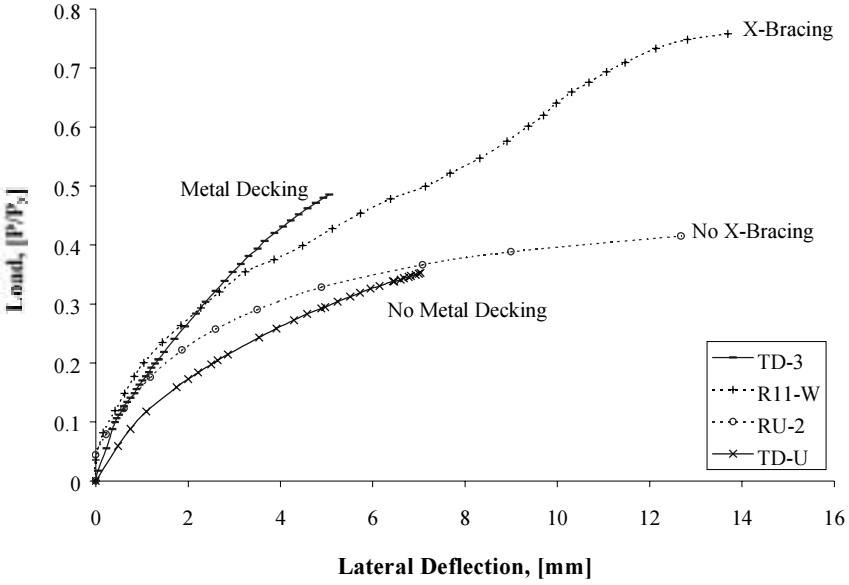

Figure 5.10 Comparison of Load-Deflection Responses Between X-Brace and Metal Deck Bracing Systems

Several differences beyond the cross sections of the specimens existed between the two test groups. The connectors on the metal deck tests had considerably closer spacing than the brace points in the X-brace tests. However, test TD-3 had an unbraced length at midspan equal to twice the unbraced length of R11-W. Finally, the outermost deck panels of test TD-3 extended past the support cross frames while the outermost brace point in R11-W was located just to the interior of the cross frames.

Significant changes in the load versus lateral deflection response occurred with both test specimens when the top lateral bracing systems were installed. The addition of the X-brace top lateral system in test R11-W increased the buckling capacity of the rectangular girder by 62%. An indication of this buckling strength increase was demonstrated by the decrease in lateral deflections of the top flanges. The smaller lateral deflections reduced second-order effects, lowering the stress levels in the top flanges. The metal deck bracing system produced similar changes in the lateral deflection response of the trapezoidal girder, which qualitatively demonstrates the increase in bending strength that the metal deck bracing system provided. In addition, the decrease in lateral stiffness exhibited by R11-W at approximately $0.4P_y$ did not occur in the metal deck tests. This phenomenon was most likely due to the effects of shortening. Because the metal decking is not susceptible to the problems associated with shortening, the stiffness decrease did not appear.

Although there were differences between the X-brace and metal deck bracing tests, the general behavior associated with the addition of the metal deck panels appeared to provide similar increases in buckling strength that the X-brace system did. Although an ultimate load capacity test was not run because the specimen was needed for other experiments, the performance of the metal deck bracing system appeared to perform better than or at worst equal to the X-brace system.

CHAPTER 6
Summary and Conclusions

6.1 SUMMARY

Steel box girder systems are being used more frequently for curved bridges because of their torsional stiffness and aesthetic appearance. These systems typically consist of U-shaped girders placed side-by-side with a composite concrete deck acting as the top flange. A critical design stage for these girders occurs during casting of the bridge deck, when the non-composite steel section must support the entire construction load, including the wet concrete. During this period the top flanges are in compression and are susceptible to lateral-torsional buckling. Lateral bracing, typically in the form of a horizontal truss system, is installed to prevent the flanges from buckling and to increase the torsional stiffness of the girders. There is currently no existing codified design method for the lateral bracing of U-shaped girders. Motivation for minimizing the bracing stems from the fact that the bracing represents a significant portion of a girder's weight and cost, and is also not utilized once the concrete deck has cured.

In order to develop a design procedure, it was first necessary to understand the effect of the top-flange lateral bracing on the buckling strength of U-shaped girders. An analytical study was conducted using elastic finite element modeling. Bifurcation loads and buckling modes obtained in the analysis were used to guide the selection of appropriate experimental test cases. Experimental tests were then conducted on scale models of a rectangular and trapezoidal U-shaped girder. Variable parameters included brace stiffness, geometry, initial pretension force, and connection detail. The two types of bracing systems investigated were an X-brace truss system and metal deck panels fixed to the top flanges. Experimental test results provided girder buckling loads and buckled shapes to compare with the analytical results. Brace forces, which could not be obtained in the analytical program, were measured to compare with current design provisions. Lastly, the performance of the metal deck bracing system was evaluated through comparison with the truss-type system.

6.2 CONCLUSIONS

Experimental tests demonstrated significant increases in the buckling strength of a U-shaped girder with a top-flange lateral bracing. As with all bracing systems, the effectiveness of the bracing depends on its stiffness. Poor connection detailing in early test cases reduced the effective stiffness of the bracing system to a point that only marginal increases in buckling capacity were observed. The modified connection detail resulted in a 66% increase in buckling capacity over the unbraced case. The unbraced buckling strength was 47% of the load necessary to cause yielding in the top flanges.

In addition to the importance of the connection stiffness, the effects of shortening were found to decrease the effectiveness of the bracing. Current design provisions for U-shaped girders consider brace points as unyielding supports. Current bracing design recommendations for stability of the top flange (Yura et al, 1992; Yura, 1993), $F_{br} = 0.004$ M/h assume an initial out-of-straightness, $\Delta_o = 0.002s$. The flexural resistance of a girder, which is normally controlled by lateral torsional buckling, is calculated using the distance between brace points as the unbraced length. Since the actual bracing only prevents the relative movement between adjacent brace points, it is susceptible to the detrimental effects of girder shortening. Bending of the girder causes the brace panels to shorten, which introduces slack in the diagonal brace members. As a result, lateral displacement of the top flanges must occur before the braces can return to their original length and subsequently engage. This lateral displacement increases the second-order bending stresses in the top flanges, which reduce the girder's bending capacity. Current design provisions do not account for the effects of shortening. For the test case with the welded X-brace connection detail,

the experimental load capacity of $0.76P_y$ was 25% less than the nominal flexural resistance of $0.95P_y$ calculated using current specifications. A simple allowable stress analysis that accounted for the effects of shortening predicted a flexural resistance of $0.72P_y$, within 5% of the experimental capacity.

Brace forces obtained from the experimental tests compared favorably with theoretical predictions. Calculated diagonal brace forces determined using methods by which current code provisions are based on followed the general trends exhibited by the experimentally measured brace forces. Differences observed were attributed to the calculated values being directly proportional to the initial-out-of-straightness of each brace panel. The test results, however, lend support to the fundamental theory by which current brace force predictions are made. The maximum measured diagonal and cross-strut brace forces reached 2.3% and 1.2% of the force necessary to cause yielding in both flanges, respectively.

Since diagonal bracing systems on the top flange are susceptible to shortening, Δ_{sh}, the brace force design recommendations given in Yura (1992) should be adjusted by Eq. (5.3) as follows:

$$F_{br} = 0.004 \frac{M}{h} \left[\frac{0.002 + (s\Delta_{sh} / b)}{0.002} \right] \qquad (6.1)$$

The preliminary results from pilot tests involving metal deck panels as the top lateral bracing system qualitatively demonstrated buckling capacity increases similar to the welded X-brace system. Although the tests did not bring the girder to failure, the similar decrease in the lateral deflections of the top flanges indicated similar increases in the buckling capacity. In addition, the detrimental effects of shortening were not evident in the metal deck tests because metal deck panels are not susceptible to the effects of shortening. The increase in buckling capacity provided by the metal deck panels appeared to perform equally or better than the welded X-brace system.

Other conclusions were:

1. The Southwell predicted buckling loads might not be reliable when the buckled shape is more complicated than a sine wave. The deformed shape of the test girder may have deviated from the sine wave because of the presence of the top-flange lateral bracing.
2. The tension diagonal braces acted as brace points for compression diagonal braces, reducing their unbraced length by one-half.

6.3 FUTURE RESEARCH

The results of the experimental program showed the increase in buckling capacity that a lateral bracing system could provide. Because of the problems associated with the removable connection detail, only one welded brace stiffness/geometry case was conducted. Additional tests may be necessary to verify that variation in brace stiffness and geometry can be adequately predicted using the current analytical models. Large displacement analyses may also be necessary to better understand the brace forces that are developed in relative bracing systems.

In addition to providing stability to the top flanges during bending, top lateral bracing systems effectively close the section and increase the torsional rigidity of a U-girder. Brace forces due to torsion in these curved girders have been predicted analytically and measured in the field (Fan, 1999), but experimental data is currently limited to only single-diagonal bracing systems.

Finally, the preliminary results from pilot tests conducted in this research study showed promising potential for the use of the corrugated metal decking as a top lateral bracing system for U-shaped girders. More extensive tests may be necessary to quantify the increase in bending strength the decking provides. In addition, the failure mechanism and demands on the fasteners are not yet known.

Part II: Torsional Behavior

CHAPTER 7
Experimental Program

7.1 GENERAL

Where Part I of this research study investigated the bending and buckling behavior, Part II focuses on the torsional behavior of U-shaped girders with top lateral bracing systems. A series of six pilot tests were conducted as a preliminary investigation to evaluate the potential capability of permanent metal deck forms to torsionally stiffen U-shaped girders. The variable parameters in these tests were the number and distribution of deck panels attached to the top flanges.

The test specimen in these tests was the trapezoidal girder used in the bending behavior experiments described in Section 3.2. The cross-sectional properties of the trapezoidal girder are shown in Figure 3.4. The girder was 12.19 m (40 ft.) long and simply supported over an 8.53m (28 ft.) span with 1.83 m (6 ft.) overhangs at each end. Loading was applied near midspan of the girder and produced a concentrated torsional moment as shown in Figure 7.1.

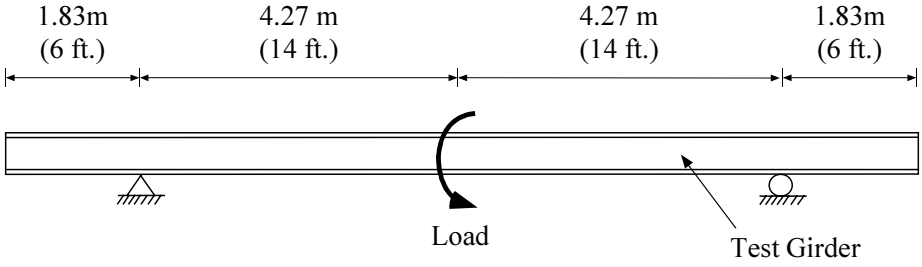

Figure 7.1 Profile of Test Setup

7.2 TEST SETUP

7.2.1 Loading and Support System

The support system for the torsional tests was also the same system used in the bending behavior tests described in Section 3.2.2. In addition to the four internal cross frames located at the girder ends and supports, an additional cross frame was placed at the location of the concentrated load as shown in Figure 7.2. This internal cross frame was used to control distortion of the cross section and also aided in transferring the torsional moment to the girder.

Load was applied to the specimen through a beam placed across the top flanges near midspan of the girder, as shown in Figure 7.3. The application of a tensile load by the hydraulic ram produced the concentrated torque. A plate welded between the loading beam and internal cross frame allowed the force transfer to occur primarily through the cross frame and not solely through the top flanges.

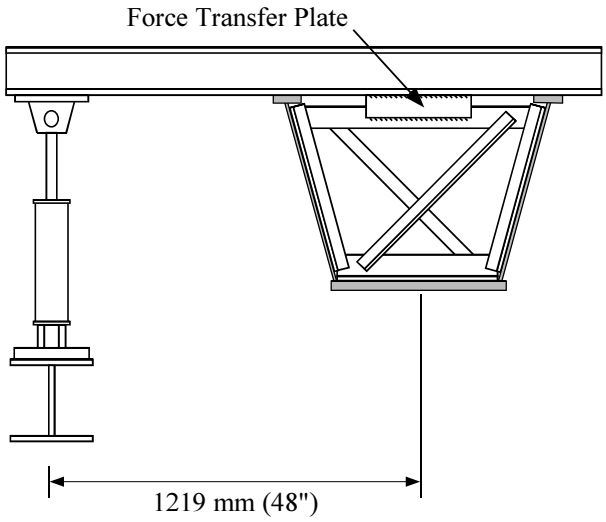

Figure 7.2 Cross Section of Test Setup at Load Point

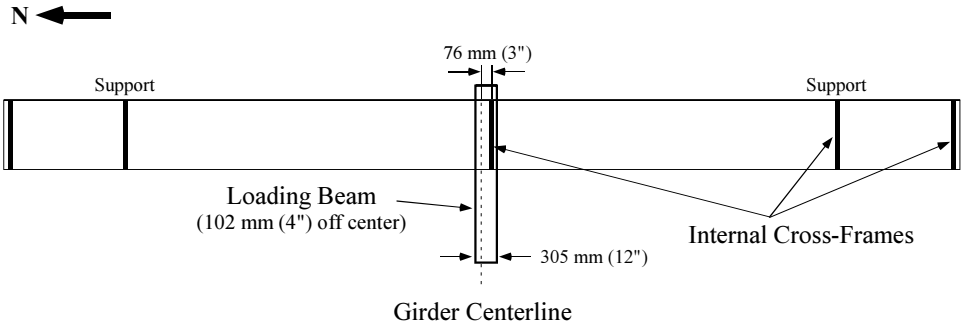

Figure 7.3 Plan View of Test Setup

7.2.2 Instrumentation

Girder rotations were measured using bubble levels placed at the load point and south support. The bubble levels, pictured in Figure 7.4, had a precision of 0.001 radians. To account for support movements, the rotation at the support was measured so the differential rotation between the load point and support could be obtained.

Figure 7.4 Bubble Level at South Support

7.2.3 Bracing System

The top-flange bracing used in the torsional stiffness tests were the metal deck panels used in the bending behavior tests described in Section 3.4. The form deck was selected out of convenience from surplus. The panels were attached to the top flanges in the same manner using Hilti ENPH2-21-L15 powder actuated fasteners. A single fastener was used in every corrugation valley.

7.3 TEST CASES

Six test cases were used to investigate the effect of the metal decking on the torsional stiffness of the girder. Initially, the girder was fully braced between the supports using ten deck panels. Each subsequent test case removed a pair of panels with the final unbraced test case having no top-flange bracing. The test cases are summarized in Figure 7.5.

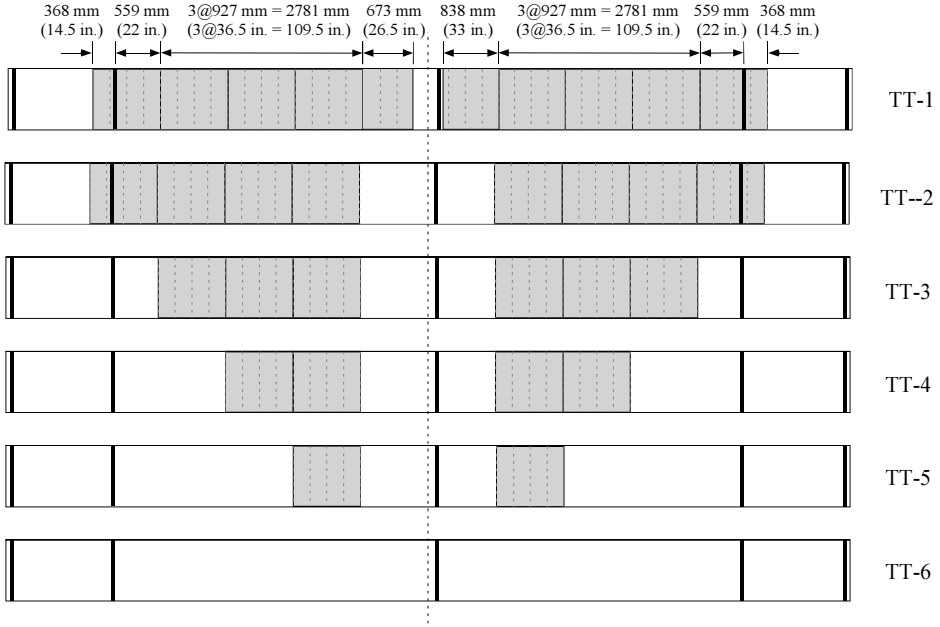

Figure 7.5 Torsional Stiffness Test Cases

CHAPTER 8
Test Results

8.1 TORSIONAL STIFFNESS

The results from the torsional stiffness tests are summarized in Table 8.1. The torsional stiffness values presented in Table 8.1 represent the concentrated torque necessary at midspan to produce a relative unit rotation between midspan and the support. Torque-twist curves obtained from each test are shown in Figure 8.1.

Table 8.1 Torsional Stiffness Test Results

Test Case	Torsional Stiffness [KN-m/rad]	% Increase Above Unbraced
TT-1	1065	77 %
TT-2	1001	67 %
TT-3	871	45 %
TT-4	724	21 %
TT-5	654	9 %
TT-6	600	--

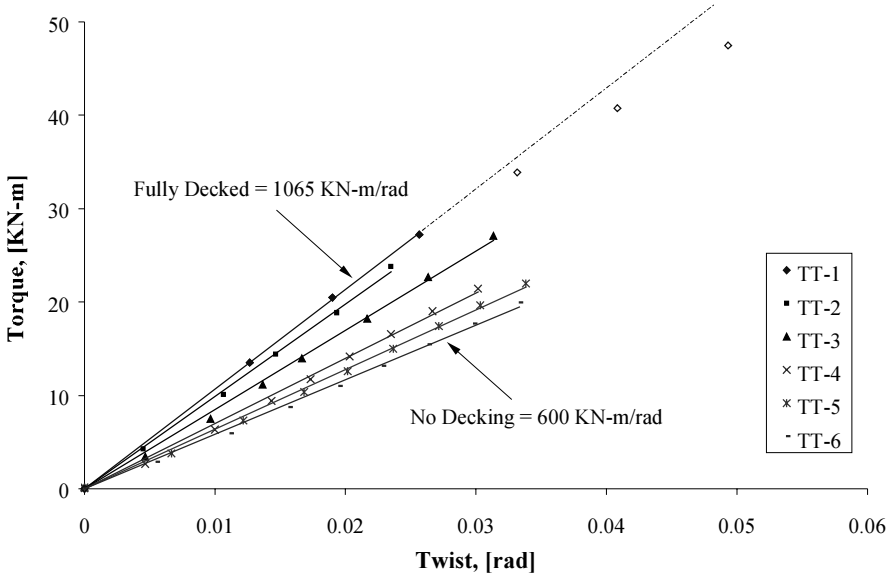

Figure 8.1 Torque-Twist Curves

The torsional stiffness for each test case was determined using a linear regression analysis. The test cases exhibited generally linear load-deflection responses. Test case TT-1 began to deviate from linear above applied loads of approximately 27 KN-m (3.1 kip-in). The torsional stiffness for test case TT-1 was

determined using only the linear data points. Those data points not included in the regression analysis for TT-1 are denoted by outlined symbols. As expected, the torsional stiffness of the girder increased with increasing numbers of deck panels attached to the top flanges. The fully braced test case TT-1 represented a 77% increase in torsional stiffness above the unbraced test case TT-6.

8.2 DECK DISTORTION

During testing, the metal deck panels visibly distorted as shown in Figure 8.2. The presence of rib stiffeners in the center of the corrugation valleys required some fasteners to be offset to one side. As the girder was loaded, the unfastened portions visibly pulled away from the flanges as seen in Figure 8.3. This phenomenon occurred with all the deck panels along the length of the girder.

Figure 8.2 Metal Deck Distortion

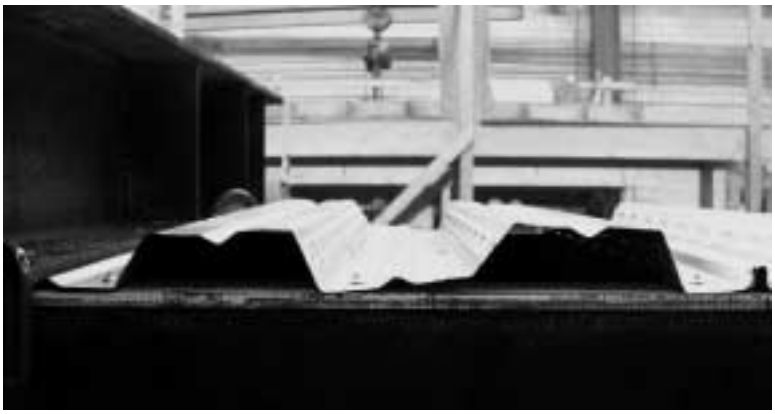

Figure 8.3 Deck Pulling Away From Top Flanges

CHAPTER 9
Analysis of Results

9.1 BACKGROUND

Members subjected to torsion have a distinguishing feature in that plane sections do not remain plane when loaded. This phenomenon causes the cross sections of members to warp. Certain sections that do not warp include circular sections and thin-walled sections in which all elements intersect at one point, such as a cruciform, angle, or tee. Depending on whether the cross section is free to warp, there is a distinction that is made between *uniform* (also referred to as pure or St. Venant) and *nonuniform* (or warping) torsion. Pure torsion resists the applied load through shear stresses in the plane of the cross sections. During loading, displacements occur both in and out-of-plane. If warping is unrestrained, the out-of-plane displacements do not induce any normal stresses. If warping is restrained, however, the out-of-plane displacements cause normal stresses to develop. The resulting normal stresses induce warping shears, which provide an additional torsional restraining moment. This moment, known as the warping torsional moment, along with the pure torsional moment combine to keep the system in equilibrium.

9.1.1 Pure Torsion

The basic governing equation for an elastic member subjected to pure torsion is given by (Basler and Kollbrunner, 1969)

$$T = GK_T\phi' \tag{9.1}$$

where T is the applied torque, G is the shear modulus of the material, K_T is the pure torsional constant, and ϕ' is the twisting angle per unit length. The pure torsional constant for open sections comprised of narrow rectangular elements can be approximated by (Basler and Kollbrunner, 1969)

$$K_T = \frac{1}{3}\sum_{i=1}^{n} b_i t_i^3 \tag{9.2}$$

where b_i and t_i are the width and thickness of each element, respectively. For closed sections, the pure torsional constant is

$$K_T = \frac{4A_o^2}{\oint \frac{1}{t(s)}\,ds} \tag{9.3}$$

where A_o is the area enclosed by the centerline of the walls and $t(s)$ is the wall thickness along the member arc length s. If the hollow cross section is made up of n elements, each of thickness t_i and width b_i, then the contour integral can be replaced with

$$\oint \frac{1}{t(s)}\,ds = \sum_{i=1}^{n} \frac{b_i}{t_i} \tag{9.4}$$

The expression for the pure torsional constant for closed shapes then becomes

$$K_T = \frac{4A_o^2}{\sum_{i=1}^{n} \frac{b_i}{t_i}} \tag{9.5}$$

9.1.2 Warping Torsion

The basic governing equation for an elastic member subjected to warping torsion is given by (Basler and Kollbrunner, 1969)

$$T = -EI_w\phi''' \tag{9.6}$$

where E is the modulus of elasticity and I_w is the warping torsion constant. The warping torsional properties for any general shape can most readily be obtained using a numerical procedure which utilizes finite difference relations. Many cross sections can be simplified by considering the section to be composed of a series of interconnected narrow, rectangular elements (Basler and Kollbrunner, 1969). Details of this procedure are presented in various references and will not be discussed beyond the example calculations provided in Appendix C.1 (Basler and Kollbrunner, 1969; Heins 1975).

9.1.3 Combined Pure and Warping Torsion

In most engineering applications, a member will resist torsional loads with both pure and warping torsional stresses. The combined torsional resistance becomes the sum of both the pure and warping components. As a result, the governing differential equation becomes

$$T = GK_T\phi'' - EI_w\phi''' \tag{9.7}$$

The relative proportion of each type of torsion present in a member depends on both its length and cross section. The parameter χ is used to determine whether pure or warping torsion predominates. This parameter is related to the member length as well as the ratio of the pure torsional rigidity GK_T and the warping torsional rigidity EI_w.

$$\chi = L\sqrt{\frac{GK_T}{EI_w}} \tag{9.8}$$

The torsional predominance of a member based on the value of the parameter χ is given in Table 9.1 (Basler and Kollbrunner, 1969).

Table 9.1 Pure and Warping Torsional Predominance

Torsional Predominance	χ
Pure Warping	< 0.3
Dominating Warping	0.3 - 2
Mixed	2 - 5
Dominating Saint-Venant	5 - 10
Pure Saint-Venant	> 10

Members dominated by one type of torsion can be approximately analyzed by neglecting the other type of torsion. For thin-walled open cross sections, Saint-Venant torsion dominates long members and warping in short ones (Basler and Kollbrunner, 1969). For idealized systems, the boundary conditions for twist and warping are summarized in Table 9.2.

Table 9.2 Idealized Boundary Conditions

Twist Restrained	$\phi = 0$
Warping Restrained	$\phi' = 0$
Warping Unrestrained	$\phi'' = 0$

9.2 UNBRACED TEST CASE

9.2.1 Upper and Lower Bound Theoretical Solutions

The results from the unbraced torsional stiffness test TT-6 were compared with theoretical predictions that account for the combined effects of pure and warping torsion. The theoretical stiffness of the unbraced section was determined by solving Equation (9.7) with the appropriate boundary conditions. The idealized structure consisted of the main span between the supports, fixed against twist at the ends as seen in Figure 9.1.

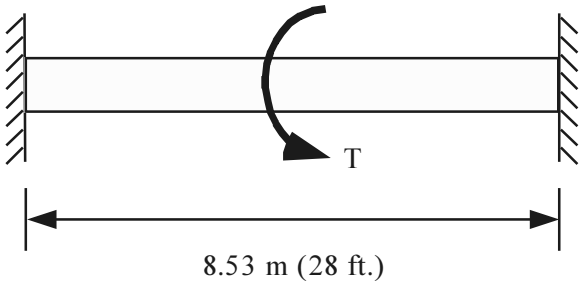

Figure 9.1 Idealized Model for Torsion Tests

Additional boundary conditions imposed were dependent on the warping restraint at the supports. The presence of cross-frames at the supports of the test specimen prevented twist but provided minimal warping restraint. The attachment of the bottom flange to the support beam produced a partial warping restraint condition. Imposing full warping restraint at the ends produced an upper bound solution while no warping restraint produced a lower bound solution. The upper and lower bound torsional stiffnesses were 1430 KN-m/rad (12660 kip-in/rad) and 386 KN-m/rad (3412 kip-in/rad), respectively. Detailed calculations may be found in Appendix C.2.

The comparison of analytical and experimental results for the unbraced test case TT-6 is shown in Figure 9.2. The experimental stiffness relative to the upper and lower bound solutions indicates the degree of warping restraint actually present in the test.

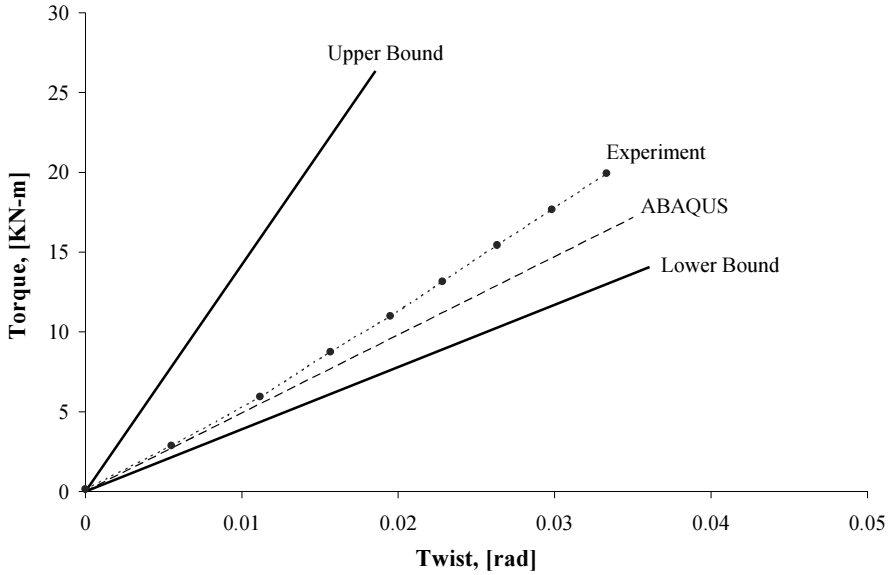

Figure 9.2 Torsional Response of Unbraced Test Case TT-6

9.2.2 Finite Element Analysis

To capture the effects of the partial warping restraint provided by the supports in the experimental test, a 3-dimensional finite element model was created using the commercial software package ABAQUS. Four-noded shell elements were used to model the girder, support beams, and internal cross-frames as seen in Figure 9.3. The loading beam was modeled using a rigid beam element connected to the top flanges and midspan diaphragm. The thickness of the diaphragms used to model the cross-frames was approximated. Variations in the thickness of the internal diaphragms had little effect on the overall torsional behavior. A comparison between the finite element solution and the experimental results is shown in Figure 9.2. The response predicted by the finite element model was 491 KN-m/rad (4345 kip-in/rad) and correlates reasonably well with the experimental results.

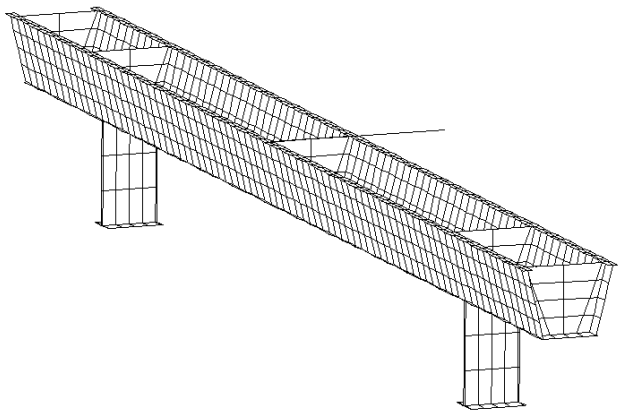

Figure 9.3 Finite Element Model for Torsion Tests

9.3 FULLY BRACED TEST CASE

9.3.1 Background

Closed cross sections are generally thousands of times stiffer than comparable open cross sections in torsion. For pseudo-closed members, such as U-shaped girders with top lateral truss systems, the increase is typically several orders of magnitude less. The reason is that the equivalent plate thickness of the bracing systems is usually very small compared to the thickness of the other plate elements comprising the cross section. Since the warping torsional component of closed sections tend to be negligible, the torsional stiffness is controlled by the pure torsion constant as defined in Equation (9.5).

Blank (1973) conducted torsion tests on open box sections stiffened using cold formed decking. The sections tested, however, consisted of channel sections connected on top and bottom by decking to form a closed-section. Although the aspect ratio is outside of the applicability for U-shaped girders, the results indicated the potential for cold formed decking to torsionally stiffen open sections. Test results showed torsional stiffness increases between 3 and 10 times. In addition, it was found that fastener slip significantly affected the torsional stiffness. McDonald et. al. (1976) tested rectangular open sections with top-lateral truss systems in combinations of bending and torsion. The torsional stiffness of the pseudo-closed sections were approximately 4 times greater than the theoretical open section. In addition, forces generated in the top-lateral bracing were reasonably predicted using the equivalent plate theory.

9.3.2 Comparison Between Theory and Experiment

The theoretical torsional stiffness of the fully braced test case was determined by estimating an equivalent plate thickness for the permanent metal deck forms. This equivalent thickness corresponded to a flat plate with the same shear stiffness as the deck forms. The Steel Deck Institute Diaphragm Design Manual was used to determine the shear stiffness of the decking (SDI 1981, 1995). Previous work by Currah (1993) has shown good agreement between the SDI deck stiffness and experimental tests. In general, the shear stiffness of deck panels is routinely an order of magnitude more flexible than flat continuous plates of similar thickness. In addition, the stiffness is primarily dependent on the cross-sectional properties of the decking and the fastener arrangement. The equivalent plate thickness of the decking was calculated to be 0.0607 mm (0.00239 in.). The corresponding theoretical stiffness of the fully decked girder was 1586 KN-m/rad (14040 kip-in/rad), versus 1065 KN-m/rad (9423 kip-in/rad) obtained from the experimental test. Detailed calculations may be found in Appendix C.3.

Differences between the theoretical and experimental stiffnesses of the fully-braced girder may be partially attributed to the fastener placement. The shear stiffness relationships developed by SDI were based on the assumption that fasteners were located in the center of each corrugation valley. Actual locations of fasteners in the experimental tests were offset as seen in Figure 8.3. In addition, the application of the equivalent plate theory is an approximate method. The correlation between theory and experiment is similar to what has been observed by others (Blank, 1973, McDonald et. al., 1976, Rao, 1964).

The experimental torsional stiffness of the fully decked girder was only 1.77 times greater than that of the unbraced case. This modest increase is due to the fact that the deck panels were made of fairly light gage material. If the thickness of the base material were increased from 20 gage to 16 gage, the equivalent plate thickness would have increased to 0.237 mm (0.00935 in.). This would have theoretically resulted in a 10-fold increase in the torsional stiffness of the girder.

Article 1.29 of the *Guide Specification for Horizontally Curved Girders* (1993) has recommendations for the minimum area of top-lateral bracing. The basis for the recommendation comes from a study by Nakai and Heins (1977) that suggests the equivalent plate thickness should be greater than or equal to 1.27 mm (0.05 in.). Satisfying the minimum equivalent thickness requirement limits warping stresses to less than 5% of the bending stresses. Although most metal deck forms have equivalent plate thicknesses that are less than 1.27 mm (0.05 in.), use of metal deck forms as top-lateral bracing may still be very useful to the

design engineer. The permanent metal deck forms could provide supplemental bracing in highly stressed regions during critical concrete pours.

CHAPTER 10
Summary and Conclusions

10.1 SUMMARY

Unbraced U-shaped girders with open cross sections have low torsional stiffness. In order to resist the torsional moments encountered during erection and curing of the concrete deck, top lateral bracing is installed. This bracing creates a psuedo-closed section that dramatically increases the girder's torsional stiffness. Steel metal decking, which is used as the formwork for the concrete deck, may alone provide the necessary torsional stiffness needed during girder erection. The torsional behavior of U-shaped girders with a metal deck top lateral bracing system was studied through a series of pilot tests. These tests, conducted on a one-quarter scale trapezoidal girder, were performed to evaluate the potential stiffening capabilities of metal decking.

10.2 CONCLUSIONS

The torsional stiffness of the unbraced trapezoidal girder was reasonably predicted using classical torsion theory. Upper and lower bound theoretical solutions were developed which accounted for full and no warping restraint conditions at the supports. The experimental stiffness fell within the theoretical solutions due to the partial warping restraint condition created by the actual test supports.

The torsional stiffness of the girder that was fully braced with permanent metal deck forms was reasonably predicted using deck shear stiffness relationships developed by the Steel Deck Institute and the equivalent plate theory. The fully braced girder showed only a modest 77% increase in torsional stiffness due to the light-gage deck panels used in the test. The use thicker gage material for the deck panels would have theoretically increased the girder stiffness by 10 times.

10.3 FUTURE RESEARCH

The torsion tests conducted in this portion of the experimental program were conducted to investigate the potential stiffening capabilities of permanent metal deck forms. Thin gage decking used in the pilot test, however, was not able to substantially increase the torsional stiffness of the trapezoidal girder. Additional experimental tests are necessary to determine the stiffening capabilities of thicker gage decking and evaluate fastener demands to ensure adequate strength.

APPENDIX A

A.1 TENSILE TEST DATA

Table A.1 Tensile Test Data

	F_{uy} MPa (ksi)	F_{sy} MPa (ksi)	F_{uu} MPa (ksi)	F_{su} MPa (ksi)	% Elongation
Top Flange	342.2 (49.6)	323.2 (46.9)	467.9 (67.9)	-	-
	341.9 (49.6)	313.9 (45.5)	469.0 (68.0)	444.1 (64.4)	37.8%
	345.4 (50.1)	321.5 (46.6)	464.6 (67.4)	441.6 (64.0)	39.3%
	343.2 (49.8)	321.9 (46.7)	470.0 (68.2)	442.7 (64.2)	37.3%
	Average	**320.1 (46.4)**		**442.8 (64.2)**	
Web	322.1 (46.7)	300.6 (43.6)	425.5 (61.7)	401.1 (58.2)	27.9%
	324.5 (47.1)	299.7 (43.5)	492.5 (71.4)	443.4 (64.3)	28.9%
	Average	**300.2 (43.5)**		**422.3 (61.2)**	
Bottom Flange	328.9 (47.7)	309.3 (44.9)	468.2 (67.9)	440.5 (63.9)	25.4%
	337.1 (48.9)	320.2 (46.4)	475.9 (69.0)	446.8 (64.8)	27.3%
	Average	**314.8 (45.7)**		**443.6 (64.3)**	

F_{uy} – Upper Yield Stress
F_{sy} – Static Yield Stress (5 minutes)
F_{uu} – Upper Ultimate Stress
F_{su} – Static Ultimate Stress (5 Minutes)

A.2 COUPLER CALIBRATION FACTORS

Table A.2 Coupler Calibration Factors

Coupler #	Calibration Factor [KN/με]
1	0.0143
2	0.0153
3	0.0152
4	0.0149
5	0.0164
6	0.0168
7	0.0164
8	0.0157
9	0.0131
10	0.0149
11	0.0155
12	0.0182

A.3 OUT-OF-STRAIGHTNESS VALUES

Table A.3 Out-of-Straightness Values for 4 Brace Panel Tests

Brace Panel (from North)	**Panel Size**	**East**		**West**	
		Δ_o	Δ_o/s	Δ_o	Δ_o/s
	[mm]	**[mm]**		**[mm]**	
1	2134	4.3	0.0020	3.5	0.0016
2	2134	4.1	0.0019	5.0	0.0023
3	2134	3.3	0.0015	2.0	0.0009
4	2134	3.1	0.0015	6.5	0.0030
		Max =			**0.0030**

Table A.4 Out-of-Straightness Values for 5 Brace Panel Tests

Brace Panel (from North)	**Panel Size**	**East**		**West**	
		Δ_o	Δ_o/s	Δ_o	Δ_o/s
	[mm]	**[mm]**		**[mm]**	
1	1707	6.5	0.0038	3.5	0.0021
2	1707	5.5	0.0032	5.0	0.0029
3	1707	2.5	0.0015	1.0	0.0006
4	1707	0.5	0.0003	3.0	0.0018
5	1707	2.0	0.0012	6.0	0.0035
		Max =	**0.0038**		

Table A.5 Out-of-Straightness Values for 10 Brace Panel Tests

Brace Panel (from North)	Panel Size	East		West	
		Δ_o	Δ_o/s	Δ_o	Δ_o/s
	[mm]	[mm]		[mm]	
1	838	3.5	0.0042	0.5	0.0006
2	838	3.5	0.0042	1.5	0.0018
3	838	2.5	0.0030	2.5	0.0030
4	838	3.0	0.0036	4.5	0.0054
5	838	2.0	0.0024	2.0	0.0024
6	838	1.0	0.0012	1.5	0.0018
7	838	1.0	0.0012	2.5	0.0030
8	838	0.5	0.0006	3.0	0.0036
9	838	1.5	0.0018	1.0	0.0012
10	838	2.0	0.0024	5.0	0.0060
		Max =			**0.0060**

A.4 TEST R4-4

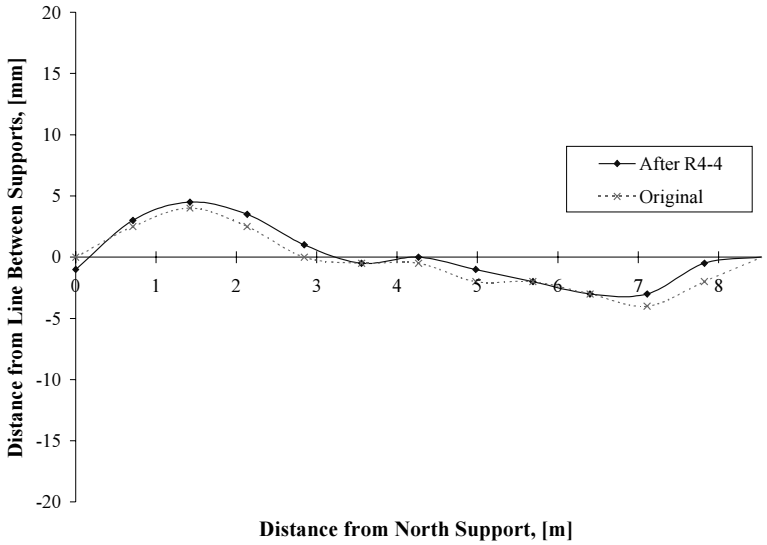

Figure A.1 Permanent Set of East Flange After Test R4-4

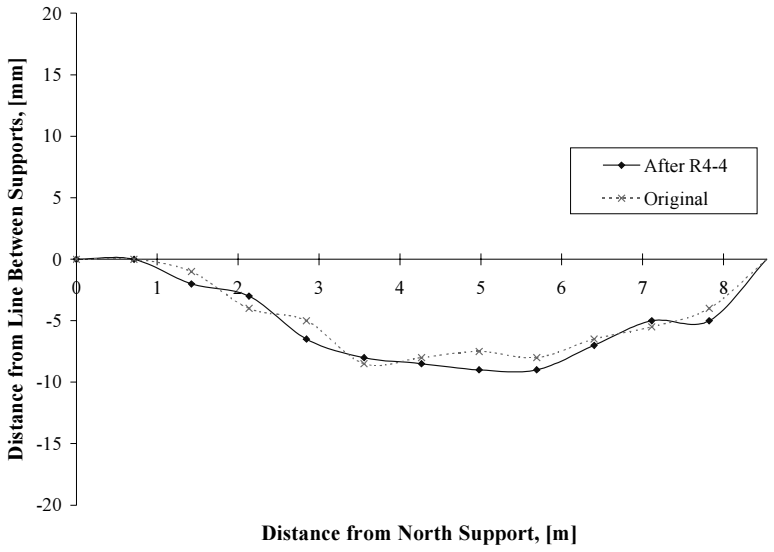

Figure A.2 Permanent Set of West Flange After Test R4-4

A.5 TEST R10-4

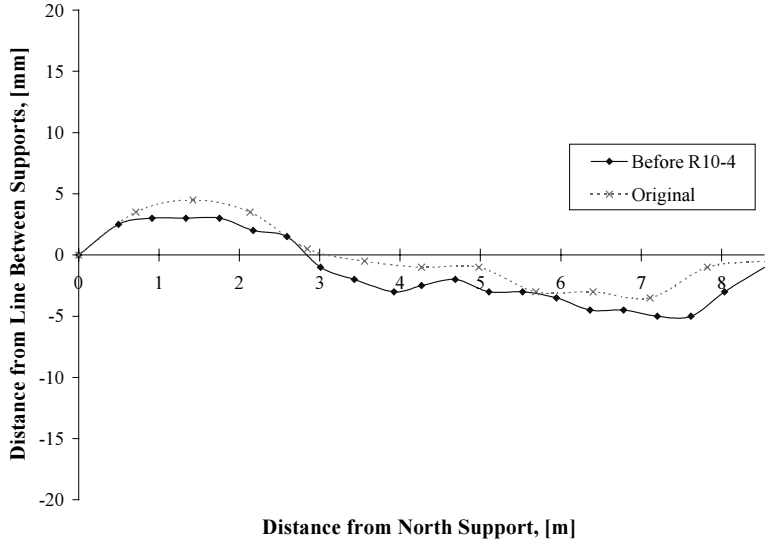

Figure A.3 Initial Imperfections of East Flange Before Test R10-4

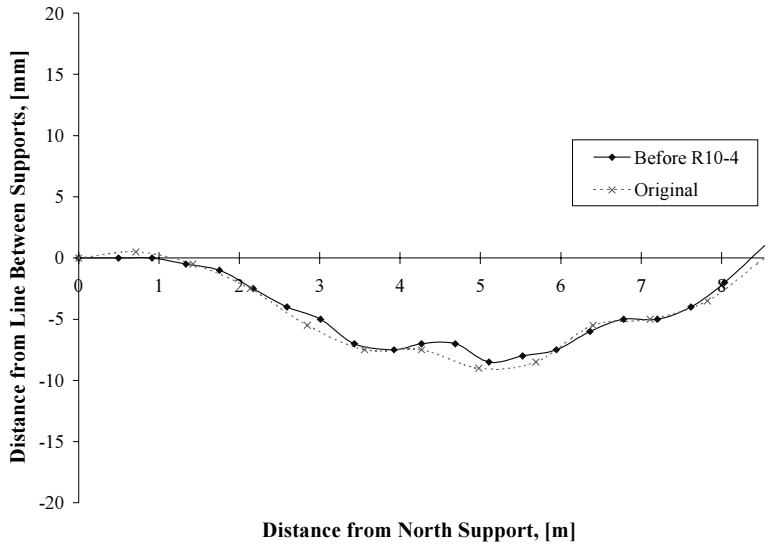

Figure A.4 Initial Imperfections of West Flange Before Test R10-4

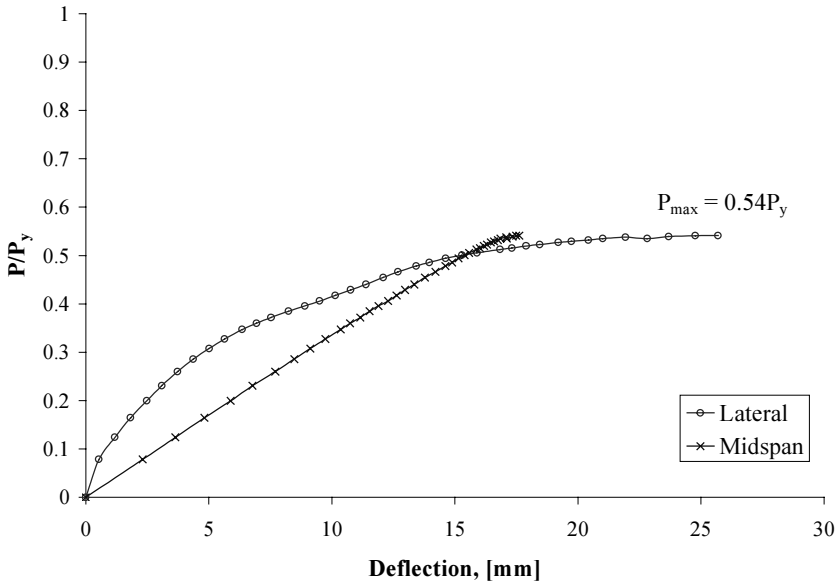

Figure A.5 Load-Deflection Response for Test R10-4

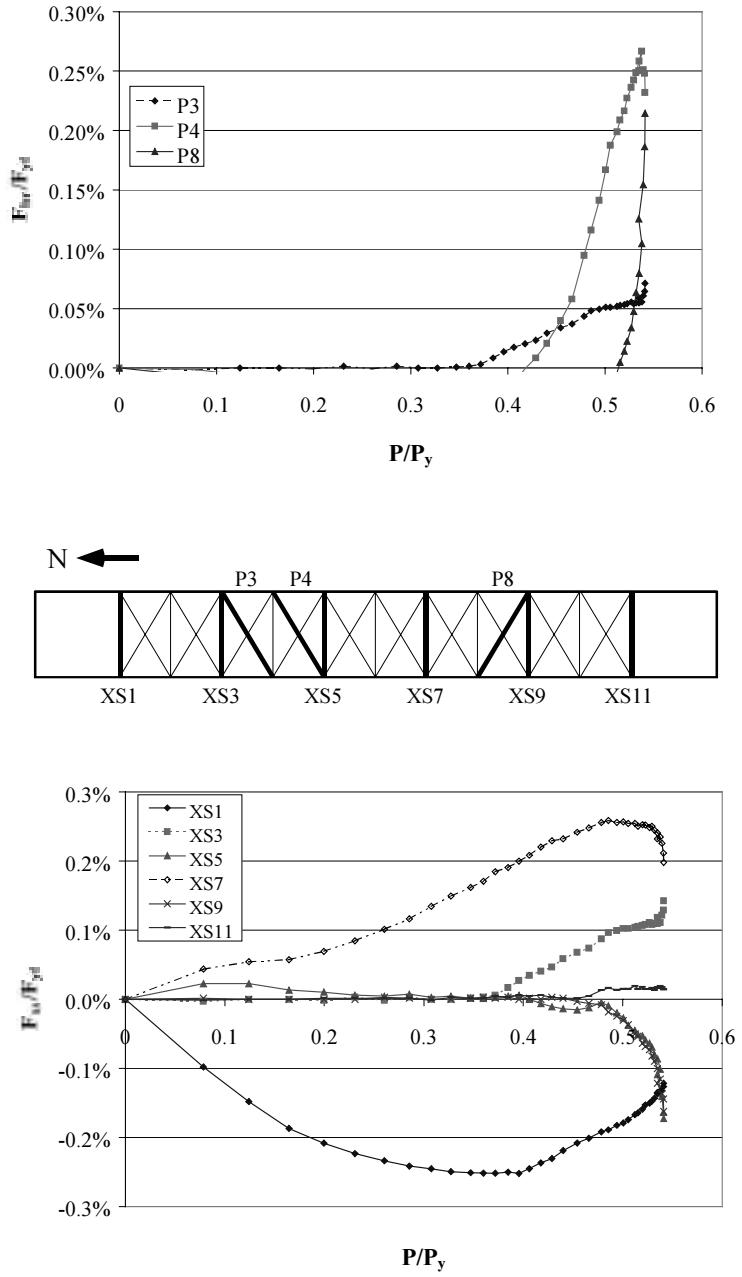

Figure A.6 Brace Force Distribution for Test R10-4

A.6 TEST R10-5

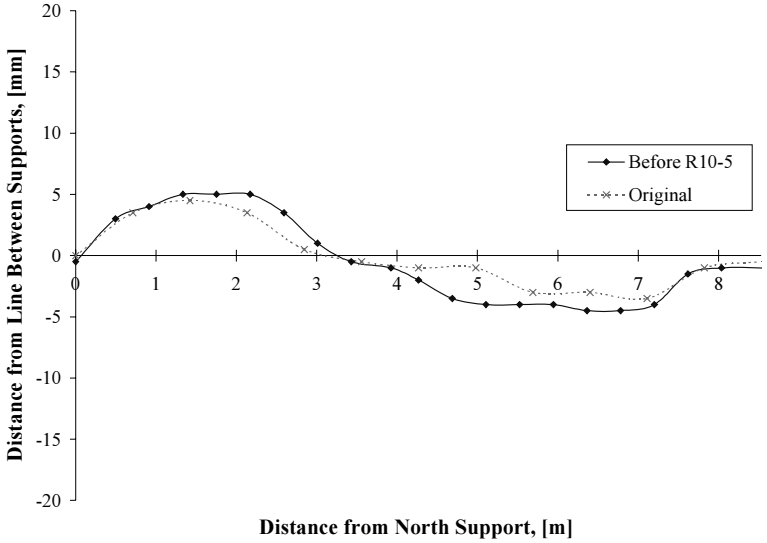

Figure A.7 Initial Imperfections of East Flange Before Test R10-5

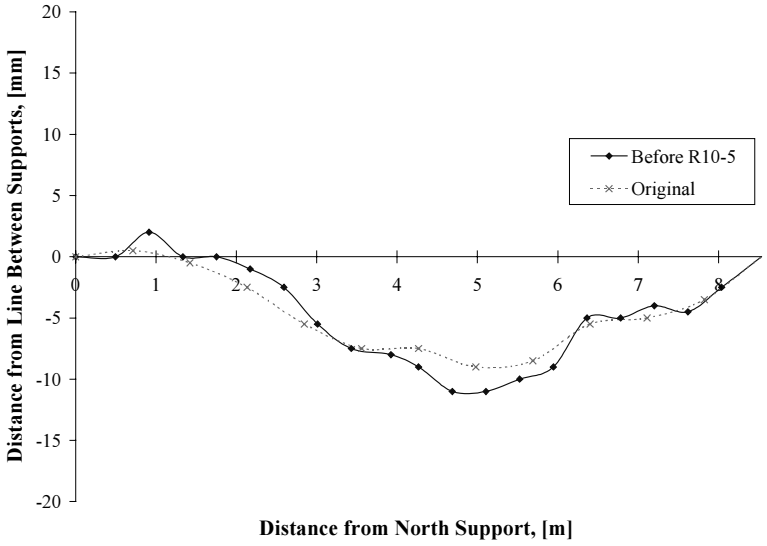

Figure A.8 Initial Imperfections of West Flange Before Test R10-5

APPENDIX B

B.1 CALCULATIONS FOR DESIGN FLEXURAL STRENGTH OF U-GIRDER

The flexural resistance of the U-girder used in the experimental program with top-flange lateral bracing was calculated using the *1998 AASTHO LRFD Bridge Design Specifications*. The equations used for lateral torsional buckling of noncompact sections are the same as those in the *AISC LRFD Specification for Steel Buildings*.

6.10.4.1.9 Noncompact Section Compression-Flange Bracing

$E = 29000\ \text{ksi}$

$F_{yc} = \text{Avg. Experimental Static Yield Stress} = 46.4\ \text{ksi}$ (see Appendix A1)

$$I_t = \frac{1}{12}(0.505)(3.056)^3 + \frac{1}{12}\left(\frac{24.813}{3}\right)(0.253)^3 = 1.21\ \text{in}^4$$

$$A_t = (0.505)(3.056) + \left(\frac{24.813}{3}\right)(0.253) = 3.64\ \text{in}^2$$

$$r_t = \sqrt{\frac{I_t}{A_t}} = \sqrt{\frac{1.21}{3.64}} = 0.58\ \text{in.}$$

$$L_p = 1.76 \cdot r_t \sqrt{\frac{E}{F_{yc}}} = 1.76 \cdot (0.58)\sqrt{\frac{29000}{46.4}} = 25.4\ \text{in}$$

Since all $L_b > L_p$ for all brace geometries considered, use 6.10.4.2.6

6.10.4.2.6 Noncompact Section Flexural Resistance Based Upon Lateral Torsional Buckling

$$D_c = \frac{I_x}{S_x} - t_f = \frac{2676}{155.0} - 0.505 = 16.8\ \text{in.}$$

$$\left[\frac{2D_c}{t_w} = \frac{2(16.8)}{0.253} = 132.5\right] > \left[\lambda_b \sqrt{\frac{E}{F_{yc}}} = 4.64\sqrt{\frac{29000}{46.4}} = 116\right]$$

where $\lambda_b = 4.64$ for members with compression - flange area

less than tension flange area

Calculate L_r

$$I_{yc} = \frac{1}{12} t_f b_f^3 = \frac{1}{12}(0.505)(3.056)^3 = 1.20 \text{ in}^4$$

$$S_{xc} = \frac{I_{yc}}{t_f/2} = \frac{1.20}{0.505/2} = 4.76 \text{ in}^3$$

$$d = 0.505 + 24.813 + 0.640 = 26.0 \text{ in}$$

$$L_r = 4.44\sqrt{\frac{I_{yc} d}{S_{xc}} \frac{E}{F_{yc}}} = 4.44\sqrt{\frac{(1.20)(25.96)}{(4.75)} \frac{(29000)}{(46.4)}} = 284 \text{ in.}$$

since all L_b are $< L_r$, use Eqn. (6.10.4.2.6a - 2)

Calculate Moment Capacity

since $\frac{2D_c}{t_w} > \lambda_b \sqrt{\frac{E}{F_{yc}}}$

$$a_r = \frac{2D_c t_w}{A_c} = \frac{2(16.8)(0.253)}{1.54} = 5.5$$

$$R_b = 1 - \left(\frac{a_r}{1200 + 300a_r}\right)\left(\frac{2D_c}{t_w} - \lambda_b \sqrt{\frac{E}{F_c}}\right)$$

$$= 1 - \left(\frac{5.5}{1200 + (300)(5.5)}\right)\left(\frac{2(16.8)}{0.253} - 4.64\sqrt{\frac{29000}{46.4}}\right)$$

$$= 0.97$$

$$M_n = C_b R_b R_h M_y \left[1 - 0.5\left(\frac{L_b - L_p}{L_r - L_p}\right)\right]$$

$$= (1.0)(0.97)(1.0) M_y \left[1 - 0.5\left(\frac{33.0 - 25.4}{284 - 25.4}\right)\right]$$

$$= 0.95 M_y$$

Summary of results for the various test cases are listed below. Nominal flexural resistance values are reported in terms of P_n/P_y because of the direct relationship between the ram load and girder moment in the experimental test setup.

Table B.1 Nominal Flexural Strength of Girder Using Current Design Specifications

# Brace Panels	Unbraced Length, L_b [in.]	$\frac{P_n}{P_y}$
10	33.0	0.95
5	66.0	0.89
4	82.5	0.86

B.2 DERIVATION OF BRACE FORCE EQUATION (5.8)

Referring to Figure 2.3

$$\Delta_T = \Delta_o + \Delta$$

$$P\Delta_T = F_{br}L$$

$$\frac{P}{L}\Delta_T = \beta(\Delta_T - \Delta_o)$$

$$\beta\Delta_o = \Delta_T\left(\beta - \frac{P}{L}\right)$$

$$\Delta_T = \Delta_o \frac{\beta}{\beta - P/L}$$

$$\Delta_T = \Delta_o \frac{1}{1 - P/\beta L}$$

Now calculating for the brace force using cosine function to convert to a diagonal brace gives:

$$F_{br} = (\Delta_T - \Delta_o)\frac{\beta}{\cos\theta}$$

$$= \left(\frac{1}{1 - P/\beta L} - 1\right)\frac{\beta\Delta_o}{\cos\theta}$$

$$= \left(\frac{P/\beta L}{1 - P/\beta L}\right)\frac{\beta\Delta_o}{\cos\theta}$$

$$= \frac{P}{\cos\theta}\left(\frac{\Delta_o}{L}\right)\left(\frac{1}{1 - P/\beta L}\right)$$

$$\therefore F_{br} = \frac{P}{\cos\theta}\left(\frac{\Delta_o}{L}\right)\left(\frac{1}{1-P/\beta L}\right)$$

In terms of calculations for the braced U-girder, replace P with M/h and L with the brace panel length, s.

$$\boxed{F_{brace} = \frac{M/h}{\cos\theta}\left(\frac{\Delta_o}{s}\right)\left(\frac{1}{1-\frac{M/h}{s\beta}}\right)}$$

APPENDIX C

C.1 CALCULATION OF TORSIONAL CONSTANTS (K_T, I_w, χ)

The pure torsional constant K_T for the open trapezoidal section was calculated using Equation (9.2)

$$K_T = \frac{1}{3}\sum_{i=1}^{n} b_i t_i^3$$
$$= \frac{1}{3}\left[(19)(0.62^3) + 2(3.02)(0.51)^3 + 2(24)(0.25)^3\right]$$
$$= 2.0 \text{ in.}^4$$

The warping constant I_w was determined using finite difference relations. Figure C.1 illustrates the simplified trapezoidal section with some important dimensions. Table C.1 lists the various warping properties for the girder. The normalized warping of an open-section is defined by

$$W_{n_i} = \frac{\sum\left(w_{o_i} + w_{o_j}\right) t_{ij} L_{ij}}{2A} - w_{o_i}$$

where

$w_{o_I} = \rho_{o\,i} L_{ij}$

$A = \sum t_{ij} L_{ij}$

t_{ij} = thickness of each element

L_{ij} = length of each element

ρ_o = perpendicular distance from shear center to element

The warping constant is given by

$$I_w = \frac{\sum\left(W_{n_i}^2 + W_{n_i} W_{n_j} + W_{n_j}^2\right) t_{ij} L_{ij}}{3}$$

The first calculation made was the perpendicular distance from each element to the shear center. The sign convention used assigns ρ_o a positive value if the shear center resides on the left-hand side of the element's axis when moving along the element from point *i* to *j*. The direction along an element from *i* to *j* coincides with the direction of the shear flow as shown in Figure C.1. Values for ρ_o are listed in column (3) of Table C.1. Summing the values of $\rho_o L$ through the loop 1-2-3-4-5-6 gives the w_o values. Because the directions of shear flow were previously established and the value of w_o was known at points 2 and 5 from the previous summing loop and are italicized in column (6) of Table C.1. Next, w_o at points 7 and 8 are back calculated while keeping in mind the direction of the shear flow. W_{ni} was then calculated using the previously defined expression. Sample calculations for selected cells are given following Table 4.1.

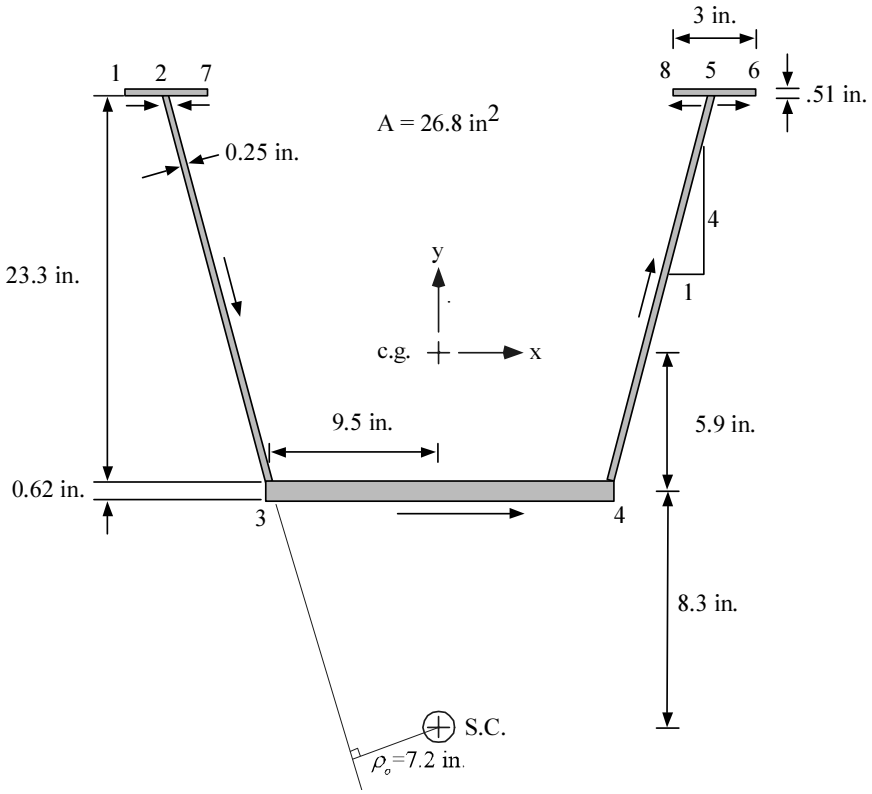

Figure C.1 Cross-Sectional Dimensions for Warping Properties

Table C.1 Warping Properties for Trapezoidal Section

(1)	(2)	(3)	(4)	(5)	(6)	(7)	(8)	(9)	(10)
Point	t_{ij}	ρ_o	L_{ij}	$\rho_o L_{ij}$	w_o	$t_{ij}L_{ij}$	$(w_{oi}+w_{oj})tL$	W_{ni}	$(W_{ni}^2+W_{ni}W_{nj}+W_{nj}^2)t_{ij}L_{ij}$
	[in]	[in]	[in]	[in^2]	[in^2]	[in^2]	[in^4]	[in^4]	[in^6]
1					0			46.3	
	0.51	-31.8	1.5	-47.8		0.75	-36		11501
2					-47.7			94.0	
	0.25	7.2	24	172.9		6.0	464		45868
3					125.1			-78.9	
	0.62	-8.3	19	-157.7		11.8	1090		73240
4					-32.6			78.9	
	0.25	7.2	24	172.9		6.0	646		45868
5					140.3			-94.0	
	0.51	-31.8	1.5	-47.8		0.75	175		11501
6					92.6			-46.3	
7					-95.5			141.8	
	0.51	31.8	1.5	47.8		0.75	-107		31707
2					***-47.7***			94.0	
5					***140.3***			-94.0	
	0.51	31.8	1.5	47.8		0.75	246		31707
8					188.1			-141.8	
Σ						26.8	2479		251391

$$A = \sum t_{ij} L_{ij} = 26.8 \text{ in}^2$$

$$w_{o2} = w_{o7} + \rho_{72} \rightarrow w_{o7} = -47.8 - (47.8) = -95.5 \text{ in}^2$$

$$w_{o8} = w_{o5} + \rho_{58} = 140.3 + 47.8 = 188.1 \text{ in}^2$$

$$(w_{o_1} + w_{o_2}) t_{12} L_{12} = (0 - 47.8)(0.75) = -36 \text{ in}^4$$

$$W_{n_2} = \frac{\sum \left(w_{o_i} + w_{o_j}\right) t_{ij} L_{ij}}{2A} - w_{o2} = \frac{2479}{2(26.8)} - (-47.8) = 94.0 \text{ in}^6$$

$$I_w = \frac{\sum \left(W_{n_i}^2 + W_{n_i} W_{n_j} + W_{n_j}^2\right) t_{ij} L_{ij}}{3} = \frac{251391}{3} = 8.4 \times 10^4 \text{ in}^6$$

The parameter χ is used to determine the relative dominance of pure and warping torsion in a member and is dependent on the member length and cross section.

$$\chi = L\sqrt{\frac{GK_T}{EI_w}}$$

$$= (336\text{ in.})\sqrt{\frac{(11{,}000\text{ ksi})(2.1\text{ in}^4)}{(29{,}000\text{ ksi})(8.4\times10^4\text{ in}^6)}}$$

$$= 0.52$$

Referring to Table 9.1 indicates the open trapezoidal girder is dominated by warping torsion.

C.2 TORSIONAL STIFFNESS FOR OPEN TRAPEZOIDAL GIRDER

Solutions for members subjected to concentrated torques can readily be found in various references (AISC 1997, Heins 1975). The upper and lower bound theoretical solutions are presented herein.

Lower Bound Solution

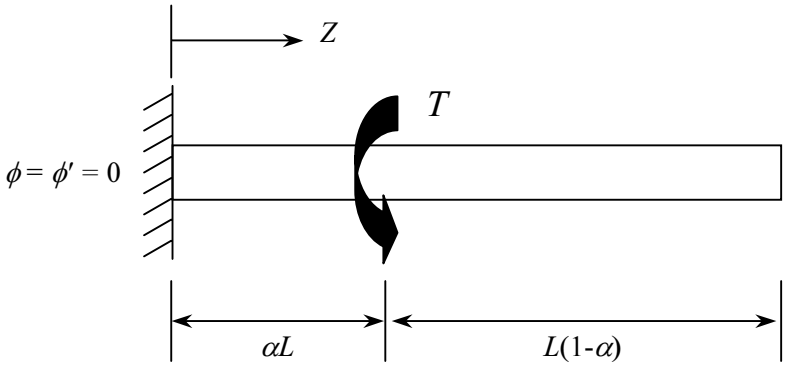

Figure C.2 Lower Bound Torsional Stiffness Model

The general solution for a cantilever with a concentrated torque is given by

$$\phi(Z) = \frac{Ta}{GK_T}\left[\left(\sinh\frac{\alpha L}{a} - \tanh\frac{L}{a}\cdot\cosh\frac{\alpha L}{a} + \tanh\frac{L}{a}\right)\left(\cosh\frac{Z}{a} - 1.0\right) - \sinh\frac{Z}{a} + \frac{Z}{a}\right]$$

where

$$a = \sqrt{\frac{EI_w}{GK_T}} = \sqrt{\frac{(29{,}000\text{ ksi})(8.4\times10^4\text{ in}^6)}{(11{,}000\text{ ksi})(2.1\text{ in}^4)}} = 325\text{ in.}$$

Using $\alpha = 1.0$, the rotation at the end of the cantilever simplifies to

$$\phi(L) = \frac{TL}{GK_T}\left(1 - \frac{a}{L}\tanh\frac{L}{a}\right)$$

Since the cantilever represents one-half of the full girder, the load and span are both reduced by one-half. Using L = 168 in. gives

$$\left(\frac{T}{\phi}\right)_{lower} = \frac{2GK_T}{\left(L - a\tanh\frac{L}{a}\right)} = \frac{2(11{,}000\ \text{ksi})(2.0\ \text{in}^4)}{(168\ \text{in.}) - (325\ \text{in.})\tanh\left(\frac{168\ \text{in.}}{325\ \text{in.}}\right)} = 3412\ \text{kip - in/rad}$$

Upper Bound Solution

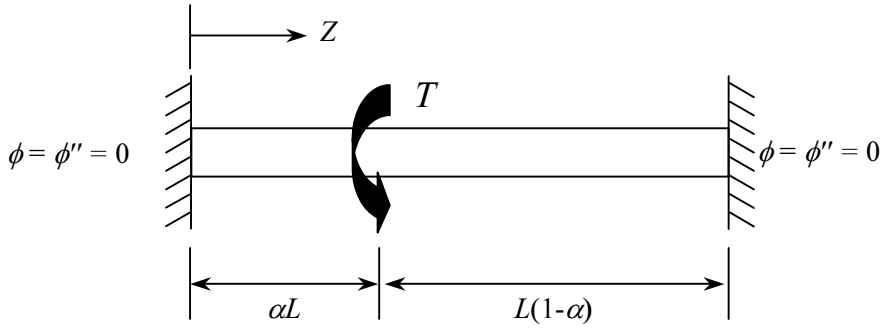

Figure C.3 Upper Bound Torsional Stiffness Model

The upper bound solution is based on no twist and full warping restraint at the ends. The torsional stiffness obtained from the solution to the governing differential equation is given by

$$\frac{T}{\phi(Z)} = \frac{(H+1)GK_T}{a}\left\{\left[H\cdot\left(\frac{1}{\sinh\frac{L}{a}} + \sinh\frac{\alpha L}{a} - \frac{\cosh\frac{\alpha L}{a}}{\tanh\frac{L}{a}}\right) + \left(\sinh\frac{\alpha L}{a} - \frac{\cosh\frac{\alpha L}{a}}{\tanh\frac{L}{a}} + \frac{1}{\tanh\frac{L}{a}}\right)\right]\cdot\left[\cosh\frac{Z}{a} - 1.0\right] - \sinh\frac{Z}{a} + \frac{Z}{a}\right\}^{-1}$$

where

$$H = \frac{\left[\frac{1}{\tanh\frac{L}{a}}\left(1.0 - \cosh\frac{\alpha L}{a}\right) + \frac{1}{\sinh\frac{L}{a}}\left(\cosh\frac{\alpha L}{a} - 1.0\right) + \sinh\frac{\alpha L}{a} - \frac{\alpha L}{a}\right]}{\left[\frac{1}{\sinh\frac{L}{a}}\left(\cosh\frac{L}{a} + \cosh\frac{\alpha L}{a}\cdot\cosh\frac{L}{a} - \cosh\frac{\alpha L}{a} - 1.0\right) + \frac{L}{a}(\alpha - 1.0) - \sinh\frac{\alpha L}{a}\right]}$$

For $\alpha = 0.5$ and $Z = L/2$, the value of the constant H becomes equal to one. The torsional stiffness then simplifies to

$$\left(\frac{T}{\phi}\right)_{upper} = \frac{4GK_T}{a \cdot \left(\frac{L}{a} - 4\tanh\frac{L}{4a}\right)} = \frac{4(11{,}000)(2.0)}{(325)\left(\frac{336}{325} - 4\tanh\frac{336}{4(325)}\right)} = 12660 \text{ kip - in/rad}$$

C.3 THEORETICAL TORSIONAL STIFFNESS OF FULLY BRACED TEST CASE

The shear stiffness of the deck panels was determined using methods outlined in the *Steel Deck Institute Diaphragm Design Manual* (1995). Additional examples of detailed calculations to determine deck panel stiffness may be found in Currah (1993).

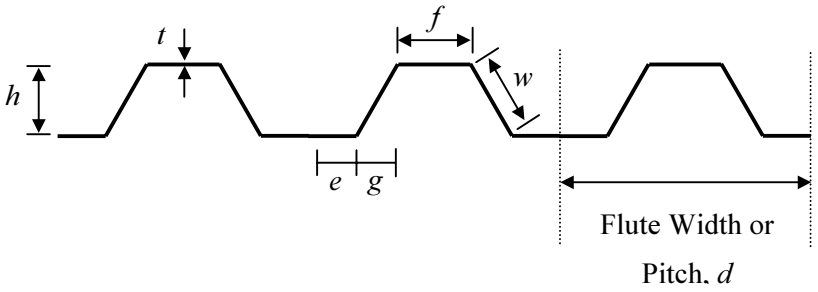

Figure C.4 Deck Cross-Sectional Dimensions

Deck cross-sectional dimensions

$t = 0.0359$ in.

$h = 2.0$ in.

$d = 12$ in.

$e = 2.5$ in.

$f = 5.0$ in.

$g = 1.0$ in.

$w = 2.236$ in.

$s = 2e + 2w + f = 14.5$ in.

The warping constant is defined in the second edition of the SDI Manual as:

$D_n = D/12L$

Where L is the deck panel length in feet and D is a constant that is calculated using equations developed in Appendix-IV of the SDI Manual. *DW1* through *DW4* represent *D*-values for end fasteners located in each, alternate, every third, and every fourth corrugation valley, respectively. The cross-sectional geometry of the decking is simplified by assuming straight elements and neglecting formed deck stiffeners.

$WT = 4f^2(f+w)$

$WB = 16e^2(2e+w)$

$PW = 1/t^{1.5}$

$A = 2e/f$

$D1 = h^2(2w+3f)/3$

$D2 = D1/2$

$V = 2(e+w)+f$

$D3 = (h^2/12d^2)[(V)(4e^2-2ef+f^2)+d^2(3f+2w)]$

$C1 = 1/[D3-D2/2]$

$C2 = 1/[e(D2/f)+D3]$

$C3 = 1/[(0.5+A)D2+D3]$

$C4 = A/[e(D1/f)+D2]$

$C5 = A/[(0.5+A)D1+D2]$

$C6 = 1/[(0.5+A)D1+D3+D2/2]$

$D4[1] = (24f/C1)(C1/WT)^{0.25}$

$D4[2] = (24f/C2)(C2/WT)^{0.25}$

$D4[3] = (24f/C3)(C3/WT)^{0.25}$

$D4[4] = (48e/C4)(C4/WB)^{0.25}$

$D4[5] = (48e/C5)(C5/WB)^{0.25}$

$D4[6] = (24i/C6)(C6/WT)^{0.25}$

$G4[1] = D4[1]$

$G4[2] = 2(D4[2])+A(D4[4])$

$G4[3] = 2(D4[3])+D4[6]+2A(D4[5])$

$C41 = A/[(1.5A+1)D1+D2]$

$C42 = 1/[D3+(1.5A+1)D2]$

$C43 = A/[(2A+1)D1+2(D2)]$

$C44 = 1/[(1.5A+1)D1+(0.5A+1)D2+D3]$

$D42 = (24f/C42)(C42/WT)^{0.25}$

$D44 = (24f/C44)(C44/WT)^{0.25}$

$D41 = (48e/C41)(C41/WB)^{0.25}$

$D43 = (48e/C43)(C43/WB)^{0.25}$

$G44 = 2(D42+D44)+A[2(D41)+D43]$

$DW1 = (G4[1])(f/d)(PW)$

$DW2 = (G4[2])(f/2d)(PW)$

$DW3 = (G4[3])(f/3d)(PW)$

$DW4 = (G44)(f/4d)(PW)$

Fastener used in the experimental tests were placed in every corrugation valley. Therefore, only *DW1* will be calculated.

$WT = 4(5.0)^2(5.0+2.236) = 723.6$

$PW = 1/(0.0358)^{1.5} = 147.6$

$D1 = (2.0)^2[2(2.24)+3(5.0)]/3 = 26.0$

$D2 = 26.0/2 = 13.0$

$V = 2(2.5+2.24)+5.0 = 14.5$

$D3 = [(2)^2/12(12)^2]\{(14.5)[4(2.5)^2-2(2.5)(5)+(5)^2]+(12)^2[3(5)+2(2.24)]\} = 7.33$

$C1 = 1/(7.33-13.0/2) = 1.20$

$D4[1] = [24(5)/1.20](1.20/723.6)^{0.25} = G4[1] = 20.3$

$DW1 = (20.3)(5/12)(147.6) = 1246$

The remaining D-values were calculated to be

DW2 = 18385

DW3 = 38817

DW4 = 62593

Equation 3.3-1 of the Second Edition of the SDI Manual represents a simplified equation for the connector slip parameter, *C*. This simplified equation is based on the assumption that the number of panels is greater than five. For purposes of this analysis, the more exact equation for *C* will be used. This equation only appears in the First Edition of the *Steel Deck Institute Diaphragm Design Manual* (SDI, 1981) on page 28 and is given by

$$C = \frac{2EtL}{a} S_f \left(\frac{n_{sh} - 1}{2\alpha_1 + n_p \alpha_2 + 2n_s \dfrac{S_f}{S_s}} + \frac{1}{2\alpha_1 + n_p \alpha_2 + n_e} \right)$$

Additional parameters are

E = 29500 ksi

W = 36 in.

L = 34 in. = 2.83 ft.

n_{sh} = 1 (single sheet)

n_s = 0 (no stitch fasteners)

n_p = 0 (single span, no purlines)

$$a = n_{sh} \cdot W$$

The distances to each fastener, x_e, is shown in Figure C.5.

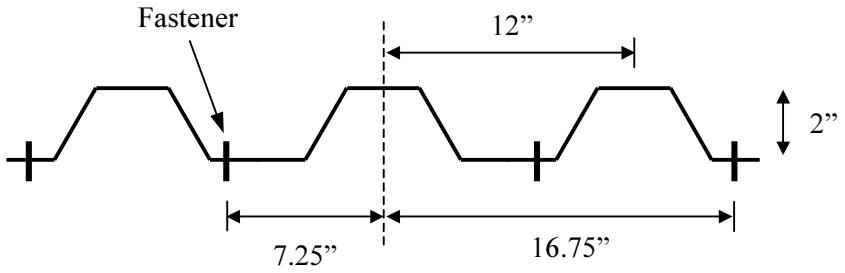

Figure C.5 Fastener Eccentricities

The term α_1 is calculated as

$$\alpha_1 = \sum \frac{x_e}{W} = \frac{2(16.75\,\text{in.}) + 2(7.25\,\text{in.})}{36\,\text{in.}} = 1.33$$

For Hilti ENP2 powder actuated fasteners

$$S_f = \frac{1.25 \times 10^{-3}}{t^{0.5}} = \frac{1.25 \times 10^{-3}}{(0.0359)^{0.5}} = 0.0066\,\text{in/kip}$$

Connector slip parameter equals

$$C = \frac{2(29500\,\text{ksi})(0.0359\,\text{in.})(2.83\,\text{ft.})}{36\,\text{in.}}(0.00511\,\text{in/kip})\left(\frac{1}{2(1.33)}\right) = 0.412$$

Calculate panel shear stiffness

$\phi = 1.0$ (for single span)

$$D_n = \frac{DW1}{12L} = \frac{1246}{12(2.83\,\text{ft.})} = 36.6$$

$$G' = \frac{E \cdot t}{2.6\left(\frac{s}{d}\right) + \phi \cdot D_n + C} = \frac{(29500\,\text{ksi})(0.00359\,\text{in.})}{2.6\left(\frac{14.5\,\text{in.}}{12\,\text{in.}}\right) + 1.0(36.6) + 0.412} = 26.3\,\text{kips/in}$$

The shear stiffness of a flat plate is given by

$$\text{G} = \frac{\tau}{\gamma} = \frac{V}{A}\frac{h}{\delta} = \frac{V}{\delta}\frac{1}{t_{eq}}$$

where G is the shear modulus of elasticity. The term V/δ is equivalent to the shear stiffness of the deck panel, G'. Thus, the equivalent thickness of the panel is given by

$$t_{eq} = \frac{G'}{G} = \frac{26.3\,\text{kips/in}}{11000\,\text{ksi}} = 0.00239\,\text{in.}$$

where G is the shear modulus of elasticity for steel. The pure torsion constant for the closed section is

$$K_T = \frac{4A_o^2}{\sum_{i=1}^{n} \frac{b_i}{t_i}} = \frac{4(595\,\text{in}^2)^2}{\frac{20}{0.64} + 2\frac{24.8}{0.15} + \frac{31}{0.00239}} = 107\,\text{in}^4$$

The overall torsional stiffness of the girder is then

$$\boxed{\left(\frac{T}{\phi}\right)_{Closed} = \frac{4GK_T}{L} = \frac{4(11{,}000\,\text{ksi})(107\,\text{in}^4)}{336\,\text{in.}} = 14040\,\text{kip - in/rad}}$$

REFERENCES

AASHTO. (1998). *AASHTO LRFD Bridge Design Specifications*—2nd Edition, American Association of State Highway and Transportation Officials, Washington, D.C.

AISC. (1997). *Steel Design Guide for Torsional Analysis of Structural Steel Members*. American Institute of Steel Construction, Chicago, Illinois.

Akay, H. U., Johnson, C. P., and Will, K. M. (1977). "Lateral and Local Buckling of Beams and Frames." *Journal of the Structural Division*, Vol. 103(9), ASCE, New York, New York, pp. 1821-1832.

Basler, K. and Kollbrunner, C. F. (1969). *Torsion in Structures.* Springer-Verlag, Berlin, Germany, pp. 14-15.

Bažant, Z. P. and Cedolin, L. (1991). *Stability of Structures.* Oxford University Press, Inc., New York, New York, pp. 19-26.

Blank, David. (1973). "Stiffening Effects of Cold Formed Decks on Box Beam Bridges," thesis presented to the University of Maryland in partial fulfillment of the requirements for the degree of Master of Science.

Currah, R. M. (1993). "Shear Strength and Shear Stiffness of Permanent Steel Bridge Deck Forms," thesis presented to The University of Texas at Austin, in partial fulfillment of the requirements for the degree of Master of Science in Engineering.

Choo, K. M. (1987). "Buckling Program BASP for Use on a Microcomputer," thesis presented to The University of Texas at Austin, in partial fulfillment of the requirements for the degree of Doctor of Philosophy.

Fan, Zhanfei. (1999). "Field and Computational Studies of Steel Trapezoidal Box Girder Bridges," thesis presented to The University of Houston, in partial fulfillment of the requirements for the degree of Doctor of Philosophy.

Galambos, Theodore V. (1968). *Structural Members and Frames*. Prentice-Hall, Inc., Englewood Cliffs, New Jersey, pp. 33-47.

Gilchrist, C., Yura, J. and Frank, K. (1997). "Buckling Behavior of U-Shaped Girders," Report No. 1395-1, Center for Transportation Research, The University of Texas at Austin, June, 67 p.

Guide Specifications for Horizontally Curved Highway Bridges, American Association of State Highway and Transportation Officials, 1993.

Load and Resistance Factor Design Specification for Steel Buildings, American Institute of Steel Construction, Chicago, Illinois, December, 1993.

Heins, Conrad P. (1975). *Bending and Torsional Design in Structural Members*. D. C. Heath and Company, Lexington, Massachusettes

Heins, C. P. and Seaburg, P. A. (1963). "Torsion Analysis." Bethlehem Steel Company, Bethlehem, Pennsylvania.

McDonald, R. F., Chen, Y., Yilmaz, C., Yen, B. T. (1976). "Open Steel Sections with Top Lateral Bracing," *Journal of the Structural Division*, Vol. 102(ST1), ASCE, New York, N.Y., pp. 35-49.

Meck, H. R. (1977). "Experimental Evaluation of Lateral Buckling Loads." *Journal of the Engineering Mechanics Division*, ASCE, EM2, April, pp. 331-337.

Nakai, H. and Heins, C. P. (1977). "Analysis Criteria for Curved Bridges." *Journal of the Structural Division*, Vol. 103(7), ASCE, New York, New York, pp. 1419-1427.

Rao, N. R. N. (1964). "Torsional Behavior of Thin-Walled Open Sections Reinforced By Bracing." Fritz Engineering Laboratory Report #354.275, Lehigh University, Bethlehem, Pennsylvania.

SDI. (1981). *Steel Deck Institute Diaphragm Design Manual.* 1st Edition. Steel Deck Institute, St. Louis, Missouri.

SDI. (1995). *Steel Deck Institute Diaphragm Design Manual.* 2nd Edition. Steel Deck Institute, St. Louis, Missouri.

Southwell, R. V. (1932). "On the Analysis of Experimental Observations in the Problems of Elastic Stability." *Proceedings of the Royal Philosophical Society of London*, Series A, Vol. 135, April, p. 601.

Taylor, A. C., and Ojalvo, M. (1966). "Torsional Restraint of Lateral Buckling." *Journal of the Structural Division*, Vol. 92(ST2), ASCE, New York, New York, pp. 115-129.

Timoshenko, S., and Gere, J. (1961). *Theory of Elastic Stability.* McGraw-Hill Book Company, New York, New York, pp. 190-191.

Trahair, Nicholas S. (1969). "Deformations of Geometrically Imperfect Beams." *Journal of the Structural Division*, Vol. 95(7), ASCE, New York, New York, pp. 1475-1496.

Winter, G. (1960). "Lateral Bracing of Columns and Beams." *ASCE Transactions*, Vol. 125, ASCE, New York, New York, pp. 809-825.

Yura, J., Phillips, B., Raju, S., and Webb, S. (1992). "Bracing of Steel Beams in Bridges," Report No. 1239-4F, Center for Transportation Research, The University of Texas at Austin, October, 80 p.

Yura, Joseph A. (1993). "Fundamentals of Beam Bracing." Structural Stability Research Council Conference - Is Your Structure Suitably Braced? April 6-7, Milwaukee, Wisconsin.

Yura, Joseph A. (1995). "Bracing for Stability-State-of-the-Art," Proceedings, Structures Congress XIII, ASCE, Boston, Massachusetts, April, pp. 88-103.

Yura, Joseph A. (1996). "Winter's Bracing Approach Revisited." *Engineering Structures*, Vol. 18(10), Elsevier Science Ltd., Great Britain, pp. 821-825.